INFORMATION QUANTIFICATION FOR SPIKE TRAINS AND FIELD POTENTIALS

A thesis submitted to the University of Manchester for the degree of Doctor of Philosophy in the faculty of Engineering and Physical Sciences

2011

By
Zareen Mehboob
Electrical and Electronic Engineering

Contents

List of Tables

List of Figures

Abstract

The University of Manchester
Zareen Mehboob
2010
Degree of Doctor of Philosophy

Neural signals are recorded from various regions of the brain and are analysed to understand the working mechanism of neurons and how they interpret external environment. The aim is to understand how this nature's supercomputer works. This helps in exploring human systems and intelligence, treat mental conditions and develop smart machines. Neural data recordings are collected from individual neurons and from populations of neurons. The single neuronal activity recordings are spike train and the activity generated from multiple neurons are field potentials. The data obtained are in enormous amount and of millisecond precision, as a consequence their processing is not a trivial task and efficient techniques are required for decoding these datasets.

This work proposes several methods for the analysis of spike train and field potentials. A self-organising map based clustering is applied to synchronous spike train and generates topographically ordered and information-preserving clusters that help interpret how stimuli features are encoded by the neurons.

An information-coupled empirical mode decomposition framework is developed for field potentials. It extracts informative oscillatory functions and information coding frequency bands in the recordings. This has several applications. The informative modes reveal underlying neuronal activities w.r.t stimuli, which otherwise have to be extracted by bandpass filters, followed by Fourier or wavelets analysis. It can also be used to analyse neuronal population activity under a medical condition or to understand neuronal interactions by information-connectivity analysis among electrodes. The proposed framework is developed into the form of a toolbox which can be used for educational and research purposes.

Declaration

No portion of the work referred to in this thesis has been submitted in support of an application for another degree or qualification of this or any other university or other institute of learning.

Copyright

i. The author of this thesis (including any appendices and/or schedules to this thesis) owns any copyright in it (the "Copyright") and s/he has given The University of Manchester the right to use such Copyright for any administrative, promotional, educational and/or teaching purposes.

ii. Copies of this thesis, either in full or in extracts, may be made only in accordance with the regulations of the John Rylands University Library of Manchester. Details of these regulations may be obtained from the Librarian. This page must form part of any such copies made.

iii. The ownership of any patents, designs, trade marks and any and all other intellectual property rights except for the Copyright (the "Intellectual Property Rights") and any reproductions of copyright works, for example graphs and tables ("Reproductions"), which may be described in this thesis, may not be owned by the author and may be owned by third parties. Such Intellectual Property Rights and Reproductions cannot and must not be made available for use without the prior written permission of the owner(s) of the relevant Intellectual Property Rights and/or Reproductions.

iv. Further information on the conditions under which disclosure, publication and exploitation of this thesis, the Copyright and any Intellectual Property Rights and/or Reproductions described in it may take place is available from the Head of Sensing, Imaging and Signal Processing Group in School of Electrical and Electronic Engineering (or the Vice-President).

Acknowledgements

I would like to say heartfelt thanks to my supervisor Dr. Hujun Yin who has been a great mentor for me, very kind and has always provided me valuable guidance, impartial advice and continuous support during my research which has helped me a lot in my research and career progression.

I am very grateful to all my colleagues, specially, Matt Mould and Aftab Khan who helped with proof reading and critical comments to help improve my thesis. I am thankful to everyone in the academics and staff without their cooperation and support my journey could not have gone that smooth.

I am thankful for the datasets, helpful comments and guidance provided by Dr. S. Panzeri, Dr. R. Vogels, Dr. Marc M. Van Hulle and Dr. Nikolay Van Manyakov. I am also grateful for all the anonymous reviewers for their helpful comments and suggestions.

I am grateful to my parents who have always supported me and always have faith in me, without them I could not have come this far. I am very thankful to Fawad Nisar, who has always been very caring and supportive and has provided me guidance whenever needed.

I acknowledge that I have been funded by HEC (Pakistan) for my studies.

Chapter 1

Introduction

Quantifying the working mechanism of brain is one of the most challenging, appealing and intriguing questions of all times. It is the brain that makes us human. Our body, senses, emotions, energy, personality, attitude, imaginations and dreams, are all controlled by this little supercomputer inside our heads.

"Men ought to know that from nothing else but the brain come joys, delights laughter and sports, and sorrows, griefs, despondency and lamentations. And by this, in an special manner, we acquire wisdom and knowledge, and see and hear and know what are fouled and what are fair, what are bad and what are good, what are sweet and what are unsavory.... And by the same organ we become mad and delirious and fears and terrors assail us.... All these things we endure from the brain when it is not healthy.... In these ways I am of the opinion that the brain exercises the greatest power in the main."

–Hippocrates,*On the Sacred Disease* (Fourth century B.C)

The science of studying the nervous system is called neuroscience; it deals with exploring the complex network of brain, spinal cord, and sensory nerve cells called neurons. The foundation of neuroscience is based on understanding the interactions among these neurons (Bear et al. 2007). The knowledge base of informatics constitutes of representation, processing, and communication of information in natural and engineered systems. Neuroinformatics combines expertise from neuroscience and other information sciences such as psychology, computer science, mathematics etc. to understand the behaviour and functionality of brain.

"Neuroinformatics combines neuroscience and informatics research to develop and apply the advanced tools and approaches that are essential for major advances in understanding the structure and function of the brain."

OECD MegaScience Forum Report, 1999

A diagram of a human brain is depicted in Fig. 1.1. It shows different portions of the brain where various types of sensory information are processed. The brain can be considered as a naturally engineered supercomputer that responds and processes different events/senses or stimuli occurring within the body and in the outer world.

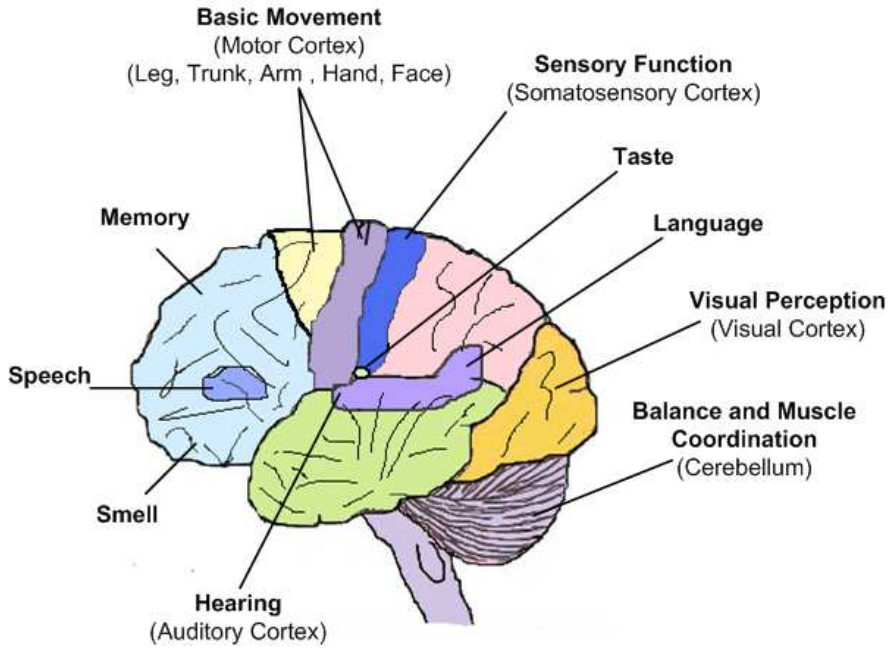

Figure 1.1: Structure of a human brain showing the coding location of different sensory information.

For every input, the brain executes an algorithm and generates an output, as shown in Fig. 1.2. As a result, you make sense and interpret the events of the outside world. In all this computation, the neurons act as 'functions' with some input and output (i/o) arguments, passing different parameters and information to each other in the form of signals. The output is finally generated within the brain or at an output terminal such as eyes, ears etc. For instance, after years of research, it is now known that if the input stimulus is an 'odour', it will go to the odour center for processing (Fig. 1.1). Similarly, a visual input is

processed in the 'vision center' (visual cortex) of the brain. It is still unknown which 'code and parameters' neurons use to represent this 'odour input' and encode this information into the brain. Thus, the aim is to learn about the programming language of the brain. Also every species' brain specifications are different as we have computers with different specifications. Humans have the most sophisticated, complicated and powerful specifications as compared to other species.

A general approach is to study the brain functionality of simple organisms whose brains are much smaller and simpler. Just a century ago, scientists discovered that the basic units of communication in the nervous system are neurons (Carey 1990, Lopez-Munoz et al. 2006). A Spanish anatomist Santiago Raman y Cajal, in 1889, gave the very first argument about neuron as a basic and an independent functional unit of brain (Carey 1990, Lopez-Munoz et al. 2006). The neuron theory and the neuron term was initially coined by a German anatomist H. Waldeyer-Hartz in 1891 (Carey 1990).

Figure 1.2: Exploring the neural code by analysing input-output relationships in the brain.

After years of research, we know that there are billions of neurons in a brain. Due to technical limitations on availability of data, it is not yet possible to learn completely about this supercomputer. Data are usually collected from a small number of neurons or from a small region of brain. Even a small region may record activity of hundreds, thousands or up to millions of neurons but this is still a small number as compared to the total neuronal population. For example, a cat has roughly 3×10^8 neurons in cerebral cortex (Roth & Dicke 2005) and a human brain consists of about 100 billion (10^{11}) neurons (Williams & Herrup 1988). From this limited amount of data, neuroscientists try to understand neural coding and information processing mechanisms in that region. This not only helps

in understanding the working mechanism of brain but also helps in diagnosing and treating different mental and physical illness and abnormalities caused in nervous system.

After recording neural signals from an experiment, neuroscientists look for relationships between stimuli and responses, and their physical, temporal and spectral attributes. Different approaches are used for analysis and based on these observations, a neural code is suggested by studying the stimulus-response (input-output) attributes and relationships. This neural code is then validated by various methods, for instance by observing correlations or synchronisation among signals. Mutual information (MI) is also used frequently for neural code analysis which measures how much information can be gained about a stimulus by observing its corresponding neuronal generated response and tells about the number of bits required to encode this neural information when quantified using logarithms to the base 2. These methods will be discussed in detail in Chapter 2.

Neural recording experiments may also look, in particular, into the input (stimulus) features that are actually coded into the brain. This is done by changing the input parameters (e.g. strong/ weak odour) and recording the resultant output (response). In such cases, the information obtained for a correct neural code will be optimal as compared to an incorrect or an incomplete code. Thus mutual information theory provides a means for information quantification as well as neural code verification (Abbot & Dayan 2001). Concepts and examples related to this approach are covered in Chapter 3.

1.1 Problem Area

The set up for neurophysiology experiments are planned to specifically address a particular problem or question of interest. The experiments may be designed to understand responses to simple or complex stimuli, or a cognitive, behavioural or memory related task. Other experiments are designed to understand different medical conditions and may compare the recordings in a healthy or unhealthy subject. Each experiment has its own objectives to gain insight into a particular problem domain.

The recordings are made usually by using single or multiple electrodes, in one or more subjects, against different stimuli/events and using several trials. Now, with the advancements in neurophysiology techniques, it is possible to obtain

recordings from multiple (16-100) channels, and from various subjects (animals/ humans) against different conditions. One approach is to repeat experiments several (10-100s) times to measure the variation in responses and account for the non-stationarity of the responses. The amount of data thus obtained, from these experiments, is huge in size and occupies several hundred Mega bytes to Giga bytes of disk space. This makes data storage, retrieval and processing a substantial time consuming task. Thus, neuroscientists need automated and robust tools for analysis of these large datasets which are efficient and user-friendly.

A number of approaches have been developed for analysis of neural recordings and neural code analysis. These are aimed to find features and attributes in the data recordings that are carrying some useful information about the given stimulus, condition or event. The brain is a non-stationary system in a sense that neurons behave in non-stationary pattern and if an input 'a' is presented several times, the neurons do not generate the same response 'b' each time. Thus, the neural recordings obtained are also non-stationary and non-deterministic in nature. Most of the signal processing methods, currently in use, offer limited applications and are less effective for analysis of these recordings. There is need for developing and improving various frameworks, tools and techniques that can help in the quantification of these large datasets. This also involves several complex and time consuming computations to find the relationship between neural responses and explore the code they are using to represent the outer world.

For instance, a typical neurophysiology experiment that involves recordings from visual cortex may involve recording the activity after presentation of a simple stimulus such as a grating. The experiment is repeated several times to account for the nonlinear behaviour of the brain. Another approach is in practice, that involves presentation of several sensory stimuli just once or may be a few times followed by recording the neuronal response in reaction to these. The idea behind this approach is that the brain is such an intelligent system that it learns and responds to the stimulus in a single presentation, it does not require several presentations of the same stimulus to learn about it or to improve its response in case of sensory stimuli. For cognitive related tasks, it is anticipated that the response or learning improves with repetition.

With the advancements in physiology and electronics technology, it is easier to conduct neurophysiology experiments. The recording procedures and standards

are improving and storage of large neural datasets is easy and getting cheaper on large hard drives locally installed on machines. However, neural data processing and analysis is yet quite time consuming and computationally expensive task. The facilities and standardized procedures for several types of neural data analysis, compression and remote data sharing are not readily available. There is an unavoidable need to develop such tools, techniques and algorithms that can help in fast, adequate and reliable data analysis. This will facilitate neural data sharing and aid in understanding and exploring the neural code and optimize procedures for extracting the useful information from the raw neural data recordings.

1.2 Aims and Objectives

The aim of this research is to find and develop robust, automated and adaptive tools that can be used for analysis of neural recordings of various types. The recordings are collected from individual neurons as well as from multiple neurons, from one or multiple sites. The recordings are either electric or magnetic potentials which vary in characteristics and represent several aspects of neural phenomena and coding mechanism. Tools are required that can facilitate neural data analysis, help in understanding and validating the neural code and can employ different methods that can reduce the amount of data while preserving the neural information in a given dataset.

As a first stage of this process, this research aims to extract an information preserving dataset from a given set of raw neural recordings. Depending on the nature of neural recording, this can be achieved by means of data analysis, correlation analysis, cluster analysis, signal filtration or decomposition, whichever technique gives the best result.

The next step involves finding ways to achieve compression of generated information preserving dataset. This aims to provide an efficient means for neural data storage, transfer, processing and analysis.

The research aims to find solutions based on the idea that all data collected in the neural recordings is not relevant to the question under consideration. There is background noise and data points which do not carry information about the events, stimuli or conditions that are currently under investigation. The irrelevant or least significant data can be discarded or filtered out, thus retaining only the

data that are useful for data exploration, feature extraction and further analysis. Hence it is intelligible that complete information in neural data recordings can be retained and used efficiently if only the informative data points are extracted from it. It can be said that information loss will be negligible or minimal in the derived dataset if procedures are developed to retrieve the information carrying points in the neural recordings.

To summarise, given a dataset of neural recordings, this research aims to develop different tools and techniques that can help in neural coding analysis and extract the 'useful' or 'informative' features or data points from it. After the feature extraction, information is re-calculated from the derived feature (data) set to measure the retained level of information. This information-preserving dataset can then be used for further analysis. This process has been shown in a simple block diagram of Fig. 1.3.

The first block of Fig. 1.3 is showing several forms of neural recordings which can be discrete (binary) spike train or continuous field potentials. These data can also be in the form of images showing activity in different regions of the brain under different conditions. Each type of neural recordings has advantages and limitations. This research covers the investigation of methods for discrete and continuous neural recordings. These can be obtained from single neurons or from neuronal networks in different brain regions.

The neural recordings or images obtained initially are analysed for neural code and may also be contaminated by some background noise. Some sort of signal filtration and processing is required to analyse the information and discard the noise. This is shown in the second block of Fig. 1.3.

The next step then involves the feature extraction process. The aim is to extract and filter out a subset of the original dataset which carries all or maximum information, or encodes the stimulus/event in almost all cases. The last step then aims to estimate the level of information preservation and information comparison between the original and the generated dataset. The objectives of this research can be summarized as follows:

1. To automate analysis of different forms of neural data recordings.

2. To develop methods for automated analysis of discrete spike train.

3. To design and improve algorithms for continuous neural recordings such as local field potentials (LFPs), magneto-encephalographs (MEGs) etc.

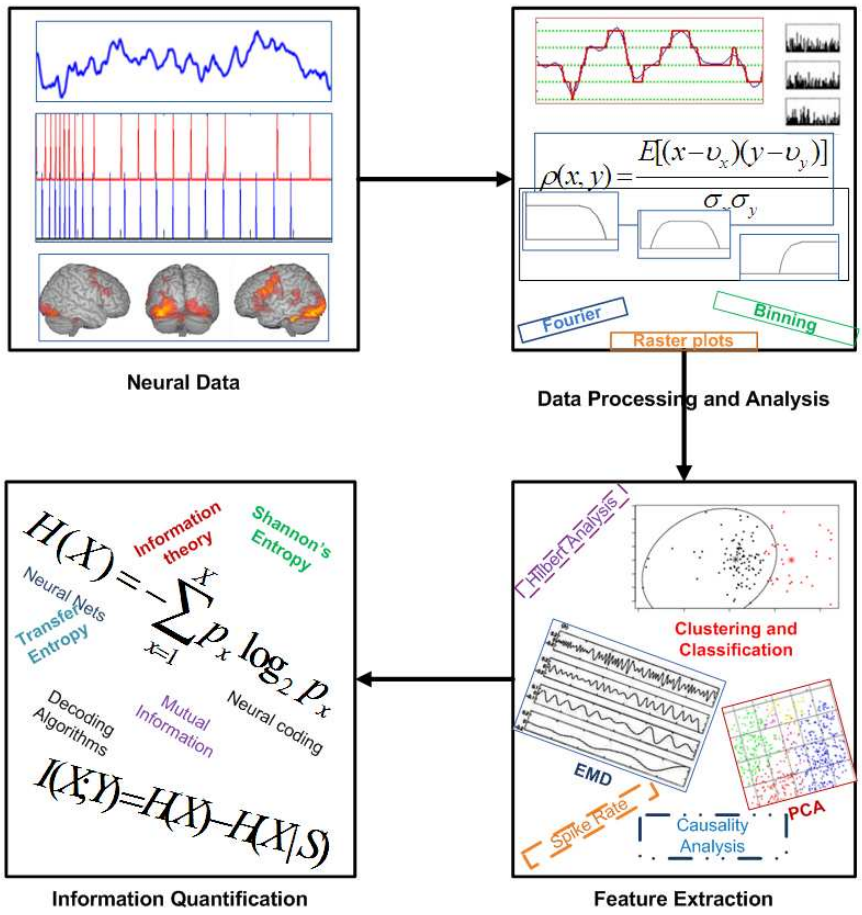

Figure 1.3: A block diagram showing the steps for information quantification analysis of the neural data.

4. To overcome the limitations of signal processing methods currently in use.

5. To investigate and validate the performance of developed tools and algorithms on various electric and magnetic field potential datasets.

To achieve these objectives, this research has explored not only the methods for discrete spike train analysis but also for continuous electric and magnetic field potentials including, electroencephalogram (EEG), magneto-encephalogram (MEGs), multi-unit activity (MUA) and local field potential (LFP) recordings. The experiments are aimed to automate the data analysis procedures and give insight into the neural coding mechanism. This helps in understanding how neurons represent the outside world within the brain.

During this research, information theoretic analysis is induced with artificial neural network based analysis for spike train clustering. Information theoretic analysis is combined with the results obtained from the application of self-organizing map (SOM). It has been found that the SOM generates topology preserving clusters. The information analysis of these clusters reveals that the information has been preserved within the clusters. The approach is automated and adaptive, suitable for the analysis of spike train which are often considered as point process data. Point processes are data which represent discrete events randomly occurring in time. These method and results are discussed in Chapter 3 and are also presented in (Yin, Panzeri, Mehboob & Diamond 2008) and (Yin, Mehboob, Panzeri & Diamond 2008).

The analysis of continuous potentials differs from the analysis of discrete spike train and these recordings also have non-stationary attributes. The discrete spike train are the activity of individual neurons whereas continuous field potential reflect combined activity of multiple/ large population of neurons. These neural signals are obtained in the form of electric and magnetic potentials from different regions of the brain. The analysis of continuous neural recordings require spectral and temporal analysis of the data in different frequency domains as the information is preserved in different frequency bands (Pfurtscheller & Aranibar 1977).

During this research, various methods, tools and frameworks for the analysis of different forms of continuous neural recordings are developed. These are widely tested on different types of neural potentials which are electric or magnetic field potentials such as LFP and MEG. Some improvements are also suggested to the

initially developed framework. Some of the findings are described in (Mehboob & Yin 2009, 2010). The developed framework introduces an information preserving signal extraction technique that retrieves the oscillatory information carrying modes from the raw and noisy potentials. The research combines knowledge from neuroscience, signal processing, mathematics and software technology to facilitate neural data analysis. This provides a solution for the automated analysis of neural signals.

The designed framework has been developed into a user-friendly and efficient MATLAB based toolbox which is available for free to offer its advantages to neuroscience community and can be used for educational and research purpose. The details of this work are presented in (Mehboob & Yin 2009, 2010, 2011). The framework is based on information-coupled empirical mode decomposition (EMD) method. EMD decomposes a given set of neural recordings into amplitude mode or frequency mode oscillatory functions. Information-carrying modes are extracted after the information analysis of these modes. The information-carrying or informative modes are the ones which are contributing to stimulus coding. Further, these information carrying oscillatory modes can be used for data compression and data transfer, significantly reducing the data size and processing time.

1.3 Thesis Organization

The rest of the thesis is organized in seven chapters. The summary of each chapter is presented in this section.

Chapter 2 covers the literature review. In this chapter, the basic structure and communication mechanism of neurons is presented, as these are the main building blocks in brain functionality. Then different forms of neural signals are discussed. A brief description of different methods is given that are currently in use for neural data analysis.

Chapter 3 is dedicated to the spike train analysis. Spikes are outputs of individual neurons and have discrete data representation. This chapter reviews the approaches for spike train analysis and presents our approach for decoding, clustering and compression of the spike train using artificial neural networks. We introduced the use of self-organizing maps (SOM) to achieve these goals.

Chapter 4 covers a review of methods for field potentials analysis and their

attributes and limitations, followed by a discussion about empirical mode decomposition (EMD) method, a signal decomposition method, and its advantages over other signal processing methods such as Fourier and wavelet analysis.

Chapter 5 presents discussion about tools for processing and analysis of continuous neural recordings. In this chapter, details of a basic framework will be presented that has been developed by us and uses EMD to extract the informative oscillations from continuous electric and magnetic field potentials. Results from analysis of different datasets are presented.

Chapter 6 presents the improved version of the framework presented in chapter 5. The comparison of the initial and enhanced version and their performance evaluation is given. The last part of the chapter presents results for our suggested approach to use the information carrying oscillations for neural data compression.

A MATLAB based toolbox has been developed, in this research, for extracting informative modes from electric or magnetic field potentials datasets. Chapter 7 covers the documentation and features of this toolbox.

Chapter 8 covers the summary of key results, conclusion and suggestions for future work and possibilities to extend the approaches developed during this research.

1.4 List of Publications

- Z. Mehboob and H. Yin, "Information quantification of empirical mode decomposition and applications to field potentials". *International Journal of Neural Systems 2011*, 21, 49-63.
- Z. Mehboob and H. Yin, "Neural data analysis and reduction using improved framework of information-preserving EMD". *IDEAL 2010*, 360-367.
- Z. Mehboob and H. Yin, "Information preserving empirical mode decomposition for filtering field potentials". *IDEAL 2009*, 226-233.
- Z Mehboob and H. Yin, "Analysis of non-stationary neurobiological signals using empirical mode decomposition." *HAIS 2008*, 714-721.
- H. Yin, S. Panzeri, Z. Mehboob and M.E. Diamond, "Decoding population neuronal responses by topological clustering". *ICANN 2008*, 547-556.

- Z. Mehboob, S. Panzeri, M.E. Diamond and H. Yin, "Topological clustering of synchronous spike train. *IJCNN 2008*, 3889-3894.

Chapter 2

Literature Review

This chapter covers basic information about the anatomy of brain, neurons, neuronal communication and different forms of neural data recordings. A brief description of various methods currently used for neural data analysis is also presented.

2.1 Neurons

Neuroinformatics aims to investigate and understand the communication mechanism and interaction among neurons. Neurons are the basic functional and communication block of the nervous system. They transmit information to each other, nerve cells, muscles or gland cells. These neuronal networks enable the brain to perform complex tasks such as movement, speech, vision and thought processes.

2.1.1 Structure of a Neuron

The basic structure of a neuron resembles other cells of the body but they have additional capability of transmitting information throughout the body. A typical neuron is composed of a cell body called soma, a nucleus, dendrite tree and an axon as depicted in Fig. 2.1. The Myelin sheath is an insulating layer over the axon. Like other cells of the body, neurons have a cell membrane and the nucleus contains genetic information. However, the reproducing rate of neurons is far less than other cells of the body, though new connections among neurons keep changing and developing throughout life. The majority of neurons in the body

receive input on the cell body and dendrite tree, and transmit output via the axon. Neurons of different organisms differ in size, shape and function according to the complexity of their nervous system (Shepherd 1988). Understanding about individual neurons and their interactions is very crucial in order to learn how neurons having different properties are linked and how they can produce simple and complex functions, such as movement, thoughts or memory development.

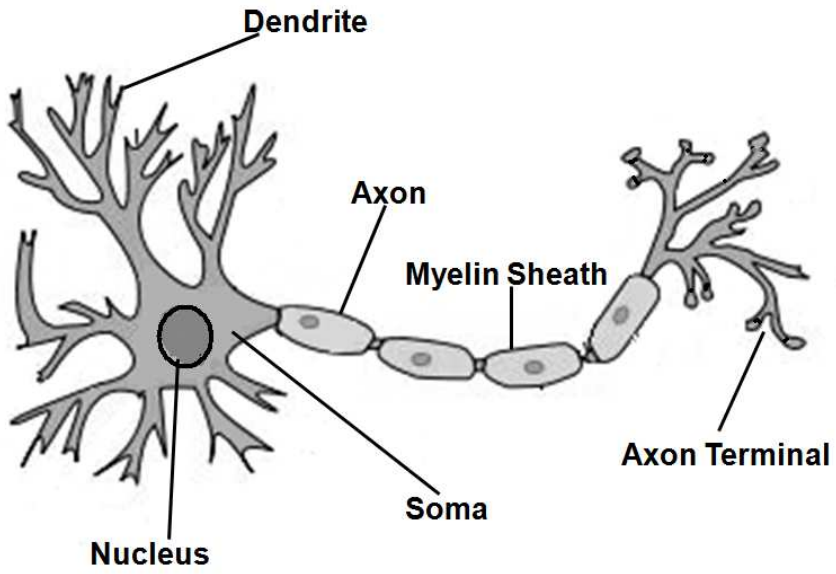

Figure 2.1: Structure of a typical neuron.

Neurons are electrically excitable cells that process and transmit information, in the body, in the form of small electric pulses (100 mV). The communication takes place via chemical and electrical connections between cells called synapses, during a process known as synaptic transmission. The dendrites receive information from sensory receptors or other neurons. This information passes through the cell body and reaches the axon. From the axon, information travels down in the form of an electrical signal known as an action potential (AP).

The chemicals responsible for synaptic connection are called neurotransmitters. More than 100 neurotransmitters have been discovered so far. Medicines and drugs usually affect these neurotransmitters. Synaptic transmission is triggered by the action potentials (Gerstein & Clark 1964).

2.1.2 Types of Neurons

Functionally, neurons are classified as afferent, efferent, and inter-neurons (association neurons) according to the direction in which they transmit impulses relative to the central nervous system (CNS) (Starr & McMillan 2007).

Sensory neurons, or afferent neurons carry impulses from peripheral sense receptors to the CNS. They carry the information from the sensory stimulus like sound, odour, taste, touch etc. and usually have long dendrites and relatively short axons. Motor neurons, or efferent neurons transmit impulses from the CNS to effector organs such as muscles and glands. Motor neurons usually have short dendrites and long axons. Inter-neurons, or association neurons, are located entirely within the CNS in which they form the connecting link between the afferent and efferent neurons. They have short dendrites and may have either a short or long axon (Starr & McMillan 2007).

2.2 Neuronal Communication – Action Potential

The neurons communicate with each other through action potentials (AP). An AP is generated by a wave of depolarization across neuronal membrane (Gerstein & Clark 1964, Shepherd 1988). During transmission of action potentials, a neuron sends information down the axon. Other common terminologies used for AP are spike and impulse. A temporal sequence of spikes is usually called a spike train.

2.2.1 Mechanism of Action Potential

The important ions in the nervous system are Sodium (Na+) and Potassium (K+) and are responsible for generation of action potential. The neuronal cell membrane is semi-permeable that allows passage of some ions and block others. When a neuron does not generate or fire an AP, it is said to be at rest. In the resting state, the inside of the neuron is negatively charged relative to the outside.

At rest, K+ ions can easily pass through the membrane whereas Na+ ions cannot pass easily. Also, there are protein molecules (A-) inside the neuron and they cannot cross the membrane either. In addition to these selective ion channels, there is a pump that uses energy to move three sodium (Na+) ions out of the neuron for every two potassium ions (K+) it gets in. Finally, the “resting

potential" is achieved at -70 mV. At this point, there are relatively more Na+ ions outside the neuron and more K+ ions inside the neuron.

In response to a stimulus, the resting potential drops and when it reaches -55 mV, a neuron fires the AP. This -55 mV acts as a threshold for occurrence of spike. The sodium channels open and Na+ ions rush into the neuron causing depolarization of neuron. The K+ channels open after a while and K+ ions start reversing the depolarization. At this time, Na+ channels start to close. This causes the action potential to go back towards -70 mV (a re-polarization). The action potential actually goes past -70 mV (a hyper polarization state) because the potassium channels stay open a bit longer. Gradually, the ion concentrations go back to resting levels and the cell returns to -70 mV. The whole process is depicted in Fig. 2.2. The three borders in the figure represent threshold level at -55 mV and initiation of an AP, followed by re-polarization and hyper polarization state.

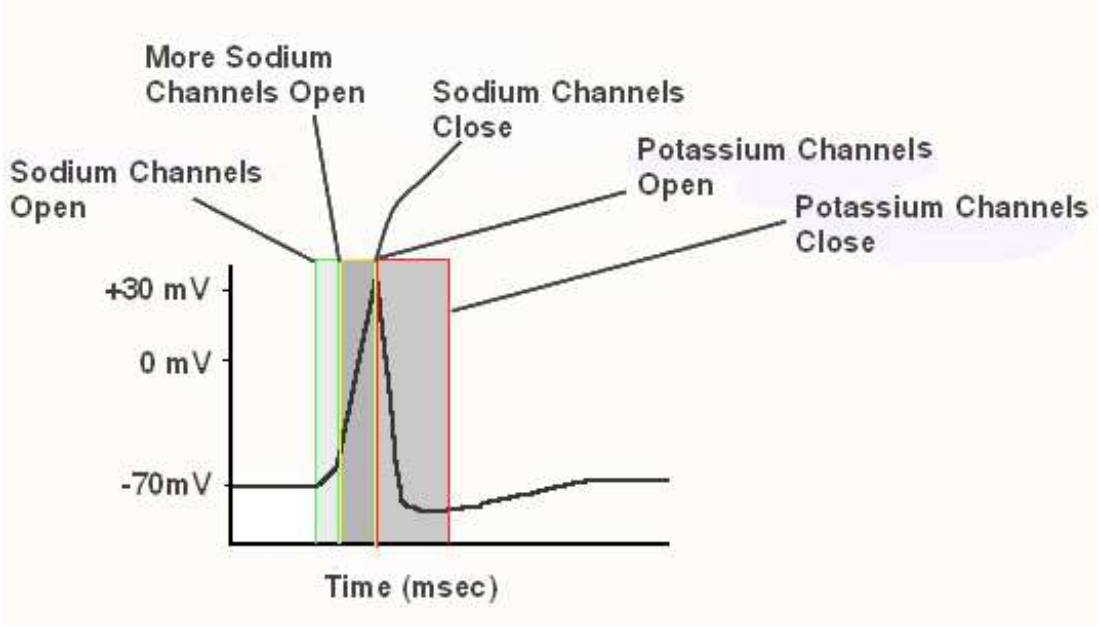

Figure 2.2: Occurrence of an AP.

2.3 Techniques for Neuronal Data Recordings

The activity of the neurons can be measured inside or outside the neurons and experiments can be conducted either in a controlled environment (or on an anaesthetized subject) or in a free environment with a conscious subject. The neurophysiology experiments that are performed in a controlled environment, outside of a living organism, are called in vitro experiments (Kitai et al. 1991). These experiments may lead to results that do not correspond to the real time situations that usually arise in a living organism. The recordings that are made in real time, in conscious subjects/animals are termed in vivo recordings (Humphrey & Schmidt 1991). For these recordings better results are expected to be achieved (Dermietzel & von Bohlen und Halbach 2006).

2.3.1 Intracellular Recording

Intracellular recording involves measuring voltage and/or current across the neuronal cell membrane (Kitai et al. 1991). Different techniques for intracellular recordings are in practice which include:

- **Voltage clamp technique**- measures the ionic current across a cell membrane when the membrane potential is held at a constant. It is used to study the ion channels properties.
- **Current clamp technique**– measures the membrane potential changes when injecting a constant current into a cell through the recording electrode. These are commonly used for measuring the neuronal action potential (spike) and can be used for intracellular and extracellular recordings.
- **Patch clamp technique**- measures voltage or current across ion channels using a micro-pipette.

To make an intracellular recording, the tip of a fine micro-electrode is inserted inside the cell, so that the membrane potential can be measured. In 1963, Hodgkin and Huxley won the Nobel Prize in physiology for explaining the underlying mechanisms in the generation of action potentials (Hodgkin & Huxley 1952, Kitai et al. 1991). They used a voltage clamp technique for intracellular recordings from the giant axon of an Atlantic squid. Today, most micro-electrodes used for intracellular recordings are glass micro-pipettes, with a tip diameter less than

1 μm, and a resistance of several mega ohms (Dermietzel & von Bohlen und Halbach 2006).

2.3.2 Extracellular Recording

Extracellular recording techniques measure the voltage and current changes outside of a cell, from nerve fibers to brain slices (Humphrey & Schmidt 1991). These extracellular recordings include:

- **Single unit recordings** – record the electrical activity of a single neuron with a small tip electrode.
- **Multi-unit recordings** – record electrical activity generated by several neurons.
- **Field potentials (FPs)** – record the field potentials generated from indistinguishable activity generated by many cells.

Extracellular FP recordings help in understanding the structure and function of a neuronal network and how these networks transform sensory information into internal representations to generate behavioural functions (Satoshi et al. 1993, Buzsaki 2004, Dermietzel & von Bohlen und Halbach 2006). The other advantage is that these recordings can be taken from conscious animals and this offers information about the spiking (output) and synaptic activity (input) of neurons in the recorded area.

2.3.2.1 Single Unit Recording

Single unit refers to a single, discharging neuron whose activity can be recorded by a micro-electrode. For extracellular recording, the electrode tip is not inserted into a single cell. Instead, it is left in continuity with the extracellular space. If the electrode tip is small enough, such a configuration may allow indirect observation and recording of the electrical activity of a single cell (Humphrey & Schmidt 1990, Dermietzel & von Bohlen und Halbach 2006).

An electrode tip introduced into a living brain will detect electrical activity generated by the neurons adjacent to it. The micro-electrode, with a tip size of about 1 μm usually detects the activity of at most one neuron. The action potentials recorded are like the action potentials that are recorded intracellularly,

but are much smaller, typically about 0.1 mV (Burns et al. 1974, Humphrey & Schmidt 1990, Dermietzel & von Bohlen und Halbach 2006).

Wire electrodes are commonly used for single unit recordings from small animals like rats. Floating electrodes are often used for larger primates like cats as there is relatively more movement between the brain and skull.

2.3.2.2 Multi-Unit Recording

An extracellular configuration, when positioned precisely, may pick up the activity of several nearby cells simultaneously, which is termed multi-unit recording. In multi-unit recordings, if extracellular micro-electrodes record more than a single cell, then the spike detector has to distinguish the cell that actually fired AP on the basis of measured waveform which requires spike sorting techniques. Spike sorting is the procedure of assigning the recorded action potentials to a neuron. A detailed review of spike sorting techniques is given by (Lewicki 1998, Quiroga 2007). If the electrode tip is slightly larger, then there is also the possibility that the electrode may record the activity generated by even more neurons. Multi-unit recording experiments are often conducted in conscious animals to record brain activity during normal behaviour (Humphrey & Schmidt 1990).

Most of the multi-unit recordings are made with sterotodes or tetrodes. Tetrodes consist of four close-by micro-electrodes that allow the visualization of individual neurons from different positions. Since the amplitude and shape of the spikes depends on the position of the neuron with respect to the electrode, the fact that the neuronal firing is seen from four different sites can improve spike sorting outcomes (Gray et al. 1995). Tetrodes usually offer a better sorting quality since ambiguous results from one channel can be extricated using the information of the other channels.

2.4 Different Forms of Neural Recordings

Neural data are recorded and analysed from different areas of the brain and at various functional levels. Data collection ranges from single neuronal recordings to multiple functional regions of the brain. Here recordings are differentiated on the basis of recording methods that involve surgical (invasive) or non-surgical (non-invasive) procedures. Non-invasive procedures are usually considered safer and carried out on human beings as well as on animals. Invasive methods are

typically conducted on animals to study and understand different phenomena in brain and surgical procedures are only administered on humans in case of serious medical conditions such as tumour or cancer. These are carried out under highly secure and hygienic environment in compliance with national regulatory bodies and institutional guidelines for the care and experimental use of animals law.

2.4.1 Invasive Neural Recordings

2.4.1.1 Spikes Trains

Extracellular recordings of action potentials are often referred to as spike train or spikes. These are high frequency signals compared to other forms of neural recordings like local field potentials (LFPs) and are usually obtained at a cut-off frequency of about 500 Hz. Since these are recordings from single cells, they are also known as single unit activity (SUA). Spikes have a discrete or binary data representation and are treated as instantaneous events (where presence of a spike is presented by 1 and absence by 0). An example of spike train representation is shown in Fig. 2.3.

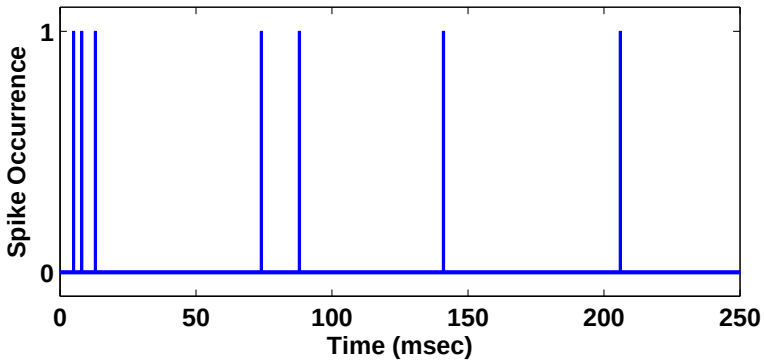

Figure 2.3: A spike train recording.

2.4.1.2 Local Field Potentials (LFPs)

Local field potential (LFP) recordings are commonly used to measure responses of local populations of neurons from a brain region, such as the cortex (Liang et al. 2005, Kreiman et al. 2006, Katzner et al. 2007). An LFP represents the sum of all dendritic synaptic activity within a volume of tissue. These are recorded using

low impedance extracellular micro-electrodes, placed sufficiently far from individual local neurons to prevent any particular cell from dominating the electrophysiological signal. The signals are usually collected at a depth of about 500 μm and then low-pass filtered and cut off around 300 Hz, to obtain the LFP (Legatt et al. 1980, Kreiman et al. 2006, Kraskov et al. 2007). The low impedance and positioning of the electrode allows the activity of a large number of neurons to contribute to the signal. The unfiltered signal reflects the sum of action potentials from cells within approximately 50-350 μm from the tip of the electrode and slower ionic events from within 0.5-3.0 mm from the tip of electrode. The low-pass filter removes the spike component of the signal and passes the LFP (Legatt et al. 1980).

LFPs are believed to represent the synchronised inputs into the observed area, which may contain thousand of neurons (Wang et al. 2008, Berens et al. 2008). The quick fluctuations in LFPs are caused by the short inward and outward currents of the action potential. This means that spike-trains play no part in LFPs (Legatt et al. 1980). A typical LFP recording and its spectral attribute is shown in Fig. 2.4.

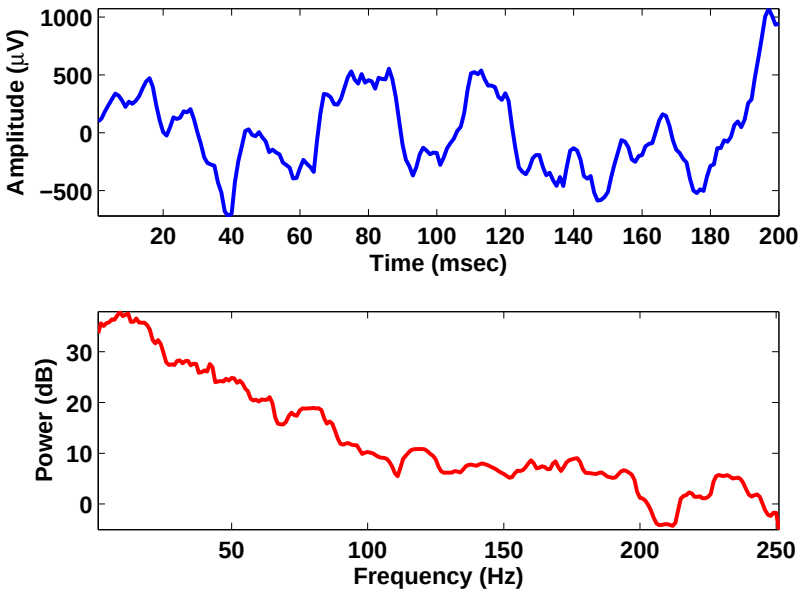

Figure 2.4: An LFP recording from the visual cortex.

LFPs are extensively studied during the past decade, mostly recorded from the visual cortex (Legatt et al. 1980, Kreiman et al. 2006, Katzner et al. 2007,

Wang et al. 2008). Various models of LFP have also been developed (Bedard et al. 2004, 2006). It is believed that different frequency bands of LFP are related to different phenomena and represent different brain activities. The LFP power has also been observed to be effected by stimulus features (Henrie & Shapley 2005, Liang et al. 2005) and the frequency bands also differ in information content. The LFP power spectrum is divided into different bands (Pfurtscheller & Aranibar 1977) as shown in Table 2.1. These frequency bands distribution is based on the electroencephalographic (EEG) signals which are non-invasive neural recordings and are discussed in the following section.

Table 2.1: Frequency bands in LFP (and EEG).

LFP Frequency Bands	Frequency Range (Hz)
Delta (δ)	1-3
Theta (θ)	4-8
Alpha (α)	9-13
Beta (β)	15-25
Low Gamma (γ)	30-50
High Gamma (γ)	75-100

2.4.1.3 Multi-Unit Activity (MUA)

MUA is the superimposed activity of many neurons whose somas are close to a micro-electrode (Stark & Abeles 2007), in a region of about 200 μm of the inserted electrode. As compared to SUA, MUA is recorded easily and is more stable over time. LFP and MUA recorded in vivo are known to convey different information about the underlying neural activity. MUAs are high frequency signals as compared to LFPs and are usually obtained from bandpass filtering the raw recording in the frequency range from 300–500 Hz up to 6 kHz. A MUA recording is shown in Fig. 2.5. Both LFP and MUA signals are considered informative for the BCI (brain computer interface) applications. MUAs are used to learn about the effects of tasks/stimuli across the population of neurons and are highly correlated signals like LFPs.

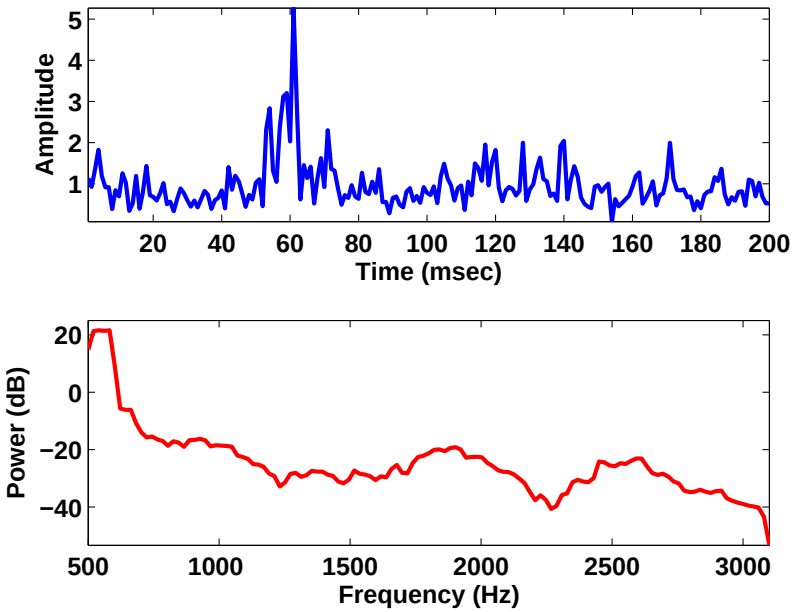

Figure 2.5: A MUA recording.

SUAs are good for learning about the tuning of individual neurons whereas the MUAs are good for understanding about the average response to stimuli across a neuronal population. It has been demonstrated that the MUA–MUA cross correlation is the sum of all SUA–SUA cross correlations between the neurons that contribute to two MUA recordings (Fries 2005, Stark & Abeles 2007).

2.4.1.4 Electrocorticographs (ECoG)

Electrocorticographic (ECoG) recordings are composed of synchronisation of the post-synaptic potentials in cortical pyramidal cells. Pyramidal neurons are a type of neuron found in areas of the brain including cerebral cortex and hippocampus. These are the neurons that were first discovered and studied by the Spanish anatomist Cajal (Carey 1990, Coles & Rugg 1996). ECoG is often referred as surface EEG (electroencephalograms) or surface LFP. However, these are invasive forms of neural recordings obtained from electrodes placement on the exposed surface of the brain. The recordings are usually taken during or after a surgical procedure for treatment of tumour or epilepsy. The temporal resolution of ECoG is 5 msec and a spatial resolution of 1 cm.

2.4.2 Non-Invasive Neural Recordings

2.4.2.1 Electroencephalograms (EEG)

EEG measures the electric potential difference across the scalp. The first EEG recordings were made on dogs in 1912 (Bear et al. 2007). EEG recordings are used in the evaluation of brain disorders, e.g. to show the type and location of the brain activity during a seizure. They are also used to evaluate conditions in coma or tumours, memory related problems or to determine brain death. EEG reflects the gradual change in the membrane potential of large population of neurons (da Silva 1991). EEG recordings are considered as multi-electrode recordings, as these are obtained from several electrodes (upto 50 or more) as shown in Fig. 2.6. These have a good temporal resolution of 10 msec but a poor spatial resolution (2 cm). Event related potentials (ERP) are the segments of EEG data that are locked to an external event and are usually studied to observe synchronisations among single trials (Coles & Rugg 1996). Details about recording procedures and analysis of ERPs can be found in (Picton et al. 1995, Coles & Rugg 1996). In case of ERPs, when similar auditory or visual stimuli are presented several times, averaging across the trials significantly reduces the effect of noise (Picton et al. 1995, Gibbons & Stahl 2007).

2.4.2.2 Functional Magnetic Resonance Imaging (fMRI)

fMRI is a neuro-imaging method that mainly relies on the paramagnetic properties of oxygenated and de-oxygenated haemoglobin and gives images of changing blood flow, in the brain, associated with neural activity. This allows images to be generated that show which brain structures are activated (and how) during performance of different tasks. Therefore, fMRI data can be used to reveal brain structures and processes associated with perception, thought and action (Logothetis et al. 2001). The resolution of fMRI is about 1–3 mm, limited by the spatial spread of the hemodynamic response to neural activity and has a poor temporal resolution (1–5 sec). Moreover, fMRI does not accurately reflect the spiking activity of neurons in a particular brain area but is related to the input coming from other brain structures (Logothetis et al. 2001).

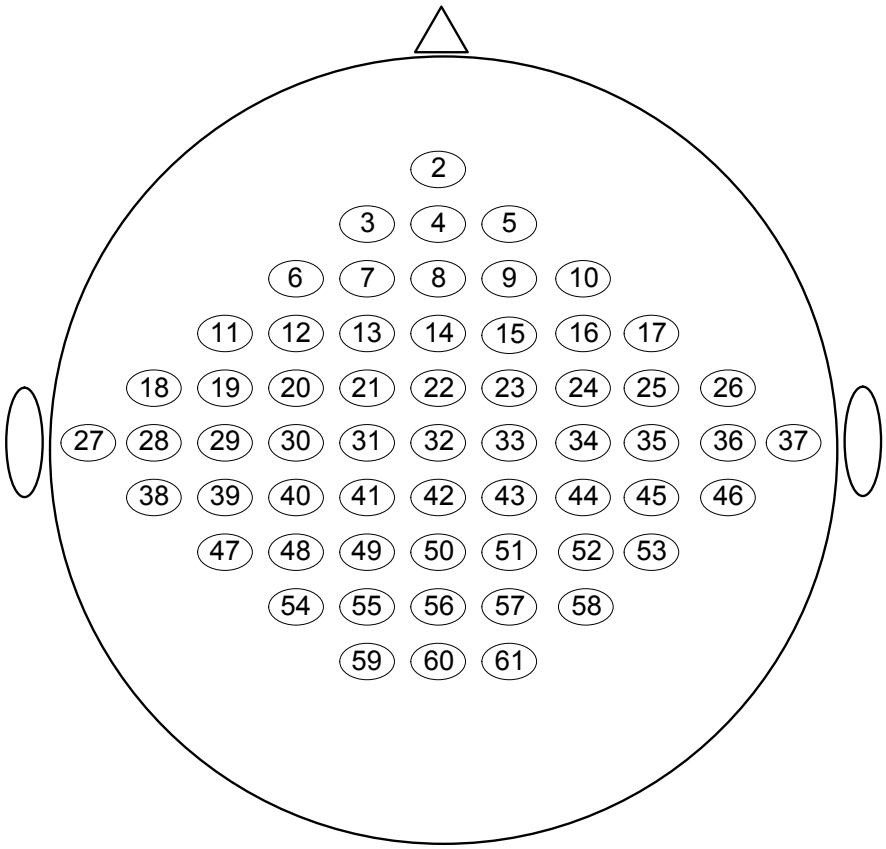

Figure 2.6: Configuration of electrodes placement on scalp during EEG recordings.

2.4.2.3 Magneto-encephalograms (MEG)

Magnetic fields are found whenever there is a current flow, whether it is in wire or in a neuronal network. The magnetic fields pass unaffected through brain tissue and the skull and therefore can be recorded outside the skull. This magnetic field is extremely small, but can be detected by sophisticated sensors. MEG technique is used to measure the magnetic fields generated by neuronal activity of the brain. It is non-invasive and the signals are usually recorded by a multichannel superconducting quantum interface device (SQUID), which is sensitive to magnetic flux. EEG is closely related to MEG as both signals are generated by the same synchronised neural activity (Hämäläinen et al. 1993). The spatial distributions in an MEG are used for localisation of brain activity in different regions and often superimposed on brain images like MRI. This provides information about both the structural and functional properties of the region under study. MEG has a very high temporal (msec) and spatial (mm) resolution as compared to other measures like fMRI (Hämäläinen et al. 1993). An MEG recording is shown in Fig. 2.7.

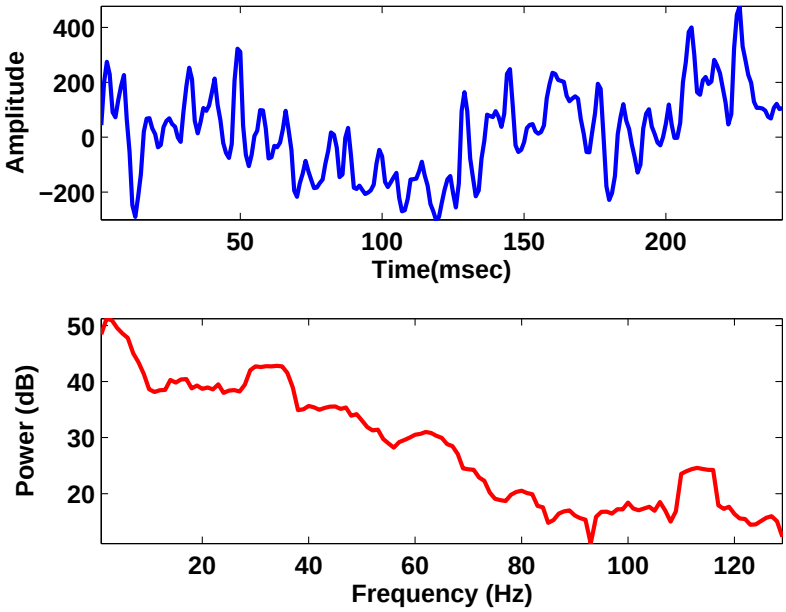

Figure 2.7: An example of MEG recording.

The shortcoming of MEG is the low strength of signals which can be easily

obscured by the noise. This is minimized by using specialized shielding that eliminates the magnetic interference found in a typical clinical environment. Mostly it is used a diagnostic tool for evaluating brain functions when planning surgical applications.

The following section presents different techniques that are in practice for analysing and decoding these different neuronal data formats.

2.5 Neural Code Analysis

The purpose of neural recordings code analysis is to decipher the language of neurons used to encode a stimulus or its features. There are several approaches in practice and are continuously under development and enhancement to aid in the process of understanding neural code mechanism. This section will briefly introduce some of the most commonly used approaches. There are several ways of looking at the problem of neural coding. One way is to find the answers of some of the basic questions such as:

1. Given a neural response, what can we say about the (known/unknown) stimulus?
2. How do neurons in an affinity encode the stimuli?
3. What is the direction of the information flow?
4. Which features of the stimuli/events are being encoded by the neural responses?
5. How to distinguish between two neural responses which are generated by two distinct or perceptually discriminable stimuli?
6. How to differentiate between a healthy and an unhealthy condition?

Given a set of spike train, field potentials or neural images, scientists aim to find answers to the questions listed earlier. A stimulus, in a neurophysiology experiment, can be regarded as a condition or event against which the neural responses are recorded and its occurrence may or may not be explicitly controlled by the investigator (Awiszus 1997).

2.6 Spike Trains Code Analysis

Spike trains are usually encoded by their rate of occurrence or temporal correlations. A spike count code is based on the number of spikes occurring after a stimulus onset, often termed as firing rate. Other temporal codes are based on the occurrence of first spike and inter-spike intervals. Spikes are represented as discrete time events and are considered as point processes (Rieke et al. 1999, Abbot & Dayan 2001) and several methods have been developed for their analysis. The analytical methods for spike train (and field potentials) can be divided into time domain and frequency domain methods, which aim to understand the association amongst the recorded neurons. These methods are briefly discussed in the following section. A detailed discussion about the spike train coding has been given by Rieke et al. (1999).

2.6.1 Spike Rate Codes

One approach to quantify the information conveyed by neuronal spikes is based on firing rate or average firing rate. For spike rate code, a post-stimulus time window is usually defined, in which the number of spikes occurrence are counted in each trial. The mean spike count over a given set of trials is calculated as:

$$Mean\ spike\ count = \frac{Total\ number\ of\ spikes\ per\ trial}{Total\ number\ of\ trials}$$

Spike rate over trials seem to work well for both static and time-varying stimuli. Sometimes the whole recording time period is sub-divided into smaller time windows called bins and mean firing rates are obtained for each bin. This is often termed as spike density. The spike density concept has also been extended for multiple neuronal recordings to analyse the group activity of neurons. All the rate codes are measured in Hz.

Firing rates are sometime calculated as temporal averages. The spike counts are obtained for a small time period and averaged over that time, that is,

$$Mean\ spike\ rate = \frac{Neuronal\ firing\ rate\ for\ time\ period\ (T)}{T}$$

Spikes temporal rate coding is observed in many cases, particularly in sensory or motor systems. In a study of touch receptors in leeches, it was found that the

spike rate was directly proportional to the strength of the touch stimulus (Kandel et al. 2000). Also, a study of rat somatosensory cortex revealed that spike rates were dependent on the kinetic features of the whiskers vibration (Arabzadeh et al. 2004).

Often it is argued that neurons cannot perform temporal averages in such a small amount of time. It is known from behavioural experiments that reaction times are often rather short. For instance, a fly can react to new stimuli and change the direction of flight within 30–40 msec (Rieke et al. 1999). Similarly, human perception also takes place in a very small time period. Visual perception requires only few hundred milliseconds (Thorpe et al. 1996, Oliva 2005). Thus, temporal averages seem to make sense particularly in case of static or slowly changing stimuli which may not require a fast reaction. However, in real time situations stimuli are hardly stationary. Even in viewing a static image, humans perform rapid changes of the direction of gaze called saccade (Thorpe et al. 1996, Oliva 2005). The image projections on the retinal photo receptors therefore change every few hundred milliseconds and this brings the hypothesis regarding other temporal spike codes.

2.6.2 Spikes Temporal Codes

Spikes temporal codes are based on the time of occurrence of spikes after a stimulus onset. This may include the time of occurrence of first spike (first spike latency) or the time of occurrence between two spikes, known as inter spike interval. Several studies have been conducted in which temporal coding was observed (Richmond & Optican 1987, Thorpe et al. 1996, Panzeri et al. 2001). It has also been found that additional information can be obtained by considering the spike timings along with the spike rates. For instance, in a study of rat barrel cortex, it is found that roughly 85% of the information about stimulus location is carried by the first spike time (Panzeri et al. 2001). Temporal codes are based on the assumption that precise spike timings are more important than spike count. In such cases, timing code is expected to provide more information than spike count code.

Temporal coding mainly deals with spike patterns. Large firing rates though increase the richness of spike patterns or the code complexity and vice versa. The information can be calculated using expansion series and the pair wise correlation between spikes. For spike timing codes, the post-stimulus window is usually

broken into the bins of size Δt and the response is taken as a 'binary word' of length $T/\Delta t$ (Panzeri et al. 2001, Panzeri & Schultz 2001, Panzeri et al. 2007). An example of first-spike-time code is shown in Fig. 2.8. The figure shows the first-spike code for a discrete and periodic stimulus. In different areas of brain, the population activation is quite common where one network can excite another. Neuronal spike train can then encode information with respect to the background oscillation.

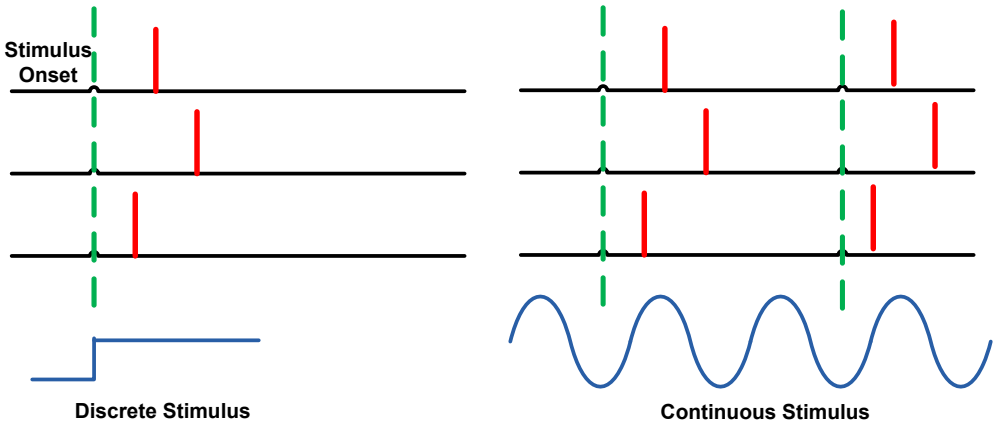

Figure 2.8: First-spike code for a discrete and continuous stimulus.

2.6.3 Spike Correlation and Synchrony

Spike synchrony codes are based on the idea that when interpreting a complex stimulus such as an image or video scene, the neighbouring neurons act synchronously. It has also been observed that precise spatio-temporal pulse patterns represent a meaningful event (Richmond & Optican 1987). Figure 2.9 shows an example where first two neurons are firing synchronously and the last two are non synchronous.

Spike times may or may not be dependent on the firing rates. Two possibilities have been suggested for stimulus encoding by spike patterns.

- Stimulus-dependent correlations.
- Stimulus-independent correlations.

For the stimulus-dependent case, a neuron fires a specific pattern for each distinct stimulus (Abeles et al. 1993). In the second case, the coding is affected

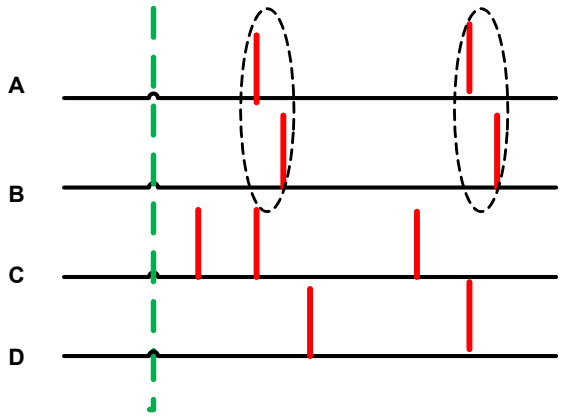

Figure 2.9: An example of spike synchrony. Neurons A and B are synchronous (C and D are not).

by interaction between the relative mean responses in different time bins. This interaction takes the form of correlations across stimuli (signal correlation) and correlations in the variability around the mean response (noise correlation). The general principle is that information decreases when signal and noise correlations have the same sign and increases when they have the opposite sign.

2.7 Methods for Spikes Codes Analysis

Several techniques have been developed for analysis of single and multi-electrode spike train data. The problem with these recordings is that they may or may not be synchronous and may inherit unknown time delays due to neuronal circuitry arrangements in the spatial domain of recording site. For this reason, we need to develop and enhance existing methods that can find hidden, non-linear relationships in data which are not clearly visible otherwise.

2.7.1 Raster plots and Histograms

For multichannel spike recordings, the data is multidimensional. 2D data visualization uses conventional plots. For the visualization of multidimensional spike train data, raster plots are most commonly used. Raster plots can also be used to compare a number of recordings from the same neuron or different neurons. An example of raster plot is shown in Fig. 2.10. It can be noticed that there are two high firing rate periods across all trials before 100 msec.

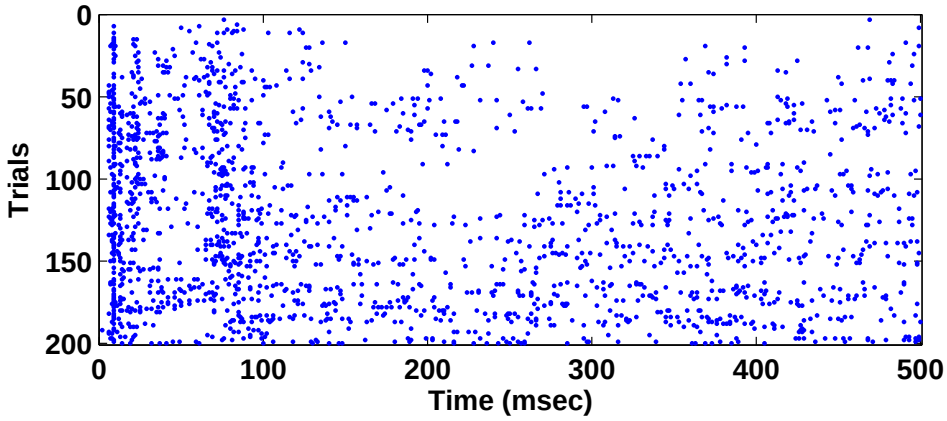

Figure 2.10: An example of a raster plot for a single neuron.

Another most common visualization tool for analysing spike density is a histogram. For the experiments in which spike timing is anticipated to convey information about the stimulus, a simplest approach is to distinguish different stimuli by temporal profiles of their firing rates modulation. Rate modulation coding is present whenever the profile of the PSTH (peri/post stimulus time histogram) differs across stimuli and can in fact carry information even in the absence of total spike count differences; the areas of the PSTHs can be equal but their profiles are different (Panzeri & Schultz 2001, Petersen et al. 2001). An example is shown in Fig. 2.11 with a firing peak right after the stimulus onset and then near 100 msec. The firing rate is significantly reduced after this period.

Another tool used for analysing the firing patterns of multiple neurons is the tunnel method. It is built on information visualization principles which include data overview, zoom, filter and on-demand data details (Walter et al. 2003). All these visualization tools are useful to observe and learn about the firing pattern of the neurons but lack in expressing complex underlying relationships in the datasets. Therefore more intricate and sophisticated tools are required for this purpose.

2.7.2 Cross-Correlogram

Spikes synchronisation between a pair of simultaneously recorded neurons can be easily visualized by a cross-correlogram as shown in Fig. 2.12 (Brown et al. 2004).

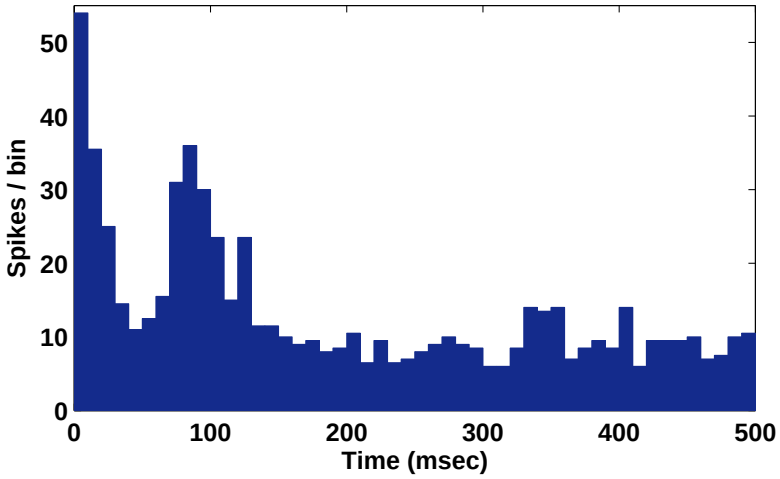

Figure 2.11: An example of a post-stimulus time histogram (bin size=10).

The spike train of one neuron is used as a 'reference' and the other's as a 'target'. The correlation is measured in time bins. Due to the inherent delay in neural circuits, a time frame for correlation must be specified. The correlation window is centred over the first spike of the reference train. The number of target spike train that fall within each bin is calculated. This process is repeated for each subsequent spike in the reference train. The results of individual comparisons are summed up to give the overall correlation. This overall correlation is then plotted as the cross-correlogram. If the cross-correlogram has a significant peak (Brillinger 1979), a correlation exists between the two trains. Cross-intensity function is also a correlation measure which gives a joint probability estimate of firing in two neurons at some time lag.

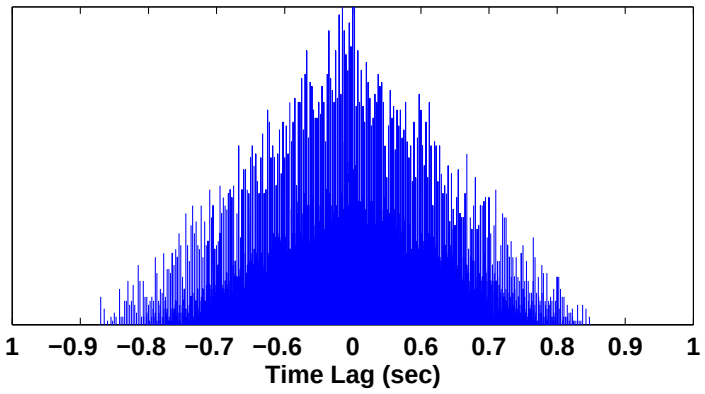

Figure 2.12: An example cross correlogram for a pair of correlated neurons.

2.7.3 Spike Pattern Classification

Clustering is a classical technique of statistical data analysis and is used in many fields for discovering interesting patterns and underlying structures of the data (Jain et al. 1999, Brown et al. 2004). Cluster analysis helps in finding clusters in multidimensional datasets and classifying them on the basis of clustering results (Lewicki 1998). Classification techniques are based on supervised learning algorithms when the class labels are already known and the algorithm assigns a new pattern to one of the predefined classes. A review of different clustering approaches is presented in Chapter 3.

2.8 Methods for Field Potentials Analysis

The analysis of continuous neural data are based on spectrotemporal analysis of neural recordings. Most of the existing signal processing methods are well suited for linear and stationary signals. However the neural signals are continuous, non-linear and non-stationary in nature. A processing method that can address the issues in analysing these signals is required.

2.8.1 Fourier Transform and Short-Time Fourier Transform

The stationary signals are analysed by the Fourier transform (FT). FT performs well on stationary and LTI (linear time invariant) systems but not all signals are time invariant and FT is capable to give only the global picture of the signal under study and lacks temporal information. FT has been used for analysis of spike train (Brown et al. 2004).

The short-time Fourier transform (STFT) is the most widely used method for studying non-stationary signals. The basic idea behind STFT is to break up the signal into small time segments and use FT to determine the existing frequencies in each segment. However, it has limited time or frequency resolution (Addison 2005), due to the Heisenberg uncertainty principle. Thus one cannot obtain both time-localised and frequency-localised information with good resolution.

2.8.2 Wavelet Transform (WT)

Wavelet transform (WT) is also a widely used time–frequency analysis method. It offers variable time resolutions for high and low frequencies. The performance of WT is dependent on the selection of mother wavelet. Each wavelet addresses differently to the time-frequency resolution problem. Examples of wavelets are Gaussian and Morlet (Addison 2005). WT and FT have been used for LFP and EEG analysis but the trade off between time and frequency energy concentrations is unavoidable due to the uncertainty principle. For this reason WT and STFT cannot simultaneously provide both good frequency and time resolution. WT has been used mostly as a de-noising technique in multiple channel analysis. A comparison of Fourier and wavelets analysis for non-stationary signals is presented in Chapter 4.

2.8.3 Principal Component Analysis (PCA)

PCA is a multivariate data analysis technique and was first introduced by Karl Pearson in 1901 (Flury 1988). It is a descriptive and feature/dimension reduction technique that aims at constructing a plane that 'best fits' a set of data points in d–dimensional space. Statistically, PCA transforms d–dimensional set of correlated data points into d pairwise uncorrelated variables called principal components (PCs). PCs are obtained by computing the eigenvectors of the covariance matrix. The first component explains the largest variance in the original dataset and the following components represent the largest amount of remaining variance. Each component is orthogonal to other components. d principal components can be retrieved for a d-dimensional dataset. This feature/dimension reduction is aimed at making data interpretation and analysis easier.

PCA is based on the assumption of global linearity and it operates on the entire feature space so it will generate a linear subspace of the original data even if the underlying structure is inherently nonlinear. PCA has been used for spike train analysis but it works well only when the underlying firing pattern also has a linear relationship (Fotheringhame & Baddeley 1997). PCA has been used for the purpose of classification of spikes at the time of spike sorting and before their storage in the form of binary arrays. This helps in assigning spikes of different shapes to their corresponding neurons in a multi-electrode array experiment (Lewicki 1998).

2.8.4 Independent Component Analysis (ICA)

ICA is an extension of PCA and factor analysis. It is a statistical tool for revealing hidden components in a multivariate dataset. The goal of ICA is to find a linear representation of non-Gaussian data so that the components are statistically independent as much as possible. Such a representation captures the essential structure of the data in many applications, including feature extraction and signal separation. ICA is normally used to separate different sources when, for example, neural signals are recorded by multi-electrodes and the data contain mixtures of distinct sources and has artefacts from background noise and sensor noise.

ICA is only suitable for the case when the number of sources is less or equal to the number of recording channels. It is based on the assumption that sources are mixed linearly, which may or may not be the case in a neuronal network arrangement (Lewicki 1998). ICA has been successfully employed for EEG analysis (Lewicki 1998) and channel separation in optical recordings in sea slug (Lewicki 1998, Brown et al. 1998), for the reason that each neuronal membrane voltage is approximately a temporally independent source (Brown et al. 1998).

An algorithm similar to ICA has been implemented for EEG analysis (Truccolo et al. 2003) to model trial-to-trial variability but it is also based on the assumption of linear mixing model of sources. The difference is that it allows for the sources to vary in specific ways from trial to trial (Truccolo et al. 2003).

2.9 Information Theory for Neural Code Analysis

Information theory is widely used for neural codes and to quantify information carried by neural responses. A common approach to neural coding is to treat the brain as a communication channel, and use information theory to quantify and compare the information about stimuli available in different candidate codes (Shannon 1948, Rieke et al. 1999, Cover & Thomas 1999, Abbot & Dayan 2001).

Information theory serves as a valuable tool for giving insight to neural coding. For instance, whether a particular neuron conveys information by millisecond precision spike timing or simply by the total spike count. The first step of information analysis is to choose the type of neural code. The second step is to compute

how much information can be extracted from the chosen response quantification. This allows assessment of the quality of the candidate neural code.

Neurons exhibit a nonlinear and adaptive behaviour (Rieke et al. 1999, Pereda et al. 2005, Andrade et al. 2008). The brain itself can be treated as a nonlinear and adaptive system, and Shannon's information theory (Shannon 1948) can help in characterising the stimulus-response relationships. During this research, it has been shown that information theory is a strong analytical tool and is applicable to all types and formats of neural data and projects the results on the same scale making them easy to analyse and compare. For this reason, a comprehensive discussion about the concept and evaluation of entropy and information is given next.

2.9.1 Information Entropy

Neural coding and decoding paradigms help in developing a dictionary for neural responses which aim to find relationships between a stimulus space S and a response space R. For instance, a response and stimulus space that consists of r_m responses and s_n stimuli is presented as:

$$R = \{r_1, r_2, r_3, ..., r_m\}$$

and

$$S = \{s_1, s_2, s_3, ..., s_n\}$$

The aim of developing a code book or dictionary is to give answers to questions such as:
What does the observed response r_1 mean when a stimulus s_1 is given?

Formally, the aim is to look for probability $p(r|s)$ (coding) or $p(s|r)$ (decoding) under some assumptions about $(S; P(s))$ or $(R; P(r))$, where $P(s)$ and $P(r)$ is the probability distribution of stimulus and response. For spike train, a popular assumption is that R is a set of integers (number of spikes per unit time), and $P(r)$ is Poisson (Rieke et al. 1999).

The next step after recording of responses is to assign a number (the information) that quantifies how well different responses discriminate between different stimuli. The first step in measuring information is thus to measure the response

variability. The most general way to do so is through information entropy (Shannon 1948). The response entropy quantifies the response variability across all possible stimuli and trials:

$$H(R) = -\sum_{i=1}^{m} P(r_i) \log_2 P(r_i) \tag{2.1}$$

where $P(r_i)$ is the probability of observing a response r_i across all trials to any stimulus, which is calculated as:

$$P(r_i) = \frac{Number\ of\ occurrences\ of\ r_i}{Total\ number\ of\ responses}$$

However, as mentioned earlier, neurons are typically non-linear (or noisy), in the sense that their responses to repetitions of an identical stimulus differ from trial to trial. This reflects variation of responses to a stimulus and also variation due to trial-to-trial noise. Thus $H(R)$ is not a pure measure of the stimulus information actually transmitted by the neuron. One can quantify the variability specifically due to noise by measuring the entropy of a fixed stimulus (that is, conditional on s):

$$H(R|S) = -\sum_{r,s} P(s)P(r|s) \log_2 P(r|s) \tag{2.2}$$

$H(R|S)$ is the conditional entropy and $P(r|s)$ is the conditional probability of observing response r given presentation of a stimulus s.

2.9.1.1 Example

Suppose in a neurophysiology experiment, stimuli from a stimulus set $S = \{1, 2, 3\}$ are chosen randomly, which result in a response space having 5 responses with $R = \{0, 1, 2, 3, 4\}$. $R = 0$ means that there is no spike in the given trial and $R = 1$ means that there is one spike (response) in a given trial Tr and so on. Each stimulus is presented 4 times, giving $Tr = \{1, 2, 3, 4\}$. We can arrange the data in a matrix whose elements are given in Table 2.2.

The entropy $H(R)$ is calculated by finding the probability of each response.

$$H(R) = H(r_0) + H(r_1) + H(r_2) + H(r_3) + H(r_4) \tag{2.3}$$

Table 2.2: An example data for illustration of information theory.

Tr	S=1	S=2	S=3
1	0	1	0
2	2	1	1
3	1	1	4
4	1	3	2

where $H(r_i) = -P(r_i) \times \log_2 P(r_i)$;

$$P(r_i) = \frac{Number\ of\ times\ r_i\ occurred}{Total\ number\ of\ trials\ (nTr)}$$

Here nTr=12 and $P(r_0)$ =2/12=0.166.

Similarly, $P(r_1)$= 6/12=0.5 and $P(r_2)$= 2/12=0.166.

$P(r_3)$=1/12= 0.0833; $P(r_4)$=1/12=0.0833.

Thus computing the entropy of R using Eq. 2.1 and Eq. 2.3 gives $H(R)$=1.96.

Now the conditional probabilities for all the responses, $H(R|S)$, is calculated by using Eq. 2.2:

$$H(R|S) = \sum_{j=1}^{3}[H(r_0|s_j) + H(r_1|s_j) + H(r_2|s_j) + H(r_3|s_j) + H(r_4|s_j)]$$

where $P(s_j) = 1/3$.

Table 2.3: Table showing conditional probability values for the given example.

R	$P(R\|s_1)$	$P(R\|s_2)$	$P(R\|s_3)$
r_0	1/4	0	1/4
r_1	2/4	3/4	1/4
r_2	1/4	0	1/4
r_3	0	1/4	0
r_4	0	0	1/4

Using Table 2.3, gives:

$$H(r_0|s_1) = -P(s_1)P(r_0|s_1)\log_2 P(r_0|s_1) = -(1/3)(0.25)\log_2(0.25) = 0.1667.$$

Similarly, $H(r_1|s_1) = -P(s_1)P(r_1|s_1)\log_2 P(r_1|s_1)$ and so on.
This gives,

$$H(R|S) = 1.44$$

2.9.2 Mutual Information (MI)

The information that the neuronal response encodes about the stimulus is the difference between the response entropy and the noise entropy and this is known as the mutual information (MI) between stimuli and responses, or simply information, given as:

$$I(S;R) = H(R) - H(R|S) = \sum_{r,s} P(s)P(r|s)\log_2 \frac{P(r|s)}{P(r)} \tag{2.4}$$

For the previous example $I(S;R)$=1.96-1.44=0.52 bits.

Thus, $I(S;R)$ quantifies how much of the information capacity provided by stimulus-evoked differences in neural activity is robust to noise. When base-two logarithm is used, MI is expressed in units of bits. 1 bit of information means that, on average, observation of the neuronal response on one trial reduces the observer's stimulus uncertainty by a factor of two. MI is zero only when the stimulus-response relationship is completely random. Application and results of MI analysis on real spike train recordings and field potentials datasets are described in Chapters 3 and 4.

Chapter 3

Spike Train Analysis

This chapter presents techniques and algorithms which have been developed during the course of this research, for decoding population activity of neurons recorded in the form of neural spike train. A general discussion on the most commonly used methods for analysing spike train is also given.

As mentioned in Chapter 2, spike train are discrete-time signals and multichannel spike data are treated as multivariate point processes (Brown et al. 2004, Abbot & Dayan 2001). Analysis of single neuronal activity is less informative than multichannel recordings. Multichannel spike recordings can give insight into the working mechanism of neuronal population for coding complex stimuli or cognitive behaviour (MacLeod et al. 1998, Nicolelis 1999). These recordings capture the activities of nearby neurons of the recording site as opposed to single neuronal recordings and give an opportunity to gain information about neuronal interactions and information processing.

3.1 Previous Work

Spike train recordings obtained from multiple channels constitute of high dimensional data and the experiments are often repeated several times for multiple stimuli. For these types of datasets, different supervised and unsupervised learning algorithms can be employed for finding underlying patterns and relationships. For example, principal component analysis (PCA) is usually used as a dimension reduction technique by retaining only the eigenvectors with maximal variance. It has also been used as a preprocessing tool for variance based sorting of multidimensional datasets and utilising the corresponding principal components (PCs)

for further investigation (Yeung & Ruzzo 2001). This approach has been used for clustering gene expression data. However, it was shown that this does not offer a significant advantage in terms of cluster formation (Yeung & Ruzzo 2001) because initial PCs failed to capture the clusters' structure.

Clustering methods are suitable for analysing large data sets (Jain et al. 1999). They divide data into different subgroups by using suitable matching criteria. Many clustering algorithms are in use, each offering its distinct advantages. Clustering algorithms are a form of unsupervised learning algorithm which aim to find a suitable representation of each class in a given unlabelled data set. In contrast, classification algorithms are based on supervised learning. Classification algorithms learn from a predefined set of classes to classify unlabelled data. Most of the clustering and classification for spike train data has been carried out for the purpose of spike detection (Lewicki 1998) or classifying spikes based on their shapes (Ent et al. 2003). This is prior to the storage of spike train as binary arrays. For spikes decoding analysis these spike bit-arrays (or spike point process data) are used. Little work has been carried out for point process classification of binary spike data.

One of the most commonly and widely used supervised classification algorithm is the K nearest neighbour (k-NN) classifier which is often used for pattern classification. For k-NN, the number of classes has to be pre-specified. Then the classification is based on proximity using a chosen distance measure between two patterns. Often Euclidean distance is used (Jain et al. 1999). The performance of k-NN is entirely based on the distance measure alone, which makes it less flexible as compare to other classification algorithms. A variation of K-means algorithm is fuzzy K-means. It also works on datasets which can be represented in d-dimensional vector space, and requires a distance measure and initialisation of k clusters at the beginning. The fuzzy K-means algorithm (Bezdek 1981, Hoppner et al. 1999) assigns to a data point a probability of belonging to each one of the K classes, instead of a unique membership label. It has also been used for spike patterns classification (Fellous et al. 2004). In this study, Gaussian smoothed spike train were used for the classification purpose and their results showed that fuzzy K-means performs better than the standard K-means algorithm.

Neural network–based clustering algorithms are an adaptive form of unsupervised learning algorithm and are more suitable for clustering spike train data when the prior information of the classes is not available. They learn patterns

from a given data set and generate clusters based on their learning.

We have shown that a self-organizing map (SOM) based clustering can offer distinct advantage for the analysis of multiple spike train data over other clustering techniques (Yin, Panzeri, Mehboob & Diamond 2008). The SOM is an unsupervised neural network based clustering algorithm (Kohonen 1997). It was suggested that the application of the SOM to spike train, interpreted as continuous functions, could yield good clustering results and help in understanding the population stimulus coding in a neuronal population (Yin, Mehboob, Panzeri & Diamond 2008). For this study, an appropriate spike distance measure was used for clustering purpose (Yin, Panzeri, Mehboob & Diamond 2008). The description of multiple spike train dataset is given which was used for the SOM training. Also , the SOM algorithm, experiments details and discussion of the obtained results are presented.

3.2 Description of Spike Trains Dataset

A dataset of multichannel spike train recorded from rat barrel cortex was used in this experiment. Further details of the experiment can be found in (Petersen et al. 2001, Arabzadeh et al. 2003, 2004). The barrel cortex is a region in somatosensory cortex in some rodents which is sensitive to inputs generated during whiskers' movements (Swadlow 1989). A 10×10 grid of 1.5 mm long electrodes with 400 μm tip-to-tip spacing was placed into the vibrissa region of the left somatosensory cortex. The waveforms emitted by a multi-unit neural cluster of about 3–4 neurons at each channel (Rousche et al. 1999) were selected offline using the software Cyberkinetics. Sinusoidal frequency and amplitude values in each trial were selected from one of the following seven values:

amplitude (A)={8, 12, 21, 33, 54, 87, and 140 μm}.
frequency (f)={19, 30, 50, 81, 131, 211, and 341 Hz}

The first stimulus was a combination of $\{A1, f1\} = \{8, 19\}$, the second stimulus was $\{A2, f1\} = \{12, 19\}$ and so on, with the last (49^{th}) stimulus having highest value of A and f, $\{A7, f7\} = \{140, 341\}$.

The resulting 49 different amplitude–frequency combinations, shown in Fig. 3.1,

were presented in pseudo-random order 200 times per stimulus. A three dimensional plot for Fig. 3.1 is shown in Fig. 3.2. Spike count variability can be seen more clearly in this figure, with stimulus $\{A7, f7\}$ having the highest spike count. The stimuli vibration duration was 500 msec with a 1 sec interval between consecutive vibrations. After delivery of the full stimulus set, all whiskers were cut 3 mm from their base and stimulated individually by a piezoelectric wafer with 1 Hz square pulses for 1 min. Neuronal clusters that gave statistically significant responses and had a clear principal whisker were selected for analysis of responses to vibration stimuli; there were 24, 16, 37, 35, and 18 acceptable electrodes in 5 experiments, respectively. The dataset which we used for analysis was from the first experiment and comprised 24 channels recordings each of 100 msec time length.

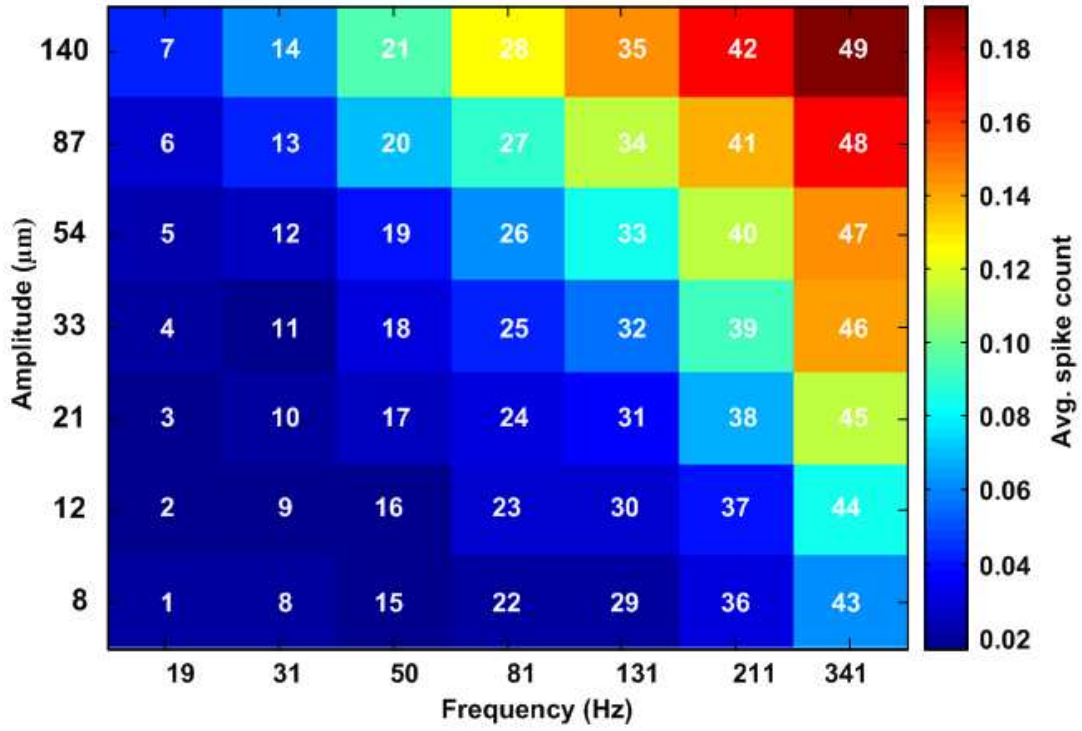

Figure 3.1: Stimulus set information for barrel cortex spike train recordings. The figure shows the combination of seven frequencies and seven amplitudes which yield a set of 49 sinusoidal whisker vibrations. Average spike count for each stimulus is shown by the color map. Average is taken across all trials and channels.

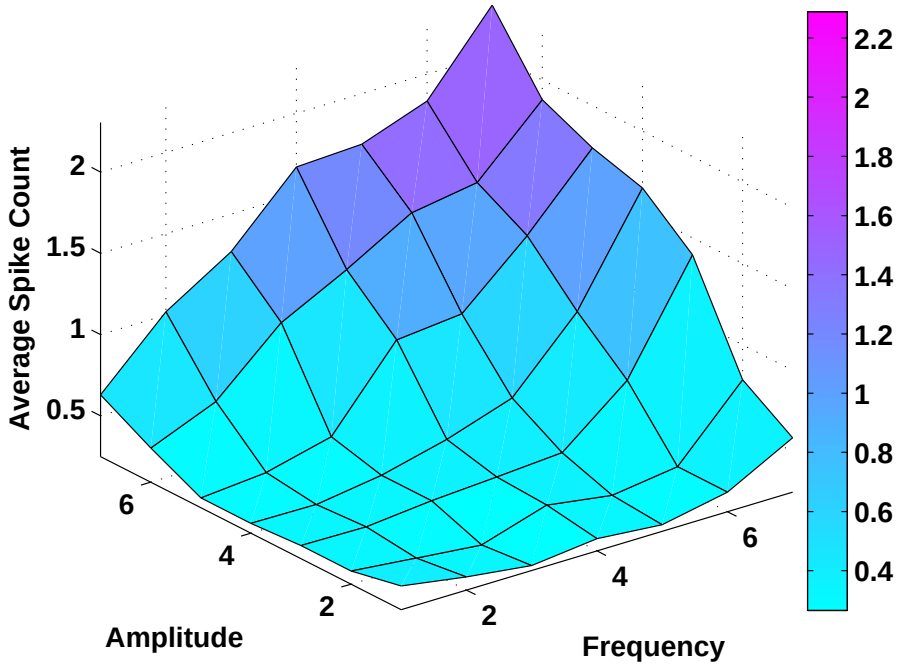

Figure 3.2: Arrangement of 49 stimuli. Colour mapping shows spike count variation across 200 trials in 24 channels.

3.2.1 Information Quantification of Spike Train Data

In this study (Arabzadeh et al. 2003, 2004), the spike count and temporal code were used for information analysis and stimulus coding. Then the first step towards neural decoding analysis of the given dataset, is to compute the mutual information (MI) based on spike count. To find about the information coding mechanism, stimuli were arranged into four different groups based on their amplitude (A) and frequency (f) values, with first group based on stimuli f values, second group on A values, third group based on product of amplitude and frequency, $A \times f$ or simply (Af) values, and fourth group according to A/f values, respectively (Table 3.1). Information quantification was then carried out for each group and it was expected that one group with maximum information would be the group which explained the neural coding mechanism of barrel cortex neurons.

Mutual information was first calculated for the dataset without any grouping and for above sets of stimulus grouping. The upper bound of information that could be transmitted by the neuronal responses is defined by the stimulus entropy (Cover & Thomas 1999). The information analysis of these different groups helps

Table 3.1: Four different approaches for stimulus grouping based on stimulus amplitude (A) and frequency (f) values.

Frequency Group (f)	Amplitude Group (A)
$f\{1\}$=[1 2 3 4 5 6 7]	$A\{1\}$=[1 8 15 22 29 36 43]
$f\{2\}$=[8 9 10 11 12 13 14]	$A\{2\}$=[2 9 16 23 30 37 44]
$f\{3\}$=[15 16 17 18 19 20 21]	$A\{3\}$=[3 10 17 24 31 38 45]
$f\{4\}$=[22 23 24 25 26 27 28]	$A\{4\}$=[4 11 18 25 32 39 46]
$f\{5\}$=[29 30 31 32 33 34 35]	$A\{5\}$=[5 12 19 26 33 40 47]
$f\{6\}$=[36 37 38 39 40 41 42]	$A\{6\}$=[6 13 20 27 34 41 48]
$f\{7\}$=[43 44 45 46 47 48 49]	$A\{7\}$=[7 14 21 28 35 42 49]
Energy Group ($A \times f$)or (Af)	Orthogonal Group (A/f)
$Af\{1\}$=[1]	$A/f\{1\}$=[7]
$Af\{2\}$=[2 8]	$A/f\{2\}$=[6 14]
$Af\{3\}$=[3 9 15]	$A/f\{3\}$=[5 13 21]
$Af\{4\}$=[4 10 16 22]	$A/f\{4\}$=[4 12 20 28]
$Af\{5\}$=[5 11 17 23 29]	$A/f\{5\}$=[3 11 19 27 35]
$Af\{6\}$=[6 12 18 24 30 36]	$A/f\{6\}$=[2 10 18 26 34 42]
$Af\{7\}$=[7 13 19 25 31 37 43]	$A/f\{7\}$=[1 9 17 25 33 41 49]
$Af\{8\}$=[14 20 26 32 38 44]	$A/f\{8\}$=[8 16 24 32 40 48]
$Af\{9\}$=[21 27 33 39 45]	$A/f\{9\}$=[15 23 31 39 47]
$Af\{10\}$=[28 34 40 46]	$A/f\{10\}$=[22 30 38 46]
$Af\{11\}$=[35 41 47]	$A/f\{11\}$=[29 37 45]
$Af\{12\}$=[42 48]	$A/f\{12\}$=[36 44]
$Af\{13\}$=[49]	$A/f\{13\}$=[43]

in understanding how stimuli features are encoded by the neurons. For example, in the first group of Table 3.1, the stimuli are arranged according to their increasing order of frequency (f) values. If the information obtained for this group is higher than all other groups and approximately equals to non-grouping information then this shows that whiskers' movements are encoded based on their frequency attributes. Similarly, in third group, the stimuli are arranged based on increasing values of product of A and f, $(A \times f)$. The information for each group was computed using Eq.3.1.

$$MI(G;R) = \left\langle \sum_{r} P(r|G) \log_2 \frac{P(r|G)}{P(r)} \right\rangle_G \tag{3.1}$$

where $P(r|G)$ is the conditional probability of observing a neuronal response r given a stimulus (s) from a group (G) in Table 3.1. $P(r)$ is the marginal probability of response r, i.e. the average of $P(r|G)$ across all stimuli; and $\langle ... \rangle$ denotes the average over all stimuli because all the stimuli were set equi-probable. A weighted average should be used in case stimuli having different probabilities.

The results obtained were identical to those reported in (Arabzadeh et al. 2003). For 100 msec post stimulus recording, maximum information is transferred in the first 10–30 msec time (Fig. 3.3). The top plot is for the MI obtained without any grouping, followed by the MI obtained from Af, f, A and A/f grouping with MI-Af grouping closest to MI with no grouping, this shows that barrel neurons encode the kinetic features $(A \times f)$ of whisker vibrations.

The spike count for each stimulus across all channels is given in Fig. 3.4 and in the colormap of Fig. 3.2. In general, the spike count increases with the stimulus number, for example, for stimulus 1–7; then 8–14 and then for 43–49, with 49 having the largest value of $A \times f$ and highest spike rate. This spike count was used in calculation of $P(r)$ and $P(r|s)$.

By reducing the stimulus set from 49 unique stimuli to 13 Af-grouped stimuli reduces the entropy but this compression does not significantly reduce the information content present in neuronal spike counts as can be seen in Fig. 3.3. The information peak for all the plots is at 30 msec. Without any grouping, at 30 msec, MI is 0.2052 bits and with Af grouping it is 0.1885 bits. At this point, the combined information of f-group and A-group is (0.08442+0.07859) 0.163 bits which is about 15% less than the (Af) information at this point (0.1885 bits). This implies that neurons do not encode A and f independently. Thus, it was

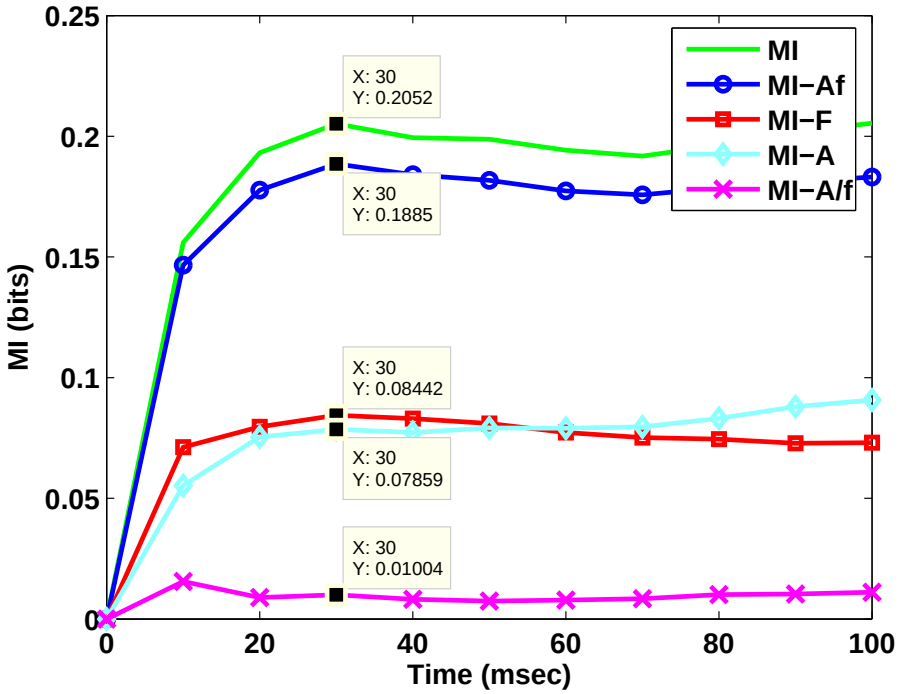

Figure 3.3: Information analysis of all groups of Table 3.1 during 100 msec. Cumulative MI is calculated across all (24) channels.

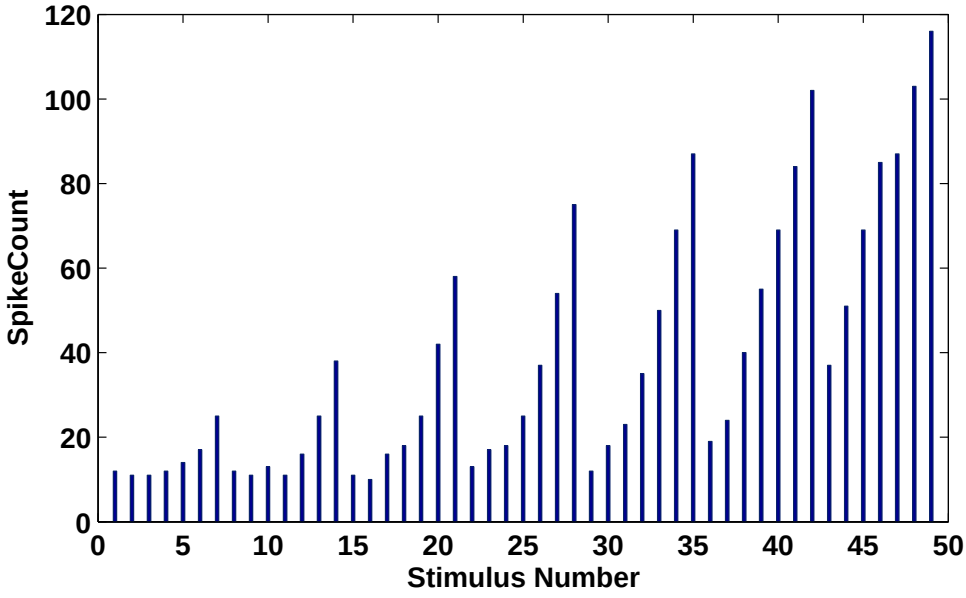

Figure 3.4: Spike count variation in the dataset.

clear that A and f have been encoded jointly and not separately. These results showed stimulus joint feature encoding and confirm that A and f are being encoded in the form of $A \times f$ (Arabzadeh et al. 2004) and not as A/f, since A/f information level is the lowest in all groups. In the next section we show that the SOM is capable of producing topology preserving clusters for this dataset. This would confirm that the SOM is able to find the underlying patterns among the multiple synchronous spike train even if the hypothesis about stimulus coding is not known prior to the SOM application.

3.3 Spike Trains Analysis Using Self-Organizing Map

3.3.1 Self-Organizing Map (SOM)

The self-organizing map is an array of nodes (or neurons), arranged in a single or multi-dimensional grid. The SOM algorithm is inspired by the working mechanism of neurons in the cortex (Yin 2002). In the beginning, the SOM nodes are initialised by small random numbers. Later, its nodes are trained in an orderly fashion, by presenting input patterns from the given data set. The node closest to given input pattern is selected as a winner; and the winner and its neighbours are updated by learning from the given input pattern, subsequently approximating the input patterns distribution. After the end of training period, similar patterns cluster together with each node representing a class pattern for input dataset.

The SOM algorithm offers an adaptive, competitive and unsupervised learning paradigm (Kohonen 1997) and is efficient in handling large datasets even in the presence of noise (Kohonen 1997, Tamayo et al. 1999). It is capable of giving simplified relational view of high dimensional, complex datasets and has also been successfully employed to different biological datasets (Mangiameli et al. 1996, Tamayo et al. 1999).

The nodes of the SOM are usually arranged on a one (or two) dimensional grid (Fig. 3.5). Each node has a W-dimensional weight vector and is connected to adjacent nodes according to the topology of the SOM. The size of W is the same as that of input patters so that they can be compared by a matching criterion.

The SOM is used to find similarity between spike train which are randomly presented in each trial. Before applying the SOM or any clustering algorithms, a

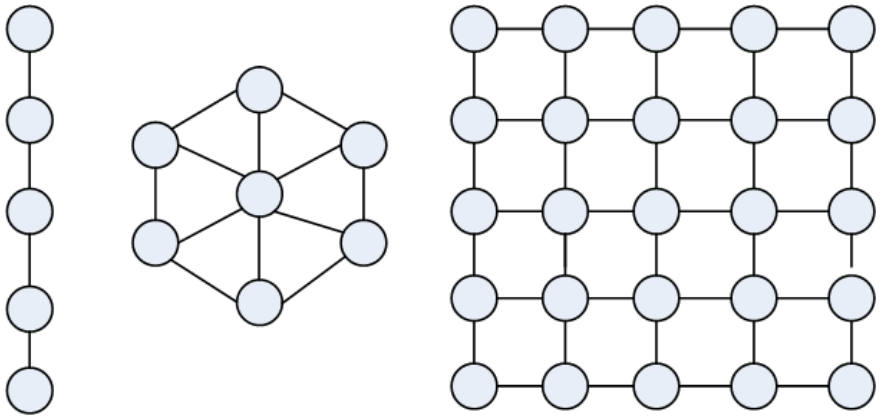

Figure 3.5: Different topologies of self-organizing map. Nodes are represented by circles and neighbourhood by lines.

similarity measure has to be defined to differentiate (spike train) input patterns. There are several distance measures for spike train such as using Euclidean distance and Gaussian kernel on spikes (Victor 2006). We proposed to use a decaying exponential kernel on the data so spike bit-arrays occupy a range of values; this developed correlations between the spikes (Van Rossum M. C. W. 2001) and gave more appropriate interpretation for spikes. The SOM algorithm for a 1-dimensional grid is presented in Table 3.2.

After the completion of training, similar nodes will be grouped together representing the main clusters in the given dataset. As mentioned in Chapter 2, one of the challenges in neuroscience is to distinguish among neural responses based on different stimuli. Cluster analysis can provide solution to this problem and can be used for analysing spike train and classifying responses, thus helping in summarizing and giving an abstract view point for data. The data in each class ideally have some common traits and often the similarity is based on a distance measure.

In this study, we suggested two types of kernel functions for interpretation of spike train and tested the performance of the SOM on these kernel-smoothed spikes. The kernel functions are:

- Gaussian kernel.
- Decaying exponential kernel.

Table 3.2: Algorithm for a 1D SOM.

1. Select number of nodes (N_d) in the SOM.

2. Initialize the weights of nodes, $\{W_1, W_2, W_3....W_{nd}\}$, to small random numbers. Vector W_1 is the weight of node 1 and so on. All weight vectors are of the same dimension as the input vector from the given dataset.

3. Initialize the learning rate (α), usually set to 0.7 or lower and the neighbourhood function (λ) equal to N_d.

4. Set a value for the total learning time (LT). This is usually set to a value roughly equal to about 5 to 10 times the number of samples in dataset to ensure that every sample has been presented a few times to the SOM and nodes have learnt about each pattern in the dataset. The learning rate and neighbourhood size should reduce slowly until the SOM completes its learning period. Set t=1.

5. At iteration t, randomly select an input spike train ($St(t)$) from the given dataset and present it to the SOM nodes.

6. Calculate the distance between the input vector and the weight vectors:

$Dist(t) = \sqrt{\sum(St(t) - W_i)^2}, i = \{1, 2, ..., N_d\}$.

7. Select a winner node, closest to the input vector.

8. Update the the winner node and weights of its neighbouring nodes as follows:

$W_i(t+1) = W_i(t) \ + \ \alpha(t) \, \lambda \, [St(t) - W_i(t)]$.
where $\alpha(t) = a/(a+t)$ and $\lambda = exp\left(-\frac{(i-u)^2}{2\sigma^2}\right)$.
a is chosen so that with each iteration the learning rate α reduces slowly from its initial value (0.7 or lower) and by the end of training period drops below 0.1 and σ is usually set between 1 and 3. i and u represent nodes in a neighbourhood.

9. $t = t + 1$, if $t < LT$ and the learning rate is above 0.1 then go to step 5, stop otherwise.

3.3.1.1 Spike Convolution with Gaussian Kernel

The clustering of spike train used to rely on binning (MacLeod et al. 1998) but a small bin size such as 1 msec is not very effective when measuring the synchronous neural activity since it is too small to capture any synchronisation. The spike train are usually stored in the form of binary arrays (bit-arrays) with 1 msec precision. A typical spike train is shown in Fig. 3.6.

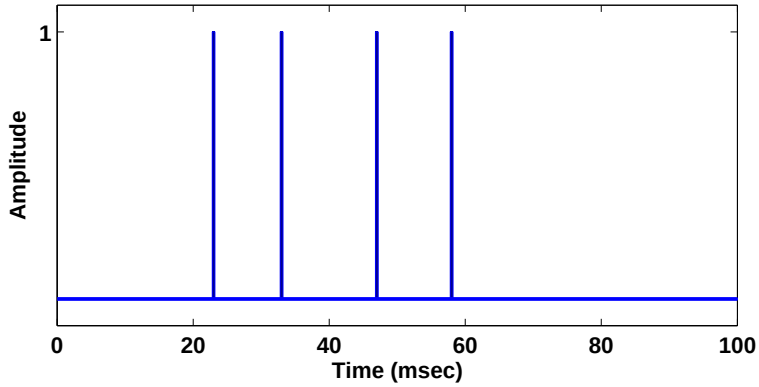

Figure 3.6: Bit-array representation of a spike train.

To convert a discrete spike train into continous functions with large bins, we first convolved spikes using a Gaussian kernel. By using kernel interpretation, each spike spreads over a range of values and this helped in capturing synchronisations. One can convolve a spike train with a Gaussian kernel by using Eq. 3.2.

$$f(t) = \sum_{k=1}^{spk} e^{-(t-t_k)^2/2\sigma^2} \tag{3.2}$$

where spk is the total spike count, k is the k-th spike at time t_k and σ is the width of the Gaussian kernel with value 0.9192. The width of Gaussian kernel was chosen so that the amplitude of the spike may vary but the spike count can be preserved by the area (spread) of the Gaussian spike. The resulting spike train of Fig. 3.6 is shown in Fig. 3.7.

3.3.1.2 Spikes Convolution with Decaying Exponential Kernel

We also used a decaying exponential kernel for spike train convolution and in order to analyse similarity among the spike train (Van Rossum M. C. W. 2001). The decaying kernel seems to be a natural choice for interpretation of binary

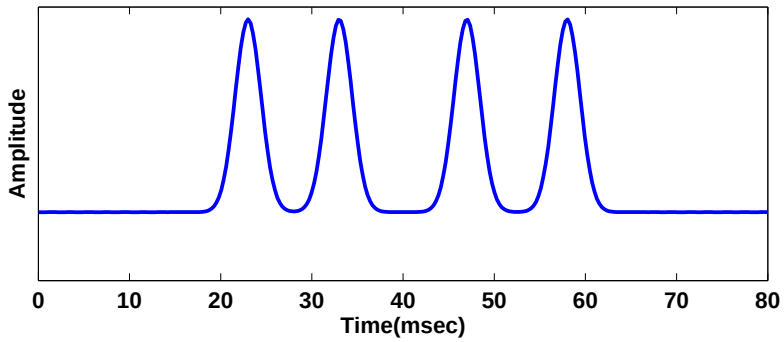

Figure 3.7: Spike train convolution with Gaussian kernel.

spikes into continuous functions, for the reason that it is more similar to the neuronal firing pattern or action potential (Fig. 2.2).

Van Rossum suggested a novel distance measure between two point processes which can be used for binary spike train (Van Rossum M. C. W. 2001). The Lempel-Ziv (LZ) measure was later suggested which was based on distinct parsing of bit-arrays and was used for clustering spike bit-arrays of similar patterns (Christen et al. 2004). It offers the advantage of comparing different spike train from one neuron and its firing pattern. However the classification results may not necessarily consider synchronisation in spike patterns (Christen et al. 2004). Victor proposed a spike distance measure based on the total 'cost' of transforming one spike into another via any insertion, deletion or time shift of spikes (Victor 2006). This is a complex method and not suitable for the purpose of clustering large datasets (Victor 2006). In comparison, Rossum's distance is computationally simpler.

A decaying exponential smoothed spike train can be expressed by the Eq. 3.3.

$$f(t) = \sum_{k=1}^{spk} e^{-(t-t_k)/\tau}\, \mu(t - t_k) \tag{3.3}$$

where *spk* is the total number of spikes in the spike train, k denotes the k-th spike and t_k its time, τ is the decaying constant with value 1.4437. The advantage of using this value is that this does not change the total spike count value. $\mu(.)$ is the unit step function. The window size (w) for spike convolution can be from 5–10 msec (Van Rossum M. C. W. 2001). Here, w=10. The resulting spike train

is shown in Fig. 3.8.

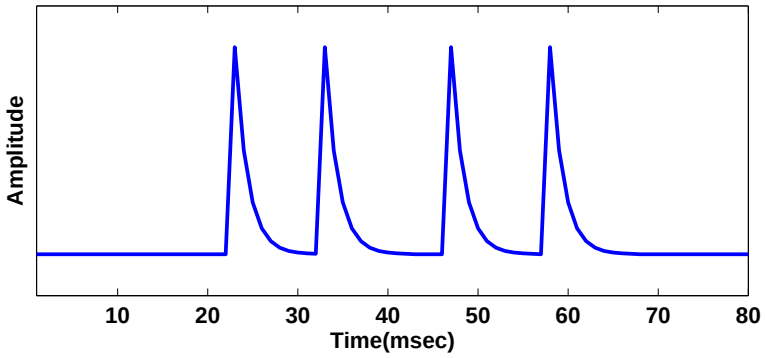

Figure 3.8: Discrete spike train convolved with decaying exponential kernel.

The spike convolution with a kernel gives a continuous interpretation of spike train in the form of an extended discrete function. We refer to a spike train as a decaying spike if a decaying exponential kernel was used for its interpretation, or as a Gaussian spike if a Gaussian kernel was used. A distance metric is then required to measure the difference between two spike train.

3.3.1.3 Distance Metric between Spikes

We used Euclidean distance to measure the similarity between the kernel-smoothed spike train. The distance between two spike train $S_i(t)$and $S_j(t)$ was calculated as,

$$d_{ij} = \left(\sum_{t=1}^{T} [S_i(t) - S_j(t)]^2 \right)^{1/2} \tag{3.4}$$

where T is the total number of time points. T=100 in this study.

3.3.1.4 Learning Parameters for SOM

Spike trains from barrel cortex neurons are shown to be a function of combined features of whiskers vibrations (Fig. 3.3) in the form of $A \times f$. Therefore we used one dimensional SOM with different number of nodes to observe the clustering performance. The best results were obtained from the 1 $\times$ 13 SOM. The SOM was trained randomly choosing a single trial at a time. The neighbourhood size

varied slowly from 13 to 1 whereas the learning rate decreased slowly from 0.6 to 0.05, shown in Fig. 3.9. The total number of iterations for the SOM was about 5 times the size of data set. All parameters were set to ensure a good convergence of the SOM (Kohonen 1997, Lau 1992, Sum & Chan 1994). The same size and parameters of the SOM were used for both decaying spikes and Gaussian spikes.

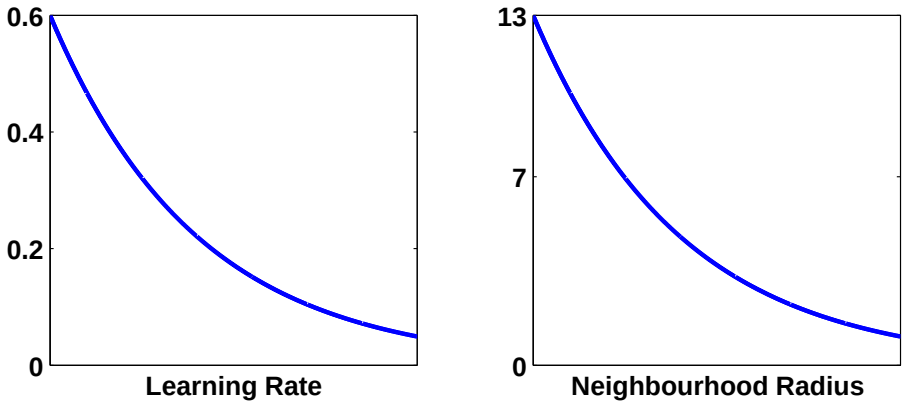

Figure 3.9: Parameters for SOM training.

3.3.1.5 Cluster Validity Check

A simple cluster validity test was applied to clusters to check the clustering quality. The Dunn's cluster validity index (DI) offers a simple yet powerful measure to check the quality of clusters separation; a larger index shows better clustering (Dunn 1974). It is expressed as:

$$DI(C) = \min_{a \in C} \left\{ \min_{b \in C, b \neq a} \left\{ \frac{\delta(c_a, c_b)}{\max_{k \in C}\{\Delta\{c_k\}\}} \right\} \right\} \tag{3.5}$$

where

$$\delta(c_a, c_b) = \min\{dist(x_a, x_b) | x_a \in c_a, x_b \in c_b\}$$

and

$$\Delta(c_k) = \max\{dist(x_a, x_b) | x_a, x_b \in c_k\}$$

C represents a set of SOM generated clusters, c_a and c_b are a–th and b–th clusters and $\delta(.)$ and $\Delta(.)$ are the inter-cluster and intra–cluster distance respectively. A large inter–cluster distance and smaller intra–cluster distance gives a large value of DI and show that clusters are well separated.

3.4 Topological Clustering – Results and Discussion

3.4.1 Gaussian Spikes Clustering Results

The best clustering result obtained by using Gaussian kernel smoothed spike train is shown in Fig. 3.10. The clusters are numbered from top to bottom with top row cluster as 'Cluster 1' with stimuli {20, 26, 28, ..., 48, 49}.

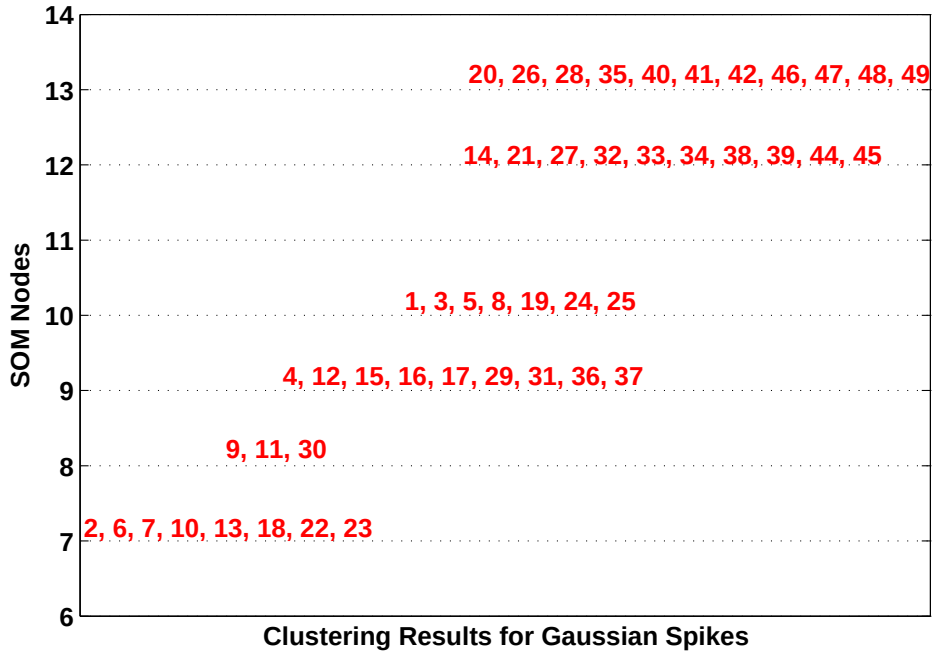

Figure 3.10: SOM clustering results using Gaussian spikes. The nodes are shown along y–axis and stimulus groups are given along x–axis.

The corresponding cluster prototypes for different spike patterns are depicted in Fig. 3.11. The 13 nodes are arranged in rows in the figure, with node 1 at top–left corner and node 13 at the bottom. The node representing 'Cluster 1' prototype is at the last node. The cluster prototypes are shown in red plots at nodes 7, 8, 9, 10, 12 and 13. The clusters may not be well separated (according to energy ($A \times f$) group) and seem to be mixing the energy groups, but smooth changes and topological ordering along the nodes are clearly visible. One of unique properties of the SOM is that the resulting clusters are either partially

or globally topologically ordered on the map and therefore has been linked with principal manifold as well as multidimensional scaling (Yin 2002, 2008). In other words, this manifold demonstrates the stimulus-response relationship.

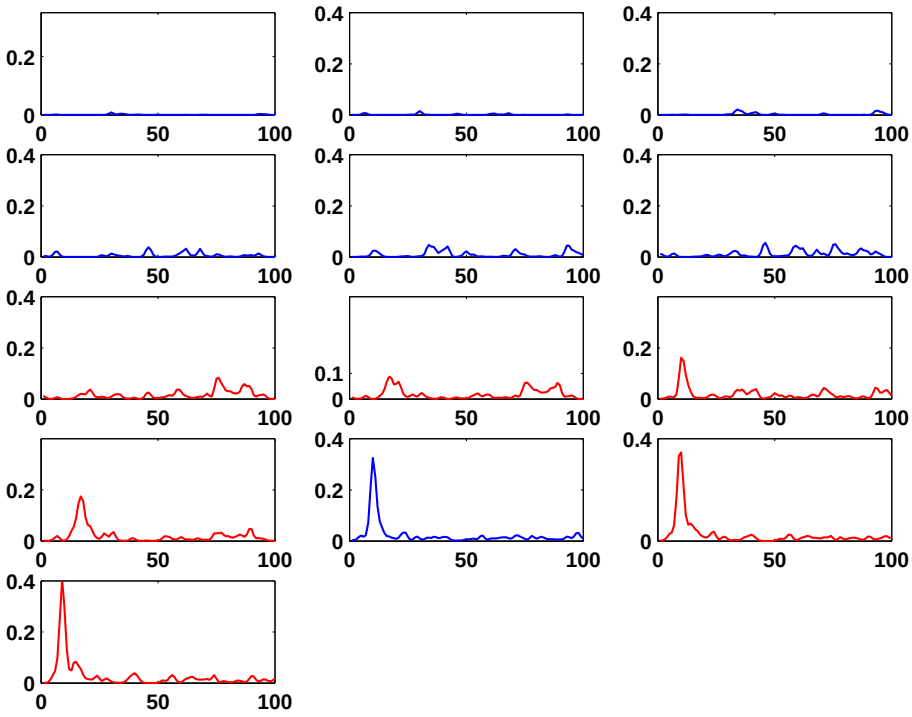

Figure 3.11: SOM nodes prototypes after training (using Gaussian spikes).

Table 3.3 shows comparison between clusters formation and their corresponding position in energy stimulus grouping and spike count (N_{spike}). The stimuli of the first two clusters are listed in Table 3.3, together with their $\log_{10}(Af)$ and $\log(N_{spike})$ values to observe the similarity between them. The $\log_{10}(Af)$ are much closer to the spike count values than their natural log values so these are shown in table. Cluster 6, for example, contains stimuli from four different sets of energy group but the variation of $\log_{10}(Af)$ and $\log(N_{spike})$ values within clusters seems bit closer. The DI for Gaussian spike clusters was found to be 0.018.

3.4.2 Decaying Spikes Clustering Results

The clustering results for decaying spikes are shown in Fig. 3.12. The clustering groups seem to follow the energy encoding more tightly than Gaussian clusters.

Table 3.3: Stimuli for first two Gaussian spike clusters, their Af values and spike count N_{spike}.

Cluster 1	$\log_{10}(Af)$	$\log(N_{spike})$	Cluster 2	$\log_{10}(Af)$	$\log(N_{spike})$
20	3.64	5.84	14	3.62	5.74
26	3.64	5.72	21	3.85	6.17
28	4.05	6.43	27	3.85	6.11
35	4.26	6.58	32	3.64	5.65
40	4.06	6.35	33	3.85	6.02
41	4.26	6.54	34	4.06	6.05
42	4.47	6.74	38	3.65	5.80
46	4.05	6.56	39	3.84	6.11
47	4.27	6.58	44	3.61	6.03
48	4.47	6.75	45	3.85	6.35
49	4.68	6.87	-	-	-

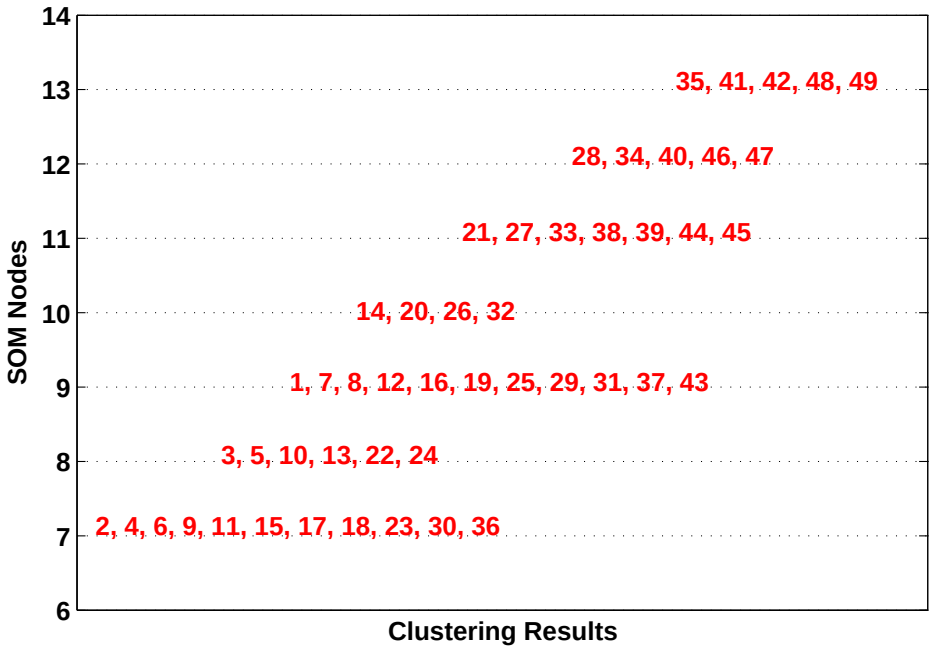

Figure 3.12: Clusters for decaying spike train across the SOM nodes. The stimulus groups are given along x-axis.

Table 3.4 shows the stimulus log values and spike counts for top four rows clusters of Fig. 3.12. By comparison of clustering results, it can be seen that stimuli clusters are better in grouping than Gaussian spike train clusters (with DI=0.046) and verifies that exponential kernel smoothing is better and more natural than Gaussian kernel smoothing. The groups also seem to approximately follow the energy grouping, though does not 'exactly' matches the energy group.

Fig. 3.2 is showing the spike count variation colormap based on the stimuli energy grouping. It can be seen from the Table 3.4 and Fig. 3.12 that clusters are formulated based on the logarithmic values of spike counts of Af stimulus grouping. The stimuli with the highest $\log_{10}(Af)$ values and similar spike counts are grouped together at node 13, then at node 12 and so on.

The SOM nodes after the training period, showing the clusters prototypes are represented in Fig. 3.13. A clear spike temporal pattern can be noticed in all cluster prototypes esp. in the last four nodes. The spiking activity is highest during first 30 msec, this shows that SOM implicitly incorporates temporal code, during clustering process, along with the spike count code.

An average response for each of the 49 stimuli is also shown in Fig. 3.14. The

Table 3.4: Stimuli of the first four clusters obtained in Fig. 3.12.

Cluster 1	$\log_{10}(Af)$	$\log(N_{spike})$	Cluster 3	$\log_{10}(Af)$	$\log(N_{spike})$
35	4.26	6.58	21	3.85	6.170
41	4.26	6.5396	27	3.85	6.107
42	4.47	6.7441	33	3.85	6.021
48	4.47	6.7488	38	3.65	5.802
49	4.68	6.8711	39	3.84	6.114
-	-	-	44	3.61	6.033
-	-	-	45	3.85	6.350
Cluster 2	$\log_{10}(Af)$	$\log(N_{spike})$	Cluster 4	$\log_{10}$(Af)	$\log(N_{spike})$
28	4.05	6.433	14	3.62	5.743
34	4.067	6.347	20	3.64	5.841
40	4.06	6.346	26	3.64	5.717
46	4.05	6.557	32	3.64	5.649
47	4.27	6.581	-	-	-

patterns depicted in the SOM nodes clearly seem to be matching and representing the stimulus pattern of each stimulus.

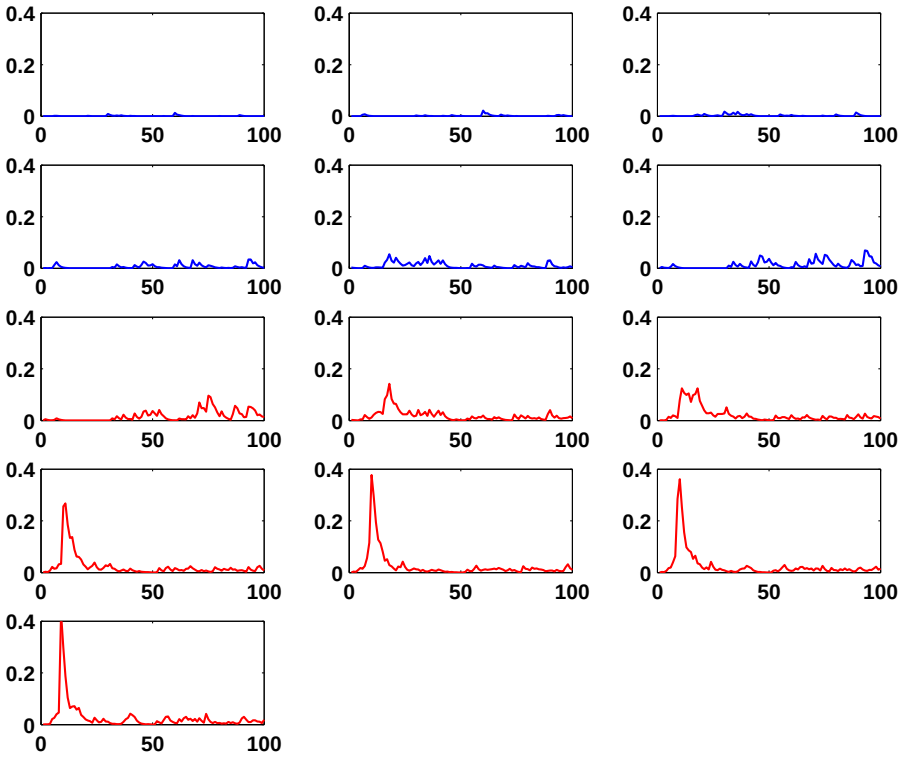

Figure 3.13: Stimuli prototypes across 1×13 SOM nodes. Decaying spike train were used for the training.

The results show that the SOM successfully generated the topological clusters of corresponding energy groups. The clustering results showed that the decaying spikes give better clustering results than Gaussian spikes and this also confirmed that decaying exponential kernel yield better and more natural continuous spike activity functions than Gaussian kernel.

3.5 Decoding Spike Trains by Clusters Information Quantification

It has been discussed earlier that in addition to spike counts, the timing of individual spikes also carry information about stimuli (Panzeri et al. 2001). It is

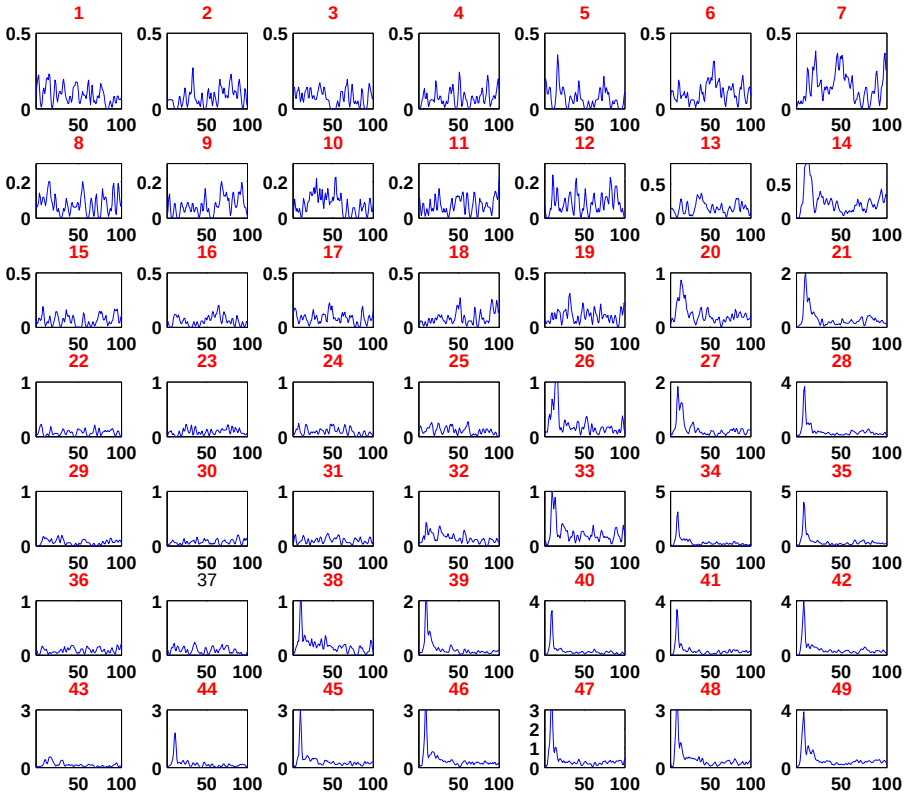

Figure 3.14: Average response of decaying spike train in 24 channels.

therefore important, to investigate whether the neurons tend to respond primarily to energy even when we take into account the timing of the individual spikes and not only the spike counts. This issue is difficult to investigate with other algorithms and alone with information theoretic analysis (Panzeri et al. 2007). We therefore suggested that the SOM combined with information theoretic analysis can help to solve this problem. In the following, clustering results obtained for Gaussian and decaying spikes are used for information quantification of clusters.

We proposed that the quality of the SOM generated clusters can be verified based on their mutual information, which can be given as :

$$MI(C;R) = \left\langle \sum_{r} P(r|C) \log_2 \frac{P(r|C)}{P(r)} \right\rangle_C \tag{3.6}$$

where $P(r|C)$ is the conditional probability of observing a neuronal response r given a stimulus (s), from a cluster (C). $P(r)$ is the marginal probability of response r, i.e. the average of $P(r|C)$ across all stimuli; and $\langle ... \rangle$ denotes the average over all stimuli.

For a good clustering result:

$$MI(C;R) \leq MI(IG;R)$$

where $MI(IG;R)$ represents the energy (Af) grouping in this case.

The result is shown in Fig. 3.15. The top line in blue is showing the MI using the grouping (MI–Af). The second plot in the figure corresponds to the mutual information of the decaying spikes clusters (MI–E). The third plot in black is for the MI of Gaussian smoothed spikes cluster (MI–Gs). It clearly shows that the decaying spikes clusters are more informative than Gaussian spikes clusters. Thus SOM for decaying spikes successfully reveals a 1-D manifold of the stimuli supporting the neuronal energy coding hypothesis based on (Af) along with spike timing code. This means that by considering both spikes temporal code and spike count code, the neuronal population is still selective mainly to stimulus kinetic feature.

The process of SOM based cluster analysis of spike train using smoothing kernel and the resultant generation of information preserving clusters is summarised in Fig. 3.16.

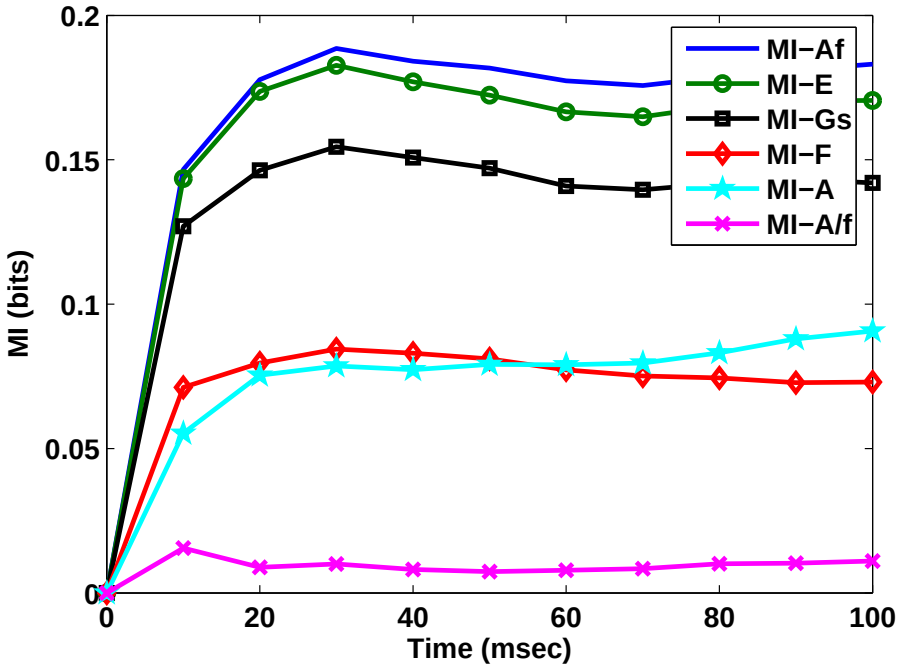

Figure 3.15: Information quantification plots for energy group, decaying spikes cluster, Gaussian spike cluster and other groups.

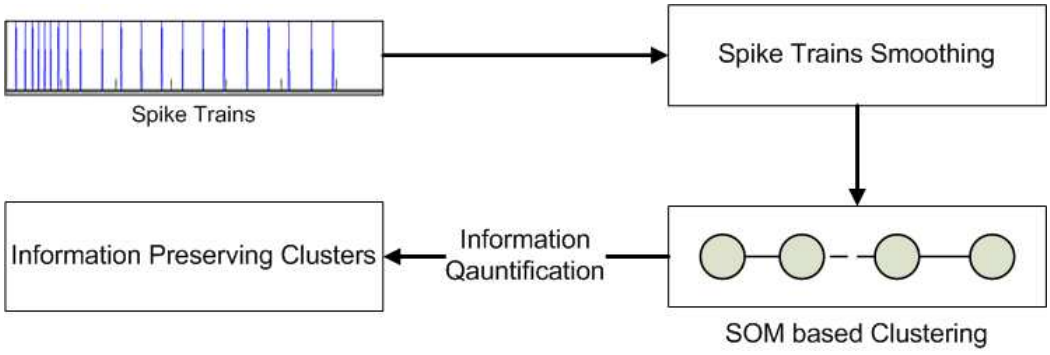

Figure 3.16: A block diagram summarizing the steps for obtaining information preserving clusters for decoding multiple spike train.

3.6 Conclusion

- The SOM can be successfully employed for decoding spike train from multi-channel recordings. The SOM yielded the topological clusters of corresponding energy groups for barrel cortex multi-channel spike data. This shows that clustering is carried out on the basis of stimulus coding.

- Also, the clustering results obtained for decaying spikes were better than Gaussian spikes clusters. This means that the decaying exponential kernel yielded better continuous spike activity functions than Gaussian spike functions. We conclude that spike train interpreted as decaying exponentials can yield better clustering clusters.

- The clustering results of the SOM reveal a 1-D manifold of the stimuli and supports the hypothesis that neurons encode only energy ($A \times f$) even when spike timing codes are considered as a potential code. This means that spike spike timing codes are implicitly included in spike train convolution with a smoothing kernel and thus SOM analysis generates information-encoding clusters.

- The SOM can generate information-preserving clusters for spike train data. The mutual information analysis of the clusters obtained for the rat somatosensory data also confirms that the clustering is analogous to the energy code and that the clustering preserves the information transfer between stimuli and the responses.

Chapter 4

Field Potentials Analysis

Field potential recordings are obtained by both invasive and non-invasive techniques in the form of EEG, LFP, ECoG, MEG etc. as discussed in Chapter 2. While they may reflect different information processing activities in brain, they all are non-stationary random processes (Rieke et al. 1999, Pereda et al. 2005, Andrade et al. 2008). Thus, signal processing techniques must be applied for their analysis. This chapter gives a brief description of some of the research work and methods that have previously been employed for analysing different forms of field potentials and reviews performance of these conventional methods.

4.1 Methods for Field Potentials Analysis

Several studies have been conducted to explore the working mechanism of neurons in different brain regions but algorithms for exploring neural codes are still crude (Pereda et al. 2005, Victor 2006) and pose two main challenges: firstly their non-stationary attributes and secondly the large number of recordings collected from multiple electrodes or micro-electrode arrays (10–100) (Victor 2006). The recording electrodes are often referred to as channels. An example of a micro-electrode array is shown in Fig. 4.1. Other possible configurations can be of 8×8 or 10×10 micro-electrode arrays. EEG data are also collected from usually more than 50 channels (Jeong et al. 2001).

It was also shown in Chapter 2 that field potentials do not have infinite periodicity, are multicomponent signals (Cohen 1992), and consist of several overlapping signals generated from the activity of multiple neurons (Cohen 1992, Pereda et al. 2005). Different mathematical transformation methods such as the Fourier and

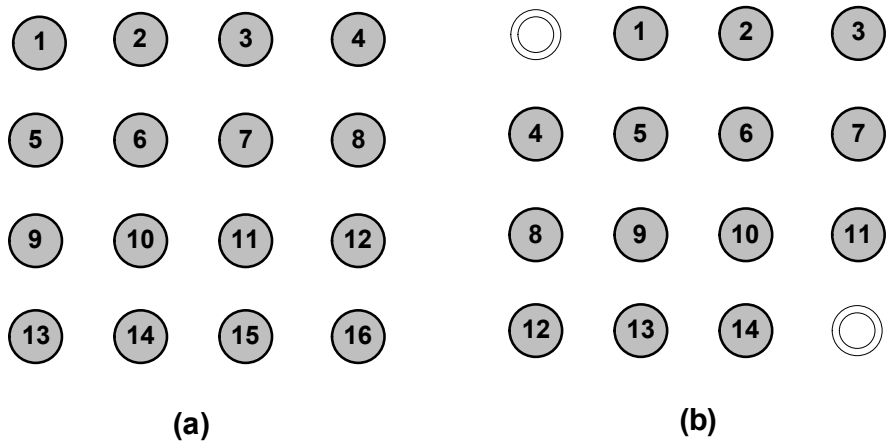

Figure 4.1: A representation of 4×4 micro-electrode array used for LFP/MUA recordings with channel numbers. On right is the array with channels (without numbers) used as reference electrodes.

wavelets are usually applied to analyse these recordings and to explore the features which are not clearly visible in the time domain (Pfurtscheller & Aranibar 1977, Mehboob & Yin 2008). Different frequency bands in field potentials correspond to different phenomena (Pfurtscheller & Aranibar 1977, Henrie & Shapley 2005, Berens et al. 2008) and are found to have different information content, thus most of the methods tend to analyse the neural code in frequency domain. These transformation methods are usually applied on different frequency bands and the recordings are first either bandpass filtered or cut-off at different frequencies of interest and the resulting sub-bands are used for neural code analysis (Pfurtscheller & Aranibar 1977, Henrie & Shapley 2005, Berens et al. 2008). However, bandpass filtering is not an ideal option for analysing non-stationary signals because the cut-off choice for filtering is arbitrary and the natural oscillations may cross these artificial boundaries. Furthermore, filtering may give rise to negative frequencies that have no physical meaning. A detailed review of these transformations is given in the following sections.

4.1.1 Fourier Analysis

The Fourier analysis is one of the common classical methods for spectral analysis of field potentials in different frequency bands and uses the Fourier transform (FT) to decompose a signal into its constituent frequencies in terms of sinusoidal functions (Brown et al. 2004, Grafakos 2004, Addison 2005). However, FT only

gives a global description of frequency components and does not provide any temporal information about the frequency components. This lack of time-localized information is one of the major drawbacks of the Fourier analysis (Addison 2005, Liang et al. 2005, Mehboob & Yin 2008). Neural field potentials have numerous non-stationary or transitory characteristics originating from several neurons and detection of these events and trends cannot be facilitated by the Fourier analysis (Addison 2005, Liang et al. 2005). Thus, FT is more useful for analysis of stationary signals when the underlying processes are linear and the sinusoidal superposition make physical sense (Pfurtscheller & Aranibar 1977, Liang et al. 2005).

A variation of FT is the short-time Fourier transform (STFT), which uses window functions (usually a Gaussian window) for the spectral analysis (Brown et al. 2004, Addison 2005, Liang et al. 2005). It is used to determine the sinusoidal frequency and phase content of local sections of a signal as it changes over time assuming piece-wise stationarity. The problem with STFT is the selection of an appropriate window size and its fixed resolution (Liang et al. 2005). A choice of wide window gives better frequency resolution but poor time resolution and a narrower window gives good time resolution but poor frequency resolution. This is because of the Heisenberg uncertainty principle by which time-localised and frequency-localised information cannot be quantified simultaneously (Brown et al. 2004, Liang et al. 2005).

Consider two multicomponent signals where *Signal 1* is obtained by superposition of three components of *Signal 2* as shown in Fig. 4.2. All the three components are present at all times in *Signal 1*, while they occur at distinct time intervals in *Signal 2*. The Fourier analyses of both signals are shown in the right side of the figure. The spectra are almost identical, lacking any temporal information about the occurrence of each component, though the two signals are clearly different.

The wavelet transform (WT) was designed to overcome the resolution problem of the Fourier analysis and aimed to give better results (Chui 1992, Liang et al. 2005, Addison 2005). A comparison of Fourier and wavelet analysis is shown in Fig. 4.3. The figure shows how the FT, STFT and wavelets operate on a signal. The FT clearly offers least flexibility as demonstrated by the examples in Fig. 4.2.

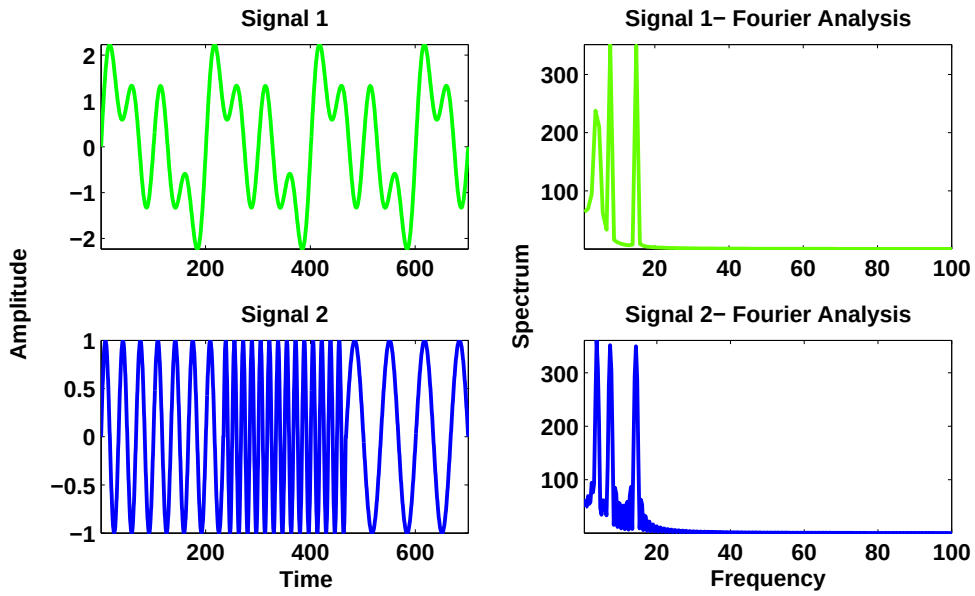

Figure 4.2: An example of Fourier analysis of multicomponent signals. Both spectrum (on right side) are similar and lack time-localized information.

4.1.2 Wavelets Analysis

WT decomposes a signal into local, time-dilated and time-translated wavelet components and is better than FT for characterising gradual frequency changes (Addison 2005, Liang et al. 2005). It uses a set of basis functions, often based on a mother wavelet, for breaking up of a signal into shifted and scaled versions of the mother wavelet. The wavelet functions generated by mother wavelets are often called as wavelet coefficients.

A mother wavelet is a waveform of effectively limited duration that has an average value of zero. Examples are Haar, Morlet, Gaussian, mexican hat (mexh) as shown in Fig. 4.4. Fourier analysis may be considered as a special case of a wavelet transform with basis functions defined by sine and cosine.

The use of different wavelets instead of sine waves clearly gives the intuition that signals with varying attributes might be better analysed with a specialised wavelet function than with a sinusoidal function. Wavelet analysis has found a wide range of applications in analysis of biological and financial data analysis, examples are given by Liang et al. (2005) and Mehboob & Yin (2008). For example, EEG recordings' transient features can be accurately captured and localised in both time and frequency context through wavelet decomposition (Adeli et al. 2003).

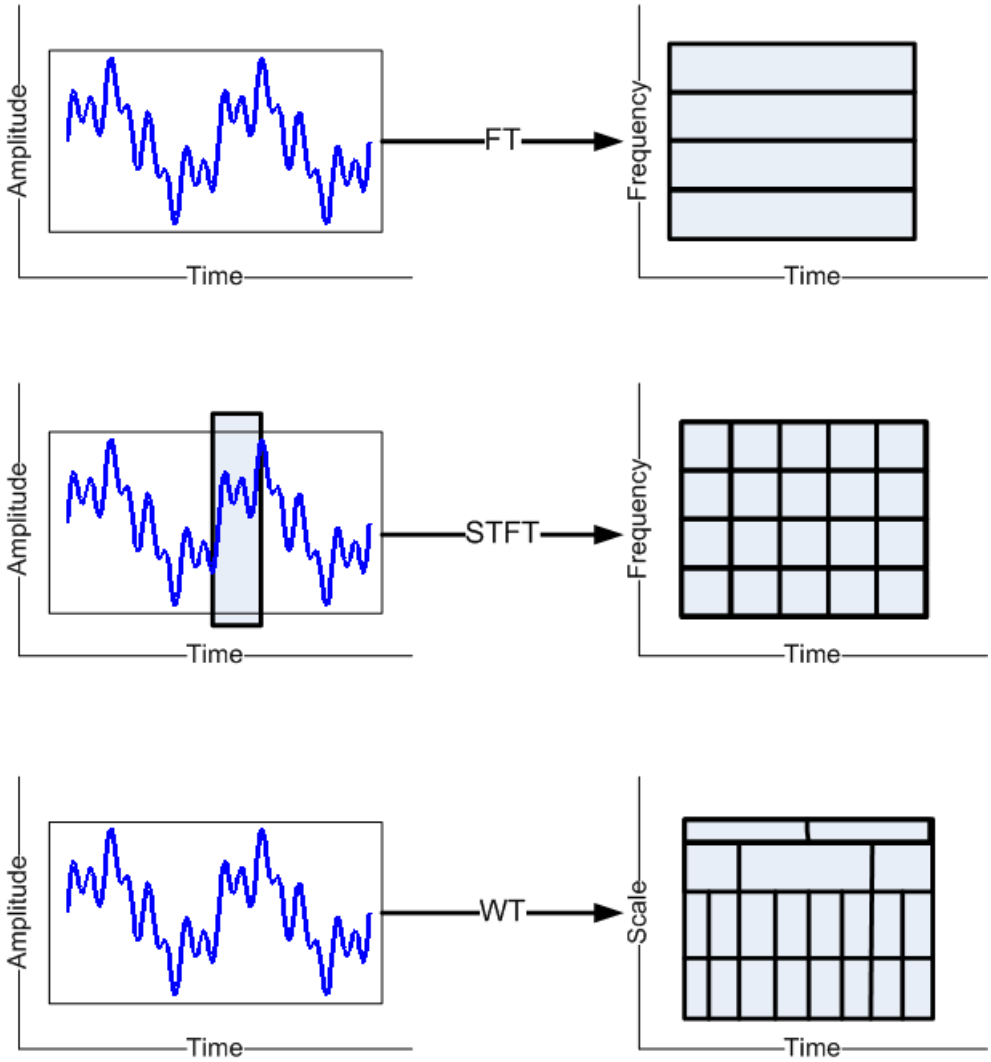

Figure 4.3: Block diagrams of Fourier and wavelet analysis. For wavelets, the term 'scale' is often used instead of frequency.

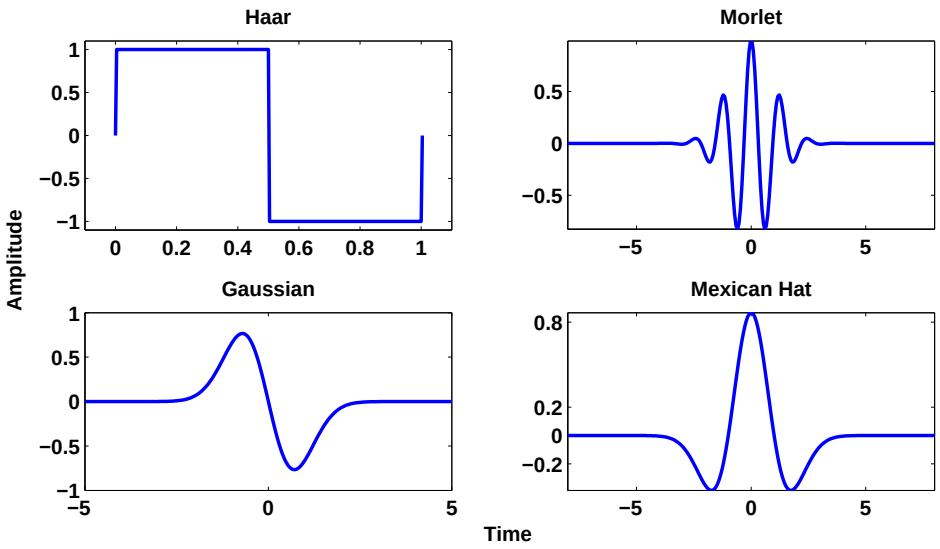

Figure 4.4: Different types for wavelets.

One of the difficulties in wavelet analysis is the selection of the mother wavelet. The same wavelet is usually used for the whole data analysis. This choice is crucial because wavelets vary in shapes and characteristics and addresses differently to the time frequency resolution problem, yielding different results on the same data, as depicted in Fig. 4.5. The toy signal is shown in the top row of the figure. As can be seen from the figure that the mexh wavelet performs better than the Morlet wavelet and is more distinct and robust in representing the individual components and characterising the frequency change.

The other limitation with wavelet analysis is that, like Fourier analysis,it also suffers from the uncertainty principle and has issues with time/frequency resolution trade-off, so a time-localized and frequency-localized information cannot be obtained simultaneously with good resolution. Therefore through wavelets analysis, a high frequency component can be located well in time domain and a low frequency component can be located better in frequency domain (Liang et al. 2005, Mehboob & Yin 2008).

The solution to these problems is offered by the Hilbert-Huang transform (HHT) which combines empirical mode decomposition (EMD) method and Hilbert transform (HT) for signal analysis. These are discussed in the following section.

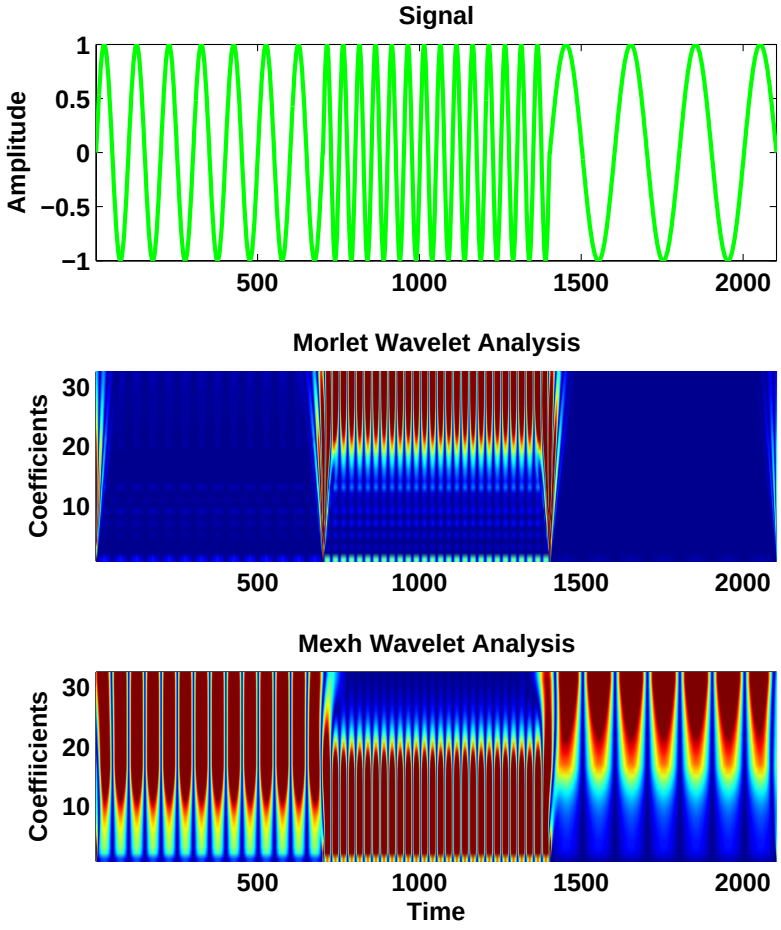

Figure 4.5: An example of signal analysis using two different wavelets.

4.2 Empirical Mode Decomposition (EMD)

Empirical mode decomposition (EMD) was first introduced by Huang et. al (Huang et al. 1998). It is a signal decomposition method that decomposes a non-stationary, non-linear time series into a number of zero mean AM/FM (amplitude modulated/frequency modulated) oscillatory functions (Huang et al. 1998, Rilling et al. 2003). It is often considered as a form of wavelet transform with the advantage that the basis functions are derived from data (Rilling et al. 2003, Flandrin & Gonçalvès 2004, Mehboob & Yin 2008), making it completely adaptive and data driven. It has been shown that EMD also behaves as WT in many cases (Flandrin & Gonçalvès 2004, Sweeney-Reed & Nasuto 2007).

4.2.1 EMD Procedure

Given a time series $x(t)$, EMD is conducted by a sifting algorithm (Huang et al. 1998) given in Table 4.1. This sifting procedure generates a number of oscillatory functions called intrinsic mode functions (IMFs) or simply modes. An IMF is defined by the following characteristics:

- An IMF has (nearly) zero mean.
- In each IMF, the number of maxima and minima differs by no more than 1.
- Each IMF (usually) lies in a narrow frequency band.

The number of iterations at step 5 of the EMD algorithm in Table 4.1 is defined by a stopping criterion in order to avoid a pure frequency modulated, constant amplitude IMF. Various stopping criteria have been proposed. Initially this was accomplished by limiting the size of normalised squared difference (SD) computed from the two consecutive sifting results (Eq. 4.1) and first used by Huang et al. (1998). A value between 0.2 and 0.3 has been found to provide good results.

$$SD = \sum_{t=0}^{T} \left[\frac{\left| h_{1(j-1)}(t) - h_{1j}(t) \right|^2}{h^2_{1(j-1)}(t)} \right] \tag{4.1}$$

Table 4.1: Algorithm for Empirical Mode Decomposition Method

1. Identify all the local maxima ($mx(t)$) and connect them by a (cubic) spline to form an upper envelope ($e_{mx}(t)$).

2. Repeat the procedure for the local minima ($mn(t)$) to produce a lower envelope ($e_{mn}(t)$). The upper and lower envelopes should cover all the data between them.

3. Find the local mean envelope $m(t)$ by averaging the two envelopes:

$$m(t) = (e_{mx}(t) + e_{mn}(t))/2$$

4. Extract $m(t)$ from $x(t)$ and obtain $h(t)$; $h(t) = x(t) - m(t)$.

5. Check if $h(t)$ satisfies the condition of an IMF. If $h(t)$ satisfies the condition of an IMF repeat the above steps with ($m(t)$) otherwise repeat the above steps with $h(t)$ until an IMF is obtained.

6. Stop the sifting process when the residual is left with only one maxima.

Huang et al. (2003) later proposed a criterion based on the number of zero-crossings and extrema. The sifting process stops when the numbers of zero-crossings and extrema stay the same and are equal or differ at most by one. Through comparisons of the individual sets with the mean, Huang et al. established an empirical guide and suggested that the number of sifting iterations should be set between 4 and 8 for the optimal siftings (Huang et al. 2003). Several EMD algorithms are available on web (Rilling et al. 2003, Lambert et al. 2003, Kim & Oh 2008, Ortigueira 2008). We tested these on different time series and found that the best results were obtained by the implementation provided by Rilling et al. (2003).

The first iteration of the sifting process is depicted in Fig. 4.6, where the upper, lower and mean envelope of a signal ($x(t)$) are shown in the first two plots. The last plot shows the first $h(t)$ obtained by subtracting the $m(t)$ from $x(t)$, which in this case is not an IMF.

During the sifting process, the number of extrema decreases from one residual to next and the complete decomposition is achieved within a finite number of steps; also the spectral bandwidth of corresponding IMFs (modes) decrease accordingly. One of the biggest strengths of the EMD method is that IMF's high

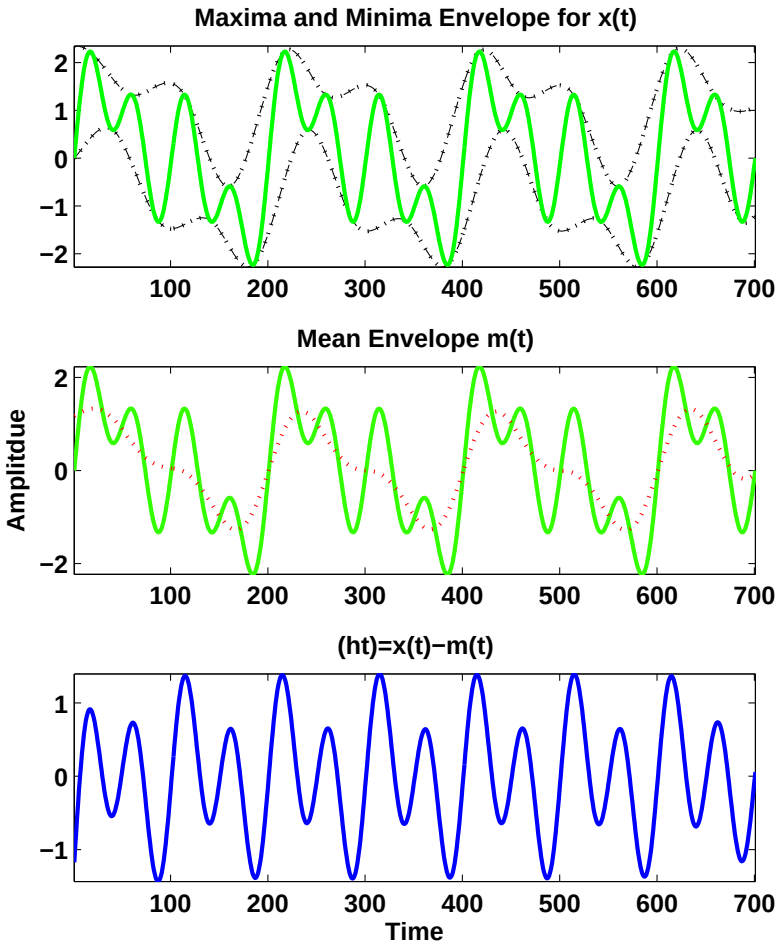

Figure 4.6: Calculation for envelopes for a signal $x(t)$ during EMD sifting.

to low frequency discrimination does not correspond by any means to predetermined sub-band filtering and is completely data-driven, which is not the case with Fourier and wavelet analysis.

The EMD sifting algorithm generates K IMFs and a residual (res_K) showing the general trend of the signal. The linear superposition of all the modes and residual gives the original recording.

$$x(t) = \sum_{j=1}^{K} IMF_j(t) + res_K(t) \tag{4.2}$$

where K is the total number of IMFs obtained from the time series ($x(t)$) and $res_K(t)$ is the residual. The number of IMFs depends on the length of the signal. A longer signal usually generates a greater number of IMFs.

The EMD analysis of a typical field potential recording is shown in Fig. 4.7. The first few IMFs are composed of high frequency components and the frequency bandwidth decreases with the increasing order of IMFs. It also shows that signals need not be explicitly bandpass filtered and the EMD can adaptively generate the underlying oscillations, each lying in a certain frequency band. These advantages make the EMD method particularly appealing for analysing continuous neural field potential recordings.

The EMD analysis of the two multicomponent signals, depicted in Fig. 4.2, is shown in Fig. 4.8. The EMD of *Signal 1* yields three IMFs, which are the original components of the *Signal 1*. Whereas the EMD of *Signal 2* generates the same signal (green plot) as it is already a narrow band signal at any particular time instant. This illustrates EMD offers better signal decomposition of multicomponent signals than Fourier analysis.

In the following section, it is also shown that spectral attributes can be better quantified using Hilbert analysis on EMD generated IMFs, when compared to Fourier and wavelets analysis.

4.3 Hilbert Transform (HT)

The Hilbert-Huang transform (HHT) makes use of the Hilbert transform (HT) and EMD method to generate the instantaneous attributes of the given signal with a good time–frequency resolution. The HT is applied on the IMFs obtained using EMD. Given a signal $x(t)$, its HT is defined as:

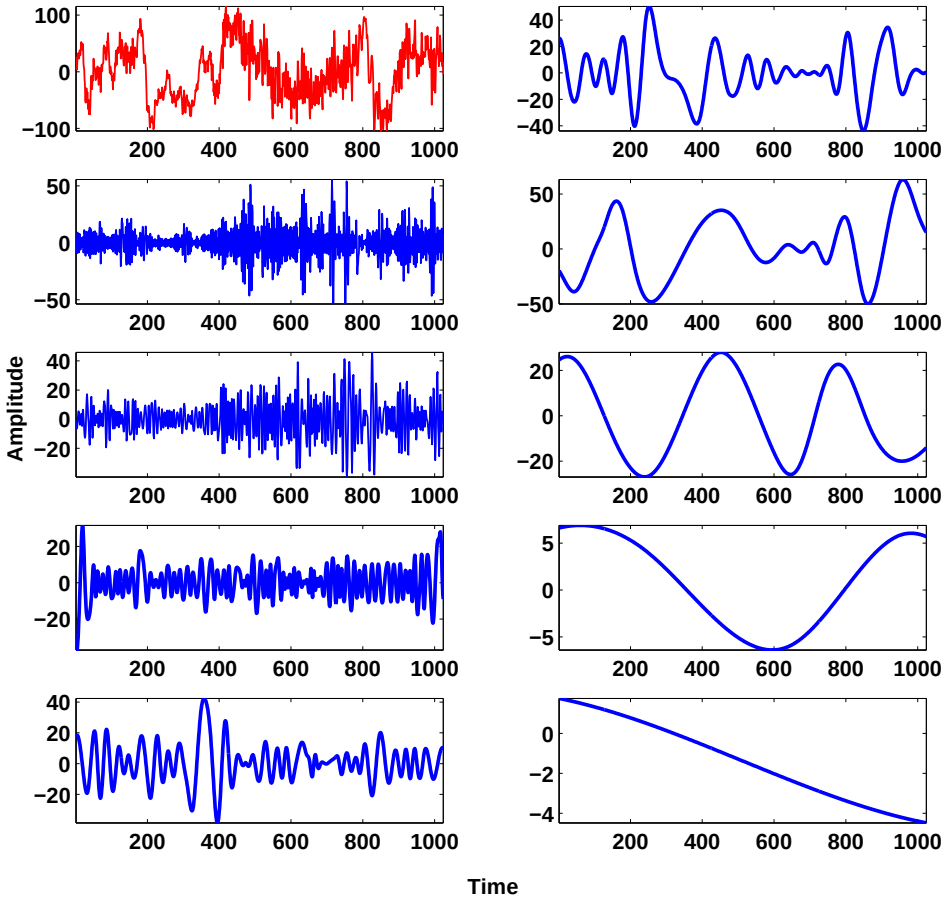

Figure 4.7: An example of EMD applied on a field potential recording. The first (red) plot on the left is the field potential with the first four extracted IMFs below it. The right panel shows the IMFs 5–7 and the residual at the end.

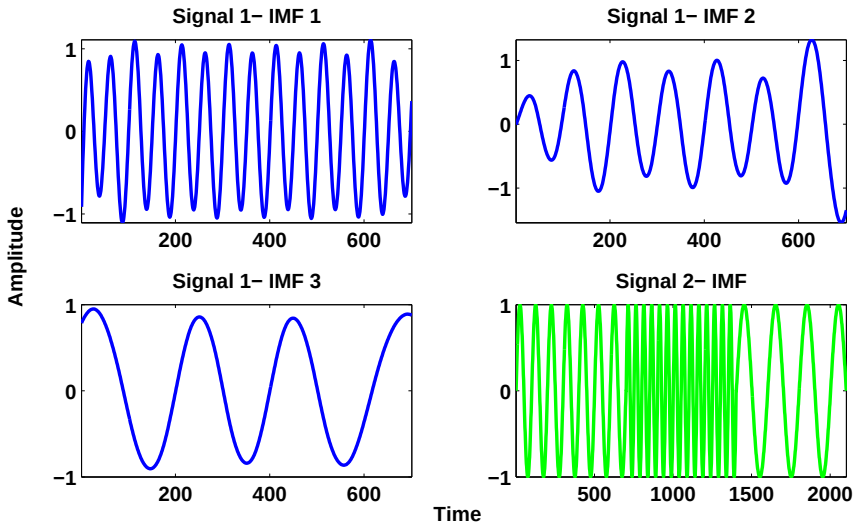

Figure 4.8: EMD of two signals and the resulting IMFs.

$$y(t) = \frac{1}{\pi} P \left[\int_{-\infty}^{\infty} \frac{x(s)}{t-s} ds \right] \tag{4.3}$$

where P is the Cauchy principal value. The analytic signal is then defined by the following:

$$z(t) = x(t) + \iota\, y(t)$$

$y(t)$ is the HT of $x(t)$. In terms of phase and amplitude, the analytic signal can be represented as:

$$z(t) = a(t) \times exp(\iota\, \theta(t))$$

$a(t)$ and $\theta(t)$ represents the instantaneous amplitude and phase respectively. The magnitude of $a(t)$ can be obtained by:

$$a(t) = \sqrt{x(t)^2 + y(t)^2}$$

the instantaneous phase (IP) and instantaneous frequency (IF) are calculated as:

$$\theta(t) = arctan\left(\frac{y(t)}{x(t)}\right)$$

$$f_{inst} = \frac{1}{2\pi}\left(\frac{d(\theta)}{d(t)}\right)$$

The Hilbert analysis of a modulated signal is shown in Fig. 4.9. Compared to its Fourier and Wavelet analysis in Fig. 4.2 and Fig. 4.5, it can be seen that the HT is able to find the time-frequency distribution and time-phase analysis more precisely without any time/frequency resolution problem.

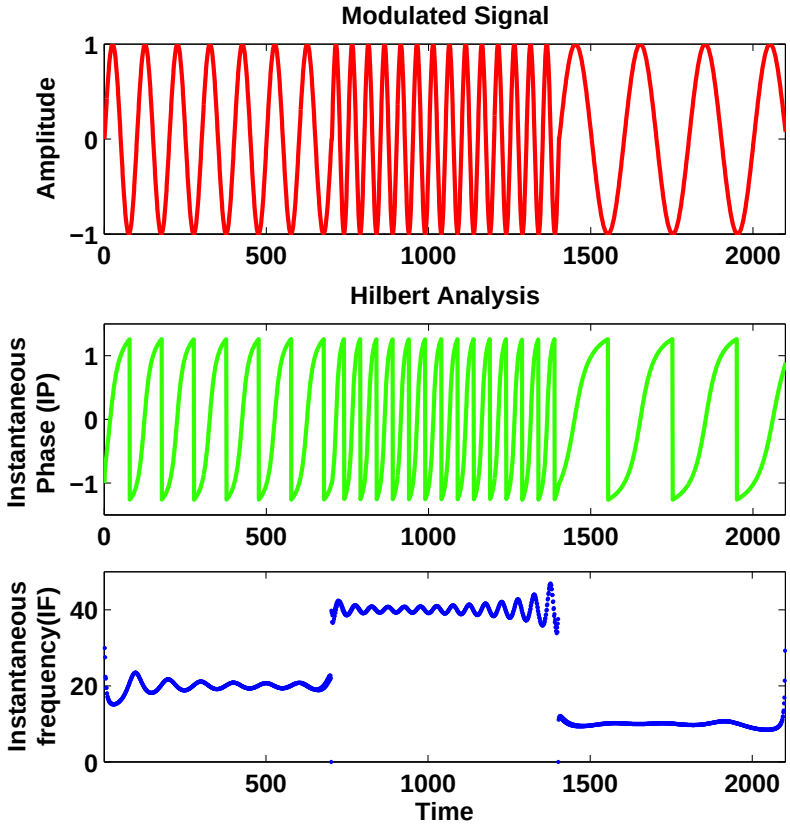

Figure 4.9: An example of obtaining IP and IF using Hilbert transform.

It has been argued by Schwartz et al. (1966), that the concept of instantaneous frequency and phase only makes sense for narrow band signals, thus wide band neural signals need to be bandpass filtered in case of Fourier and wavelets for analysis. This is, however, not the case when the instantaneous attributes are extracted by using HT on IMFs.

Since its development, EMD has been successfully applied to many engineering problems. In a study, a lower mean-squared error was found between IMFs and original artificial components using EMD compared with using the wavelets

(Liang et al. 2005) and it was also demonstrated that improved time-frequency resolution was achieved by EMD as compared with the STFT and the WT; pointing out the advantage of avoiding arbitrary bandpass filter cut-offs (Liang et al. 2005, Sweeney-Reed & Nasuto 2007). Compared with WT, EMD method shows a superior performance on selectivity and the precision of data analysis and thus proves to be a powerful tool for adaptive multi-scale analysis of short-time nonlinear and non-stationary signals (Flandrin & Gonçalvès 2004). EMD has also been used as a noise removal tool to obtain trend of a signal (Boudraa et al. 2005, Weng et al. 2006) and also for the signals corrupted by additive white Gaussian noise. Their results showed that the de-noising scheme based on EMD performs better than the wavelet approach (Boudraa et al. 2005, Weng et al. 2006, Khaldi et al. 2010). EMD and the Hilbert spectrum has also been applied to EMG signals. The results show that it may provide an increase in the spectral resolution and also gives an insight into the underlying process of the muscle contraction (Andrade et al. 2008).

4.3.1 Phase Synchronisation Analysis using HHT

EMD and HT have also been employed for phase synchronisation analysis in neural recordings. Phase synchronisations play an important role in attributing relationships among field potentials (Lachaux et al. 1999, Sweeney-Reed & Nasuto 2007, Mehboob & Yin 2011). It is a phenomenon by which two neurons tend to oscillate with relative phase angle and is observed in several studies (Lachaux et al. 1999, Sweeney-Reed & Nasuto 2007, Manyakov & Hulle 2008, Sweeney-Reed & Nasuto 2009, Mehboob & Yin 2011). HHT analysis gives the advantage of instantaneous phase and phase synchronisation analysis among non-stationary and non linear signals as it avoids the need of bandpass filtration. This is not achievable by WT or FT as they would involve bandpass filtering and might fail to capture the synchronisation as the phase progresses in a physical system (Huang et al. 1998). A comparison of neural synchrony analysis using Hilbert and wavelet analysis is reported by Quyen et al. (2001). An attempt has also been made for analysing phase locking between IMFs of the field potential recordings in which phase synchronisations were successfully located between artificially generated EEGs (Sweeney-Reed & Nasuto 2007).

4.4 Summary and Conclusion

A comparative summary of Fourier, wavelets and Hilbert-Huang analysis is presented in Table 4.2. The table shows that the HHT (EMD and HT) is indeed a powerful tool for analysing data from nonlinear and non-stationary processes like field potentials, for the following main reasons:

- The EMD is an adaptive and data driven method.
- Using EMD method eliminates the need of bandpass filtering.
- The IMFs are amplitude and/or frequency modulated functions, as a result their spectral attributes do not suffer from the time or frequency resolution problem when the frequency is defined through Hilbert transform.

Table 4.2: A comparative summary of Fourier, wavelet and HHT analysis.

	Fourier	Wavelet	EMD and Hilbert
Basis	*a priori*	*a priori*	adaptive
Frequency	convolution, global	convolution, regional	differentiation, local
Presentation	frequency	time-frequency	time-frequency
Nonlinear	no	no	yes
Non-stationary	no	yes	yes

Chapter 5

Information Preserving EMD

The characteristics and advantages of using EMD and Hilbert analysis for non-stationary data and field potentials are discussed in Chapter 4. Based on these, we proposed an information-theoretic framework that could combine the attributes and advantage of information theory and EMD analysis (Mehboob & Yin 2009) for decoding field potential recordings.

The schema of information-preserving EMD (IP-EMD) is based on filtering information carrying intrinsic mode functions (IMFs) from the raw field potential recordings. We found that IP-EMD can give a clearer and more informative representation of the data, through informative IMFs, that also tells about stimulus coding in different frequency ranges (Mehboob & Yin 2009).

This chapter presents application of information theory on field potentials and some important observations regarding EMD and IMFs obtained from different field potentials which led to the foundation of IP-EMD framework. The steps involved in the framework's algorithm and some results from LFP analysis are discussed.

5.1 Information Theoretic Analysis of Field Potentials

The information analysis of field potentials is similar to that of information–theoretic analysis of spike trains, but the main difference is that the information quantification is carried out in spectral domain to explore the information coding frequency ranges.

Information analysis has been used in numerous studies for LFP (Kreiman et al. 2006, Ray et al. 2008), EEG (Date 2001) and gene expressions data analysis (Ido Priness & Ben-Gal 2007). Different frequency bands are found to be informative in different brain regions (Pfurtscheller & Aranibar 1977, Liang et al. 2005, Belitski et al. 2008, Berens et al. 2008). LFPs, being considered as a candidate alternative to spiking activity (Kreiman et al. 2006), are easier to measure and have been shown to carry information regarding stimulus. Attempts have also been made to systematically compare information content of LFPs and spike trains (Belitski et al. 2008). For instance, it was found that in monkey inferior temporal cortex, neuronal inputs convey selectivity for complex shapes and may have an underlying organization spanning several millimetres (Kreiman et al. 2006).

It has also been suggested, based on the information analysis, that the intensity of sensory input is encoded in the timings of action potentials relative to the phase of gamma oscillations in LFPs, thus converting amplitude information to a temporal code. Spikes and LFPs recorded from secondary somatosensory cortex, in awaken monkeys, showed weak coupling between spikes and LFP oscillations in the gamma range (40–80 Hz) (Ray et al. 2008). Strong couplings were found between spikes and LFP oscillations in high gamma band. However, the phase relationship of neither low–gamma nor high–gamma oscillations changed with stimulus intensity. This showed that, in somatosensory cortex, LFP gamma oscillations are synchronised with spikes, but their phase does not vary with stimulus intensity (Ray et al. 2008). In recordings from visual cortex of monkeys, it was found that low frequency LFPs carry different information than the corresponding spike trains (Belitski et al. 2008). Research on relationship between EEG and spikes showed that only gamma and delta bands corresponded to spike activity (Logothetis et al. 2001).

The mutual information analysis of field potentials involves two main steps, with slight variation in estimating probabilities for discrete and continuous stimuli recordings. The two steps are:

1. Spectrum estimation of field potentials.

2. Spectrum quantization of field potentials.

5.1.1 Spectrum Estimation

The first step for field potentials' information quantification requires power spectrum estimation. This can be done by means of any parametric or non-parametric method. However, it has been demonstrated earlier that a parametric method such as Fourier analysis may not give optimal results. To obtain a global spectral power distribution, it has been suggested that a non-parametric method gives better results, such as multi-taper method (MTM) and Welch method, which are not prescribed by an *a priori* model (Percival & Walden 1993). MTM method, for instance, attempts to reduce the variance of spectral estimates by using a small set of tapers rather than the unique data taper or spectral window (Percival & Walden 1993, Arabzadeh et al. 2003). For these reasons, it is preferable to estimate spectral density using MTM and has been used for neural data analysis (Panzeri et al. 2007, Belitski et al. 2008, Mehboob & Yin 2009).

The multitaper method is an extension of single taper approaches. The data is divided into overlapping subsets which are individually tapered and then Fourier transformation is applied. The individual spectral coefficients of each subset are averaged to reduce the variance. The multitaper approach can minimise the spectral leakage while reducing the variance of the estimate by averaging orthogonal eigen-spectrum estimates. The orthogonal tapers are Slepian sequences used as tapers on the windowed time series. Therefore spurious correlations are not introduced when the orthogonal data tapers are combined to obtain an average spectrum. A comparison of spectral estimation by Fourier and MTM is shown in Fig.5.1. The spectrum obtained by MTM method is clearer with reduced variance.

5.1.2 Spectrum Quantization

The field potentials and their spectra are continuous valued functions and therefore require a pre–processing step for estimation of probabilities. This process involves quantization of responses and is often termed as binning (Strong et al. 1998, Panzeri et al. 2007, Belitski et al. 2008). An example of equi-spaced binning is presented in Fig. 5.2 with two different bin sizes. The choice of bin size is arbitrary but a bin size yielding higher information is preferred over other bin sizes (Panzeri et al. 2007). However this does not affect the overall information profile. The binning method is important since the MI estimation is affected by it and

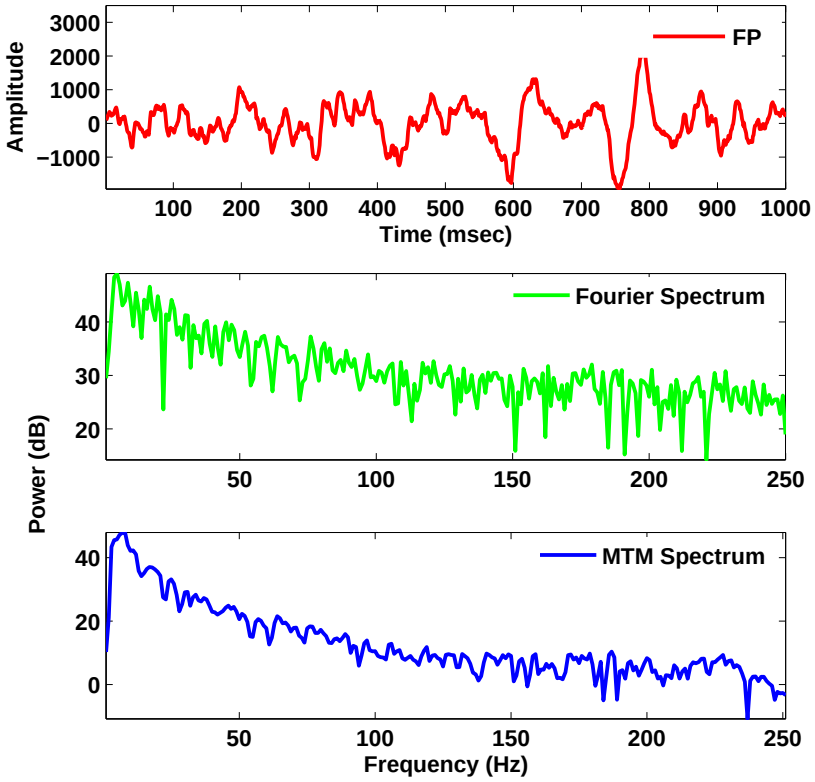

Figure 5.1: An example of spectral analysis of a typical field potential recording using MTM.

the results may be subject to biasing due to the errors in probability estimation (Panzeri et al. 2007). More information about binning strategies can be found in (Victor 2006).

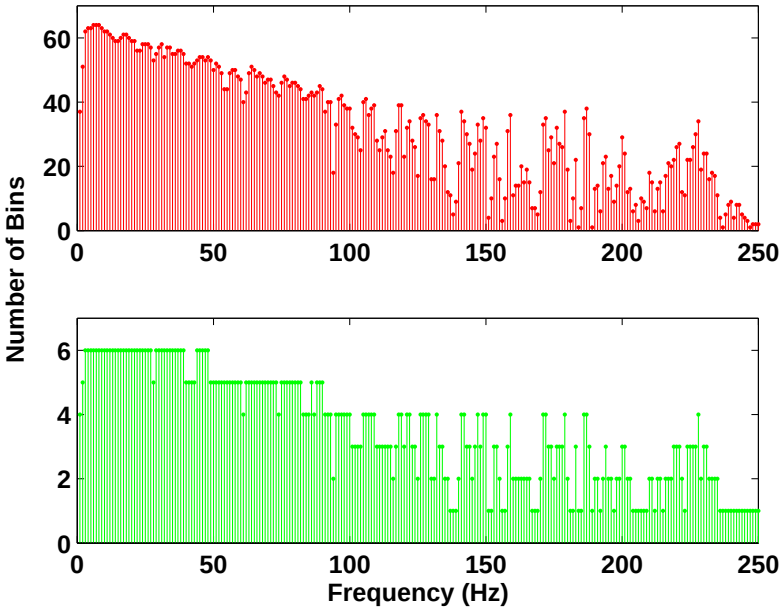

Figure 5.2: An example of field potential spectrum discretization or binning. The plot at the top shows the quantization in 64 bins and the bottom plot shows the discretization in 6 bins.

5.1.3 Stimulus Presentation

In a field potential recording experiment, stimuli can be discrete or continuous. For example an audio stimulus can be formed by small discrete set of monotonic tones or a prolonged audio recording. Similarly, a discrete visual stimulus can be composed of gratings of varying orientations or different spatial or temporal resolution. Discrete visual stimuli can also be in the form of images of different objects, people etc., whereas a continuous visual stimulus can be a video or a natural scene. Example of different visual stimuli are shown in Fig. 5.3.

Information analyses for discrete and continuous stimuli recordings vary slightly, therefore we developed specialized approaches for analysis of these two types of stimuli recordings and these will be discussed in this chapter. The storage of neural recordings, esp. field potential recordings, are based on the nature of stimuli.

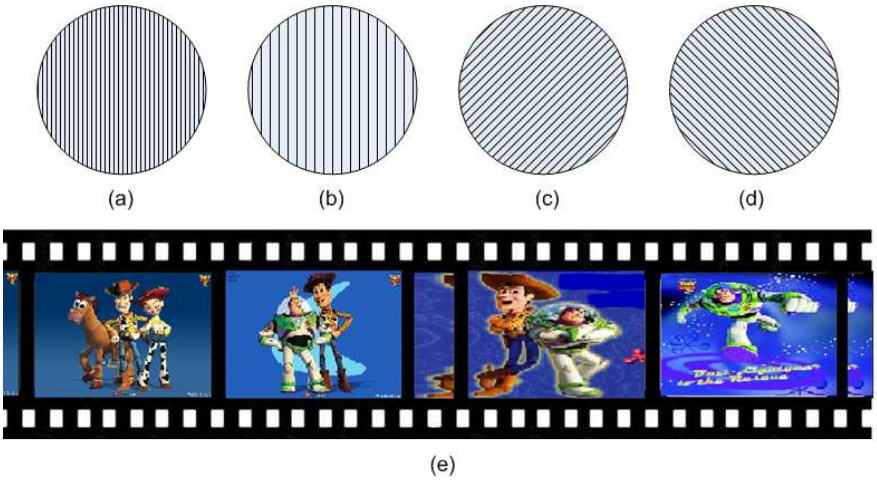

Figure 5.3: Different forms of discrete and continuous stimuli. Stimuli (a) to (d) are discrete visual stimuli with different spatial resolution and orientation. Stimulus (e) shows representation of continuous visual stimulus in the form of a video reel.

A possible representation can be in the form of three dimensional or four dimensional matrices. For multi-channel continuous stimuli recordings, the data can be arranged in the form of :

$$Data\ Matrix = Response(R) \times Trial(Tr) \times Channel(C).$$

For a set of discrete stimuli, the data can be arranged as:

$$Data\ Matrix = Response(R) \times Trial(Tr) \times Stimulus(S) \times Channel(C).$$

For a continuous stimulus, responses are usually divided into small windows (Strong et al. 1998, Belitski et al. 2008) for estimation of information in each window and observing the change in information level with time. The choice of window length is arbitrary but should be at least equivalent to subject's perception time of stimulus, for example, at least 2 msec to perceive the gist of a scene (Gunduz & Principe 2009).

5.1.4 Mutual Information Quantification

The MI calculation for field potentials is based on the probability distribution of responses' power spectrum $R_{pwr}(f)$ across all the stimuli and trials. The probability estimate is carried out by discretization obtained from the binning procedure. For field potential recordings, the mutual information (MI) analysis equation takes the form:

$$I(S; R_{pwr}(f)) = \sum_{s} P(s) \sum_{r_{pwr}(f)} P(r_{pwr}(f)|s) \log_2 \frac{P(r_{pwr}(f)|s)}{P(r_{pwr}(f))} \tag{5.1}$$

where $P(s)$ is the probability of the stimulus (in case of discrete stimulus) or stimulus windows (for continuous stimulus). $P(s)$ is equal to the inverse of the total number of stimuli if the stimuli are discrete, otherwise the total number of stimulus windows in case of continuous stimuli recordings. $P(R_{pwr}(f)|s)$ is the probability of observing a power spectrum $R_{pwr}(f)$ at frequency f and in response to a single trial to stimulus s and $P(R_{pwr}(f))$ is probability of power $R_{pwr}(f)$ across all trials in response to any stimulus. $MI(S; R_{pwr}(f))$ quantifies the reduction of the uncertainty about the stimulus that can be gained from observing the power at frequency f in one trial. For base 2 logarithms, $MI(S; Rpwr(f))$ is expressed in units of bits.

5.2 Proposal for the IP-EMD Framework

The design of the IP-EMD framework was based on few observations, discussed in the following.

5.2.1 Important Observations

1. The sum of all IMFs and residual gives the original recording as discussed in Chapter 4.

2. The IMFs extracted from field potentials lie in certain/narrow frequency bands. A typical LFP recording and its IMF spectral distribution is given in Fig. 5.4.

3. Cumulation of spectra from all IMFs is equivalent to the spectrum of original recording as shown in Fig. 5.5.

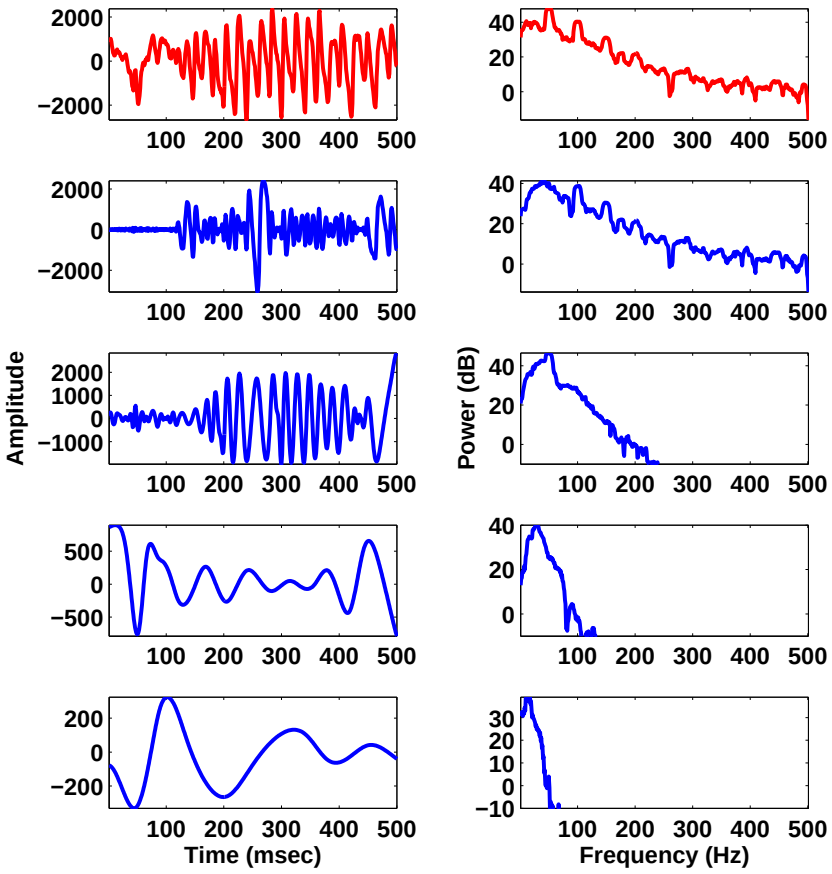

Figure 5.4: An LFP recording and its first four IMFs (on left), their corresponding power spectra are shown on the right. The bandwidth decreases from IMF 1 to IMF 4.

4. Each IMF varies in information content, shown in the following section.

This proposed method can also be used for the neural code analysis of other non-stationary continuous neuronal recordings like MEGs, ERPs etc and is able to extract the information carrying oscillatory modes. The block diagram of framework is shown in Fig. 5.6.

5.2.2 Information Quantification of FPs and IMFs

As shown in the block diagram, the first step after EMD is information quantification from FPs and their corresponding IMFs. Information quantification for

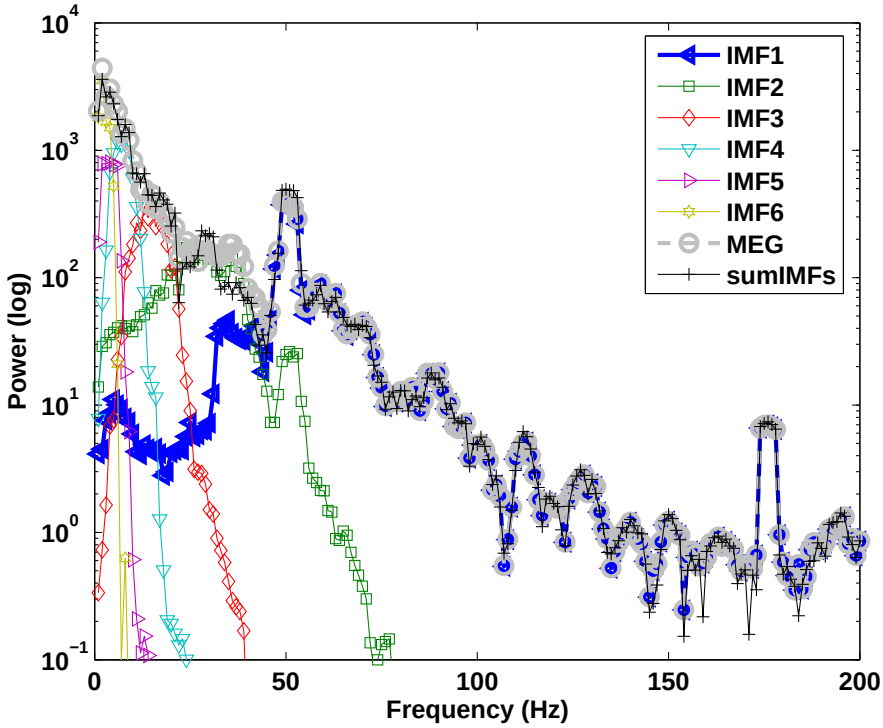

Figure 5.5: An example of spectral distribution of an MEG recording and its corresponding 6 IMFs. The cumulative sum of spectra of IMFs 1 to 6 (black line) is equal to the spectrum of MEG (grey line).

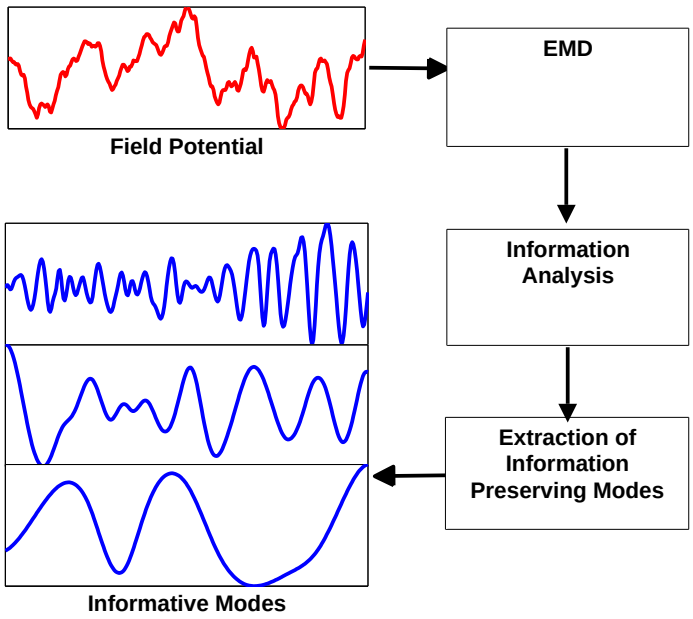

Figure 5.6: A block diagram of the IP-EMD framework for extraction of informative modes from field potentials.

field potentials is given by Eq. 5.1. The information between stimuli and IMFs can be obtained by Eq. 5.2, which is a variation of Eq. 5.1.

$$MI_{IMF}(S; IMF_{pwr}(f)) = \sum_{s=1}^{n} P(s) \sum_{imf_{pwr}(f)} P(imf_{pwr}(f)|s) \log_2 \frac{P(imf_{pwr}(f)|s)}{P(imf_{pwr}(f))} \tag{5.2}$$

where $IMF_{pwr}(f)$ is the magnitude of the power of an IMF at a particular frequency, f.

We presented the argument that information content of all IMFs should be equivalent to the information content of original recordings, since the IMFs are obtained from the decomposition of original recording. Also in the case of field potentials, not all the IMFs participate in encoding the stimulus information as only certain frequency bands have been found to be informative in different sensory stimuli and medical conditions such as epilepsy (Pfurtscheller & Aranibar 1977, Liang et al. 2005, Belitski et al. 2008). This means that if only the informative IMFs can be extracted then ideally their information content should be equivalent to that of the original recordings as given in Eq. 5.4.

$$MI_{IMF_K} = MI_R \tag{5.3}$$

$$MI_{IMF_{best}} \leq MI_R \tag{5.4}$$

We analysed the information content of individual IMFs from a given set of field potential recordings and found that the information content of each IMF varies, as can be seen in Fig. 5.7. From the figure, it is clear that IMFs have different information content per frequency as compared to the original recording. However, at this point, it is not known which IMFs are taking part in the stimulus coding.

The average information content of several LFP recordings and their subsequent IMFs is presented in Table 5.1. The data is from visual stimuli where the activity is largely in the gamma band (Liang et al. 2005, Belitski et al. 2008), which is mainly constituted by the first IMF, therefore the information content in the first IMF is much greater than in the other IMFs but it is not known which other IMFs are contributing to the information coding. For other sensory stimuli,

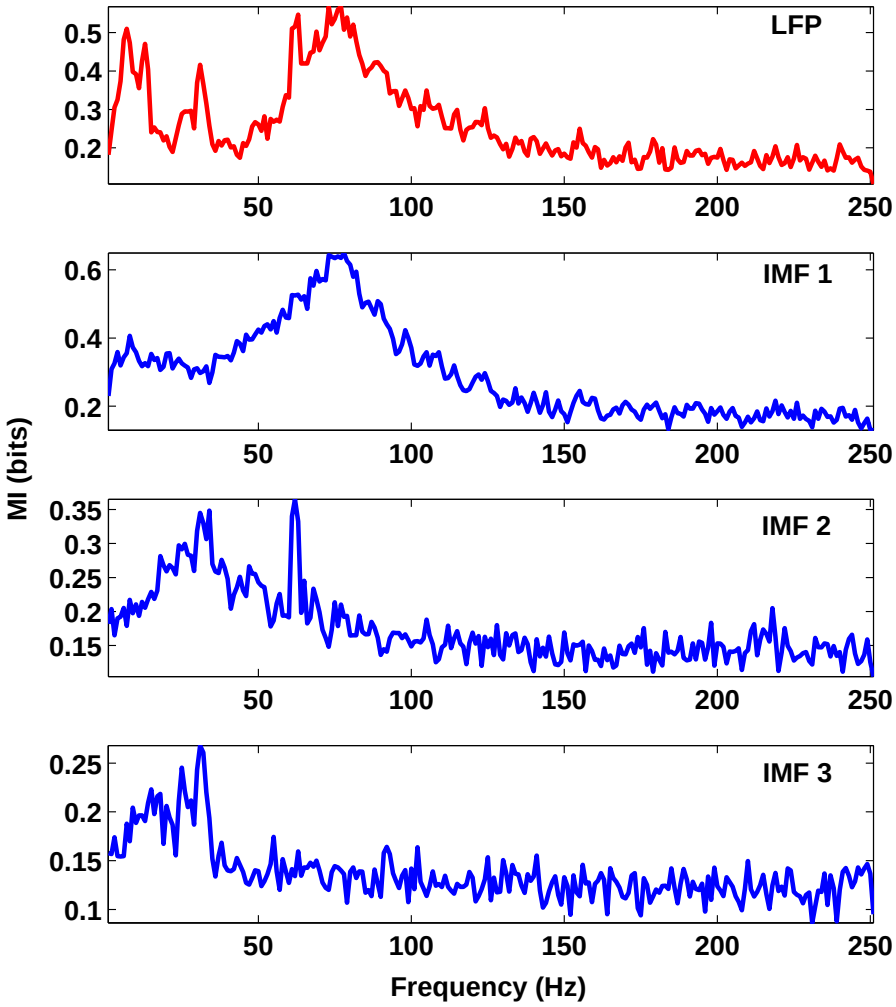

Figure 5.7: MI of an LFP recording and its first 3 IMFs.

Table 5.1: Average information content in LFP and corresponding IMFs.

LFP	IMF1	IMF2	IMF3	IMF4	IMF5
0.1183	0.0985	0.0267	0.0108	0.0038	0.0022
0.2158	0.1910	0.0398	0.0116	0.0040	0.0023
0.2711	0.2481	0.0457	0.0174	0.0116	0.0071
0.1804	0.1477	0.0331	0.0152	0.0051	0.0045
0.1449	0.1275	0.0335	0.0129	0.0047	0.0034
0.1311	0.1191	0.0296	0.0092	0.0034	0.0019
0.2150	0.1789	0.0307	0.0156	0.0084	0.0066

such as auditory stimuli, a lower order IMF may be the dominant information carrier. This means that order of informative IMFs depend on the nature of stimuli and the recording site. Therefore IP-EMD algorithm will extract different IMFs for different datasets.

5.2.3 Extraction of Information Preserving Modes

The last block of the Fig. 5.6 involves the extraction of informative IMFs or modes based on the information quantification results. Initially we used correlation for searching and extracting of informative modes (Mehboob & Yin 2009), then we used correlation entropy (CorrE) which significantly improved the performance of IP-EMD and is discussed in detail in Chapter 6. The algorithm details are given in the following section.

5.3 IP-EMD Algorithm Implementation

We developed IP-EMD algorithm in such a way that it can be used to extract the information carrying modes from any type of field potential (FP) recordings. The proposed method computes information content from the spectral attributes of decomposed IMFs. In this way it also quantifies the spectral coding in LFPs. The algorithm is composed of four basic steps.

- Application of EMD to FP recordings.
- Calculation of power spectra from FPs and corresponding IMFs.
- Discretization of the power spectra and calculation of mutual information (MI) of FPs and and corresponding IMFs.
- Extraction of the information carrying modes.

The IP-EMD framework can be used for data recorded against continuous or discrete stimuli by introducing a slight variation in the information analysis steps. We assumed that the data is arranged in the format given in Section 5.1.3. For analysis of continuous stimulus case, one can first divide the responses/recordings into small stimulus windows (rearrange R, $R = M \times S$) and then apply the EMD method to them. The other approach is to compute the IMFs first from the whole recording R and then divide the recordings and IMFs into stimulus windows. It was found that the latter approach gives better results in terms of frequency resolution and information analysis (Mehboob & Yin 2009). For discrete stimuli, the response matrices do not require any windowing as data for each stimulus is already stored in a separate dimension. The algorithm for finding the informative IMFs is presented in Table 5.2.

The EMD analysis can be carried out online or offline (Rilling et al. 2003). We carried out the IP-EMD analysis offline on the data recordings obtained in different experiments.

5.4 Results and Discussion

5.4.1 Results for Discrete Stimuli Recordings

The MI analysis for an LFP dataset against discrete stimuli is presented in Table 5.3. The recordings were made using a 4×4 array and two channels were used as reference electrodes. The first rows in the table represent the most informative IMF and the other rows show the subsequent informative IMFs and cumulative MI level. For example, only 3 or 4 IMFs out of resultant 8 in total have been found to be the informative ones and addition of remaining IMFs has little effect on the overall information level. This is shown in Fig. 5.8 and Table 5.3. The first and third columns show the informative IMFs and the second and fourth columns show the cumulative MI correlation values.

Table 5.2: Algorithm for extraction of information preserving modes.

1. Apply EMD to each FP of all the trials. This gives K number of IMFs for each trial.

2. For continuous stimulus case, divide each FP and IMF into suitable stimulus windows. Skip this step in case of discrete stimulus.

3. Calculate power spectrum density of all FPs and IMFs using multi-taper method Percival & Walden (1993).

4. Calculate MI for th FPs using Eq. 5.1, store it as MI_{FP}.

5. Calculate MI for all IMFs using Eq. 5.2. This gives $MI_{IMF}(n)$, n=1,2,...K.

6. Take each $MI_{IMF_n}(n = 1, ...K)$ and compare its percentage MI correlation with MI_{FP}.

7. Choose the best informative IMF that has the maximum MI correlation with the FP and store it to a set of $MI_{bestIMFs}$.

8. Choose the next informative IMF by adding each of the remaining MI_{IMFs} to the MI of selected IMFs and compute the correlation between their MI and MI_{FP}. If the correlation is greater than the previous value+0.05, it means that this IMF is adding significant amount of information. Choose this IMF as the next best IMF and update the collection of best IMFs. Otherwise quit.

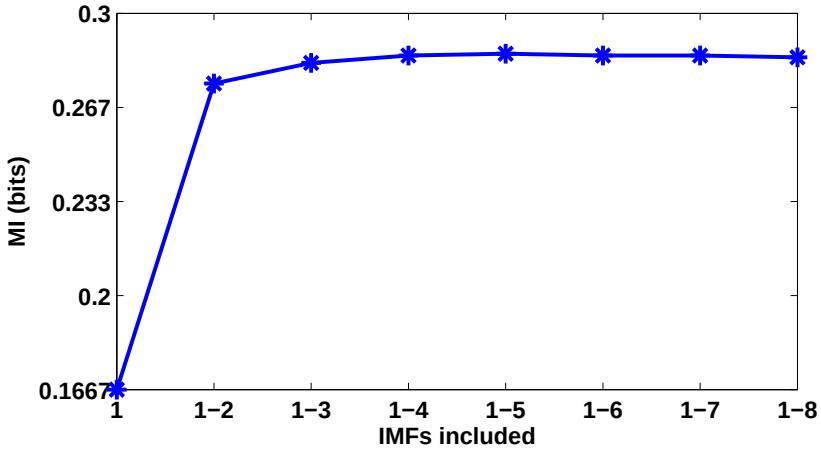

Figure 5.8: Cumulative MI levels of dominant IMFs. First 3 IMFs contain most significant information and adding more IMFs has little effect on information.

As can be seen in Fig. 5.8, adding insignificant IMFs does not alter the information content, these IMFs can thus be omitted. This indicates that a few informative IMFs are sufficient, in terms of information preservation and in representing and decoding the signal. For an artificially generated set of recordings, the profile of the Fig. 5.8 might be similar. But for a random dataset it will be simply flat as there will be no consistent probability distributions and mutual information in random signal.

Table 5.3: Results for single channel analysis against discrete stimuli.

Channel 1		**Channel 2**	
IMFs	MI Corr.	IMFs	MI Corr.
IMF_1	0.9218	IMF_1	0.8794
IMF_3	0.9520	IMF_3	0.9280
IMF_5	0.9709	IMF_5	0.9654
-	-	IMF_7	0.9708
Channel 3		**Channel 4**	
IMFs	MI Corr.	IMFs	MI Corr.
IMF_1	0.8872	IMF_1	0.7905
IMF_3	0.9423	IMF_3	0.9139
IMF_5	0.9866	IMF_5	0.9811
Channel 5		**Channel 6**	
IMFs	MI Corr.	IMFs	MI Corr.
IMF_1	0.9050	IMF_1	0.7758
IMF_3	0.9560	IMF_3	0.9365
IMF_4	0.9750	IMF_5	0.9770
-	-	IMF_7	0.981

A threshold (e.g. 0.05) is added to the information criterion in the step 9 of the proposed algorithm in Table 5.2 to ensure that the MI correlations increases by a sufficient amount with the inclusion of the next IMF. Examples of information comparison between several LFPs and their information preserving IMFs are shown in Fig. 5.9 which depicts a high level of information preservation and strong correlation between the cumulative MI of extracted IMFs and MI of LFP.

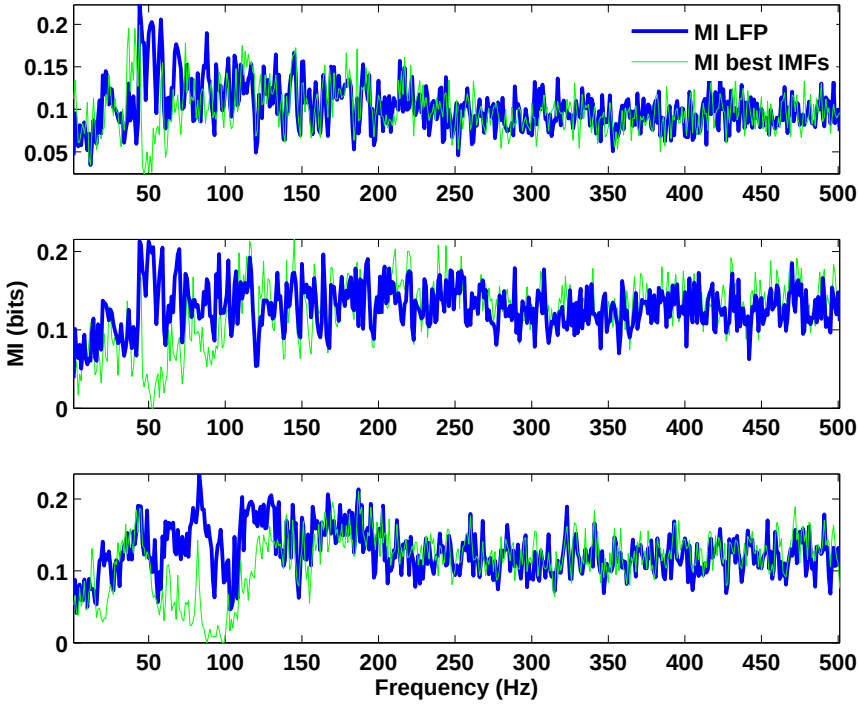

Figure 5.9: Information comparison between LFPs and the best (information preserving) IMFs obtained for channels 1-3.

5.4.2 Neural Data Classification using Extracted Modes

To verify and evaluate the performance of IP-EMD we used single trial binary classification to assign a trial to its parent class using different IMFs (Manyakov & Hulle 2008). We used the support vector machine (SVM) for this purpose, which can find an optimal hyper-plane to separate two classes. In SVM, a set of trials is divided into two groups. One group is used to train the SVM and then its classification performance is tested on the other group. Many SVM tools are currently available online. A complete list is given at (Hsu et al. n.d.). We used the SVM toolbox available from Chang & Lin (2001) and used the suggested parameters and grid search method given in the practical guide to SVM (Hsu et al. n.d.).

For classification purpose, each discrete stimulus was considered as a class. The data was divided into two pairs. One used for training and the other for

testing. Using the IMFs obtained from a trial, we evaluated if SVM can successfully identify the parent stimulus class. As mentioned earlier, the total number of IMFs obtained for this set was IMF_K=8 and from the IP-EMD analysis, sum of three (1,3,5) or four IMFs (1,3,5,7) were found to be most informative (Table 5.3) in almost all cases. We tested the classifier performance using (1+3)-IMF, (1+3+5)-IMF, (1+3+5+7)-IMF and (1+2+3...+8)-IMFs.

Results are presented in Table 5.4. The first 6 rows correspond to the 6 channels given in Table 5.3. From the table, it is clear that the classification performance is optimal by using only the informative IMFs (third column) in majority of the cases. For the second and ninth channel, four IMFs (1,3,5 and 7) were informative so the classification performance improved by inclusion of 7^{th} IMF, as can be seen from the table. The table shows that adding other (non-informative) IMFs does not significantly increase the information content. The reason is that most of the significant information is carried by the frequency ranges covered in these few IMFs and also proves that IP-EMD successfully extracted the informative modes from the LFP recordings.

Table 5.4: Percentage accuracy of single trial binary classification of LFPs using informative modes.

Channel	(1+3)-IMF	(1+3+5)-IMF	(1+3+5+7)-IMF	(1-8)-IMF
1	75	76.39	72.22	73.61
2	71.42	78.57	85.71	78.57
3	35.71	78.57	42.85	28.57
4	71.42	71.42	64.28	71.42
5	75	75	68.75	68.75
6	50	87.5	87.5	81.25
7	50	93.75	87.5	75
8	56.25	75	81.25	81.25
9	64.28	78.57	78.57	71.42

5.4.3 Results for Continuous Stimuli Recordings

The IP-EMD framework was also applied on recordings for continuous stimuli. For this dataset, it is found that the most informative IMFs lie in the gamma

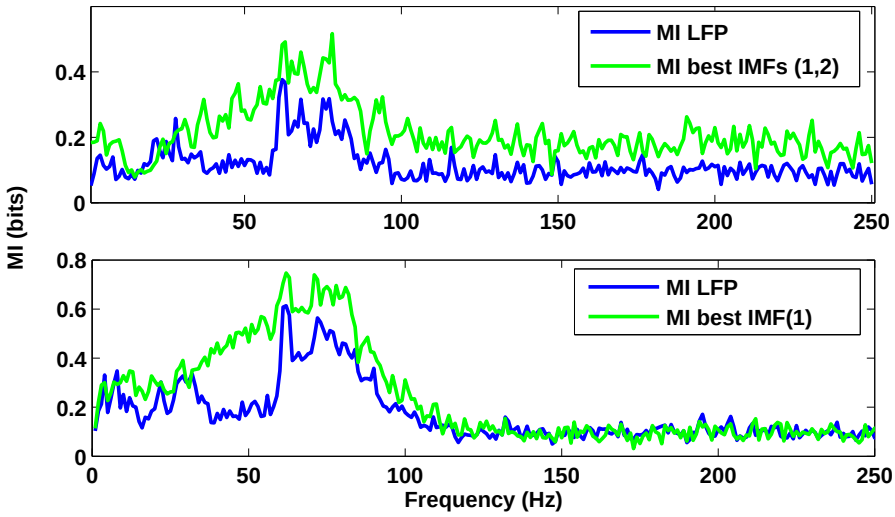

Figure 5.10: Results from two channels of the data recorded against continuous visual stimuli.

band and are carrying majority of the information. Addition of remaining IMFs showed minor effect on the information level. The MI analysis results from two channels are shown in the Fig. 5.10.

From the figure, it is evident that the largest peaks of information are in the frequency range between 50-100 Hz.An LFP recording and the information carrying oscillation (IMF_1) for the top case is shown in Fig. 5.11, which is clearly showing about 70 Hz oscillation as the main contribution and is not directly visible in the original LFP. The EMD, thus, has a clear advantage in this regard as these informative oscillations cannot be automatically extracted by other methods discussed previously, like FT or WT.

It is also important to note here that only one or two IMFs were extracted for this dataset and the information preservation is not completely satisfying the Eq. 5.4. The (green) plots for MI best IMFs, in Fig. 5.10, are exceeding the information threshold of LFPs. This shows biasing in the information estimation from best IMFs. To reduce this biasing and improve the performance of IP-EMD, we suggested few enhancements in the basic framework (Mehboob & Yin 2010) which will be presented in Chapter 6 along with the applications in which IP-EMD can be used for analysing neural field potentials.

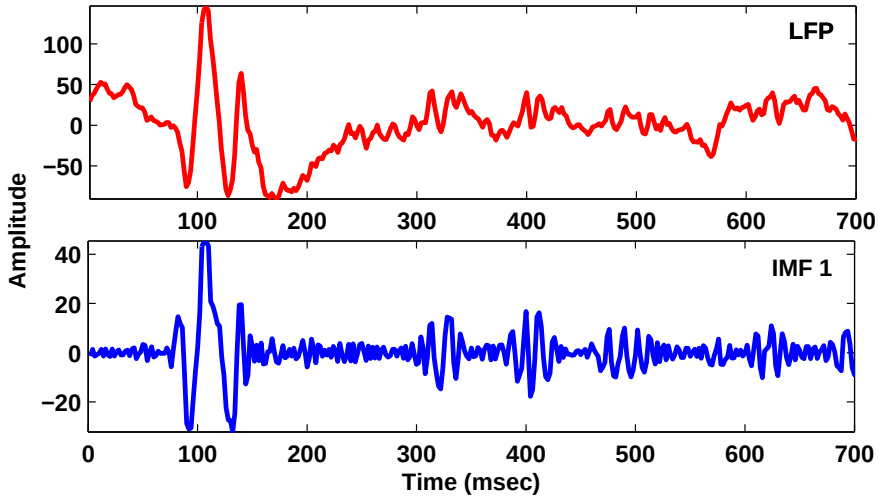

Figure 5.11: The LFP recording from the top channel in Fig. 5.10 and the extracted information carrying oscillation.

5.5 Summary and Conclusion

EMD can decompose a non-stationary signal into a number of IMFs. However, the information content of the IMFs vary radically and this shows that including all modes are not necessary in an information-preserving sense, as the stimuli may not be encoded by all the modes or all the frequency bands. Information-preserving EMD can thus be used to identify the most informative modes which give insight into the neural coding mechanism and a much clearer and informative representation of data and the extracted modes can also be used for further analysis as will be shown in Chapter 6.

Chapter 6

Improved Framework and Applications of IP-EMD

This chapter presents several improvements to the initially developed IP-EMD framework. By using the updated version, results obtained from the basic framework are further improved and it shows an increased level of information preservation with minimal biasing, which was previously observed. This is achieved by introducing changes in the information quantification procedure and more sophisticated criteria for extraction of informative modes. The chapter is organised as follows. First, it gives comparisons of the results obtained from the basic framework and the improved version, then the algorithmic details of the improved IP-EMD framework are given, and in last section various applications and advantages of IP-EMD for field potentials analysis are discussed.

6.1 Improved Algorithm for IP-EMD

The basic algorithm of IP-EMD was built on five steps which are shown in the block diagram of Fig. 6.1. However, in the results obtained from the basic framework, it was observed that the combined information from best IMFs was subjected to some biasing (e.g. left of Fig. 6.2) and ideally this should not be the case. The total information from best IMFs should be approximately equal to or less than the information in the original field potential and the information preservation from best IMFs should satisfy the condition of Eq. 5.4. To resolve this issue, we carefully analysed each step of the IP-EMD algorithm in Table 5.2 and finally suggested changes for the third and fifth block of the Fig. 6.1 (Mehboob & Yin

2009).

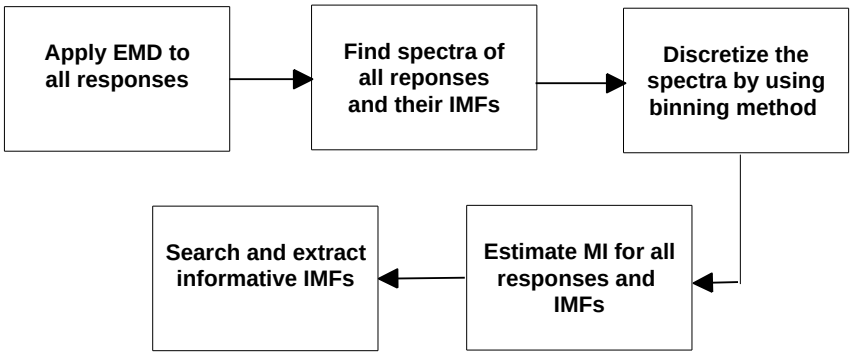

Figure 6.1: Block diagram for IP-EMD algorithm.

In the previous algorithm, for MI estimation, the binning was applied individually to the spectrum of each IMF and in few cases it resulted in biased MI estimation. This can be seen clearly in the left side plots of Fig. 6.2, shown by green lines where MI of the extracted IMFs exceeds the MI of the original response. These are the results shown previously in Fig. 5.10 in Chapter 5. From further analysis, it is found that the biasing effect can be effectively minimized by applying binning across spectra of all IMFs and then estimating the MI for each IMF individually.

The improved results are shown in the right side of Fig. 6.2, obtained from the MI estimations using new version of IP-EMD. By comparing the previous and new results it can be seen that there are two main differences, one is the reduced bias in information level, which is because of improvements suggested for block 3 of Fig. 6.1. The second difference is extraction of a greater number of best IMFs in the latter case, which is due the changes made at step 5 of Fig. 6.1.

In the previous approach, the filtration of informative IMFs was based on the cross correlation measure between MI(R) and MI(IMFs). Cross correlation is suitable for finding linear similarity between two time series (Brillinger 1979). Due to this reason, It was also observed previously that only one or two IMFs were retrieved in most cases, where other lower order IMFs could have been extracted. For instance, on left side of Fig. 6.2, it can be seen that there are three peaks of information with the largest peak lying in the range of 50-100 Hz and there are two smaller peaks below 50 Hz. The previous algorithm extracted only 1 or 2 IMFs lying in the gamma band, which shows weak information preservation.

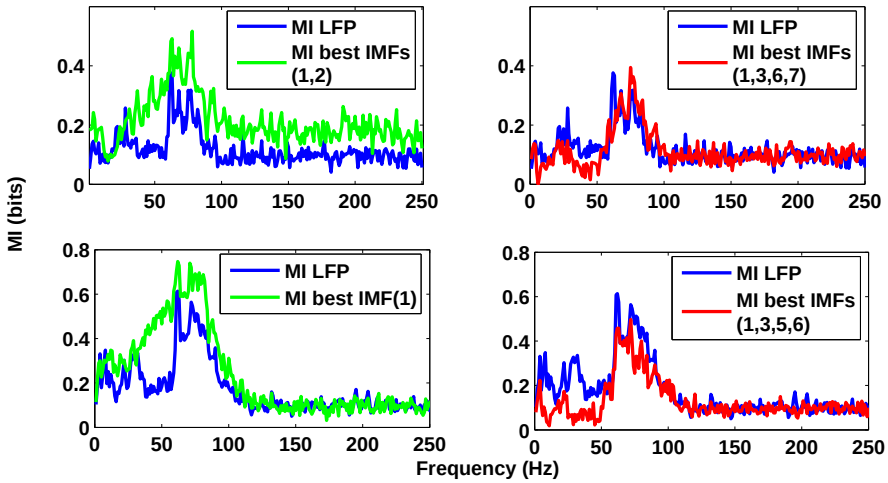

Figure 6.2: The comparison of results obtained by using previous proposed algorithm for IP-EMD and its updated version.

It was anticipated that using a nonlinear similarity measure could improve the extraction procedure and might result in extraction of more informative IMFs which may otherwise be missed by using the linear correlation. For this reason, we replaced the linear similarity measure with a nonlinear and more localized similarity measure called the cross correlation entropy measure or CorrE (Gunduz & Principe 2009). CorrE is a localized similarity measure based on information theoretic learning and can be used to find similarity between two random processes (Gunduz & Principe 2009) and to detect nonlinear characteristics in a given signal. The CorrE between two random variables can be found by:

$$CorrE\,(X,Y) = \frac{1}{L}\sum_{k=1}^{L} G\,(x_k - y_k) \tag{6.1}$$

where G is the Gaussian kernel of size ρ.

and

$$\rho = 0.9 \times (\sigma L^{-\frac{1}{5}})$$

L is the data length and σ stands for the minimum of the empirical standard deviation of data and the data interquartile range scaled by 1.34 as defined in Silverman's rule (Gunduz & Principe 2009). The kernel size works as a window to find similarity in the given area.

Our experiments showed that using the CorrE significantly improved the informative IMF extraction process. This can be noticed in the right plots of Fig. 6.2 where four IMFs are extracted instead of just one or two with a (combined) less biased information and better preservation of MI. Other examples are given in Table 6.1.

Table 6.1: Comparison of the results obtained in different channels from first version of IP-EMD framework and improved version.

	IMF extraction using correlation		IMF extraction using CorrE	
Channel No.	IMFs	MI Correlation	IMFs	MI CorrE
1	1,2	0.75-0.83	1,3,6,7	0.81-0.97
2	1	0.79	1,3,5,6	0.77-0.94
3	1,2	0.69-0.76	1,4,6,7	0.81-0.89
4	1,5	0.56-0.64	1,3	0.63-0.75
5	1,4	0.64-0.74	1,3,4,5,6	0.78-0.96

Table 6.1 shows comparison of the results obtained from the previous and improved IP-EMD. The first column of the table shows the IMFs extracted using the previous method and the third column shows the IMFs extracted using the enhanced framework. The second column shows the initial correlation between the MI(R) and MI of first extracted IMF (MI bestIMF1) and the final correlation between MI(R) (or MI(FP))and all the extracted IMFs (MI bestIMFs). The fourth column shows the initial and final CorrE between the MI(FP) and MI(bestIMFs). The first two rows of the table corresponds to the MI plots of Fig. 6.2. MI plots for last 3 rows are shown in Fig. 6.3.

The details of the algorithm are given in Table 6.2. The algorithm has been tested on several LFP, MEG and ECoG datasets. As shown previously, this version of IP-EMD framework performs better than the previous version. The new IP-EMD framework and the extracted informative modes offer many advantages and can be used in several applications.

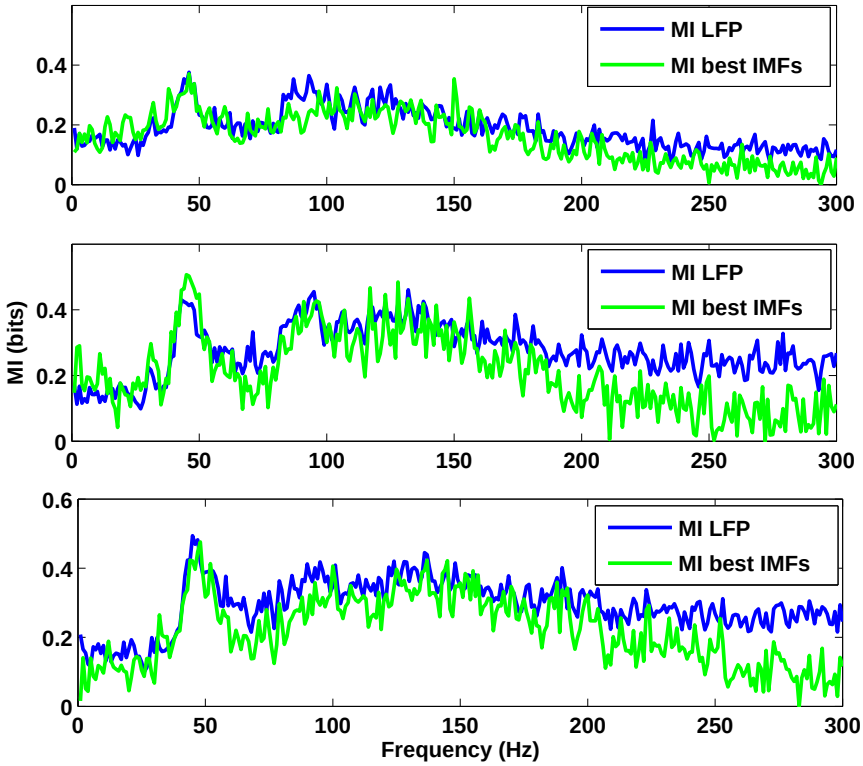

Figure 6.3: MI plots for LFPs and best IMFs extracted by improved algorithm for IP-EMD and using CorrE. MI-CorrE values are shown in last 3 rows of Table 6.1.

Table 6.2: Improved algorithm for information preserving EMD.

1. Apply EMD to all the responses or field potentials (FP) trials. This gives K IMFs for each trial.

2. For continuous stimuli recordings, divide each FP and IMF into suitable stimulus windows. Spike this step in case of discrete stimuli.

3. Calculate power spectrum density of all FPs and IMFs using MTM.

4. Discretize the FP power spectra for each frequency into equi-spaced bins and calculate MI for the FP using Eq. 5.1, store it as MI_FP.

5. Take the power spectra of all IMFs and discretize the spectra at each frequency into equi-spaced bins. Calculate MI for each IMF using Eq. 5.2. This gives MI_IMF (n), n=1,2,...K. (Note: In the previous algorithm, binning was applied on each IMF separately).

6. Take each IMF one by one and calculate the CorrE between active region of that IMF to the same region of MI_FP by Eq. 6.1. The active regions are the FP frequency bands with highest peaks of information.

7. Select the IMF with highest CorrEntropy and term it as maxCorrEntropy. Then select the IMF with next highest CorrE and add that IMF to the previous one. Calculate the CorrE of the resultant mode and the LFP. If the new CorrE is higher than the maxCorrE then keep this IMF and update the maxCorrE, else repeat the same procedure with the IMF of next higher CorrE. Repeat the same procedure for all IMFs CorrEntropies so that at the end a set of most informative IMFs will be obtained.

6.2 Applications of IP-EMD

The algorithm has various applications for field potentials analysis. The following section lists some of the applications and the results obtained on several LFP and MEG data sets.

6.2.1 Single Channel Analysis

One of the direct applications of IP-EMD is using single channel recordings which may be obtained from single electrodes as in EEG/MEG or by using multi-electrode arrays as in LFP or MUA.

A single channel study on a set of MEG recordings was also conducted. The data was recorded to study the coding analysis in motor cortex and analyse how wrist movement in different direction is encoded into the brain (Waldert et al. 2008). There are four discrete stimuli with wrist movement in forward, backward, left and right directions.

The result obtained using the improved IP-EMD framework is shown in Fig. 6.4. The figure shows activity in three frequency bands, which are reflected in the decomposed results. The extracted IMFs from a single trial recording is also shown in Fig. 6.5.

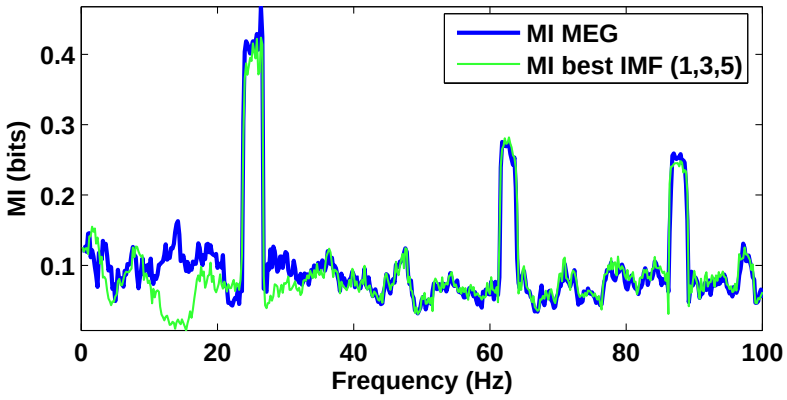

Figure 6.4: IP-EMD analysis on single channel MEG data.

6.2.2 Neuronal Population Activity Analysis

When data is recorded from multiple single electrodes or from a micro-electrode array, all the data can be collectively analysed using IP-EMD. This can be termed

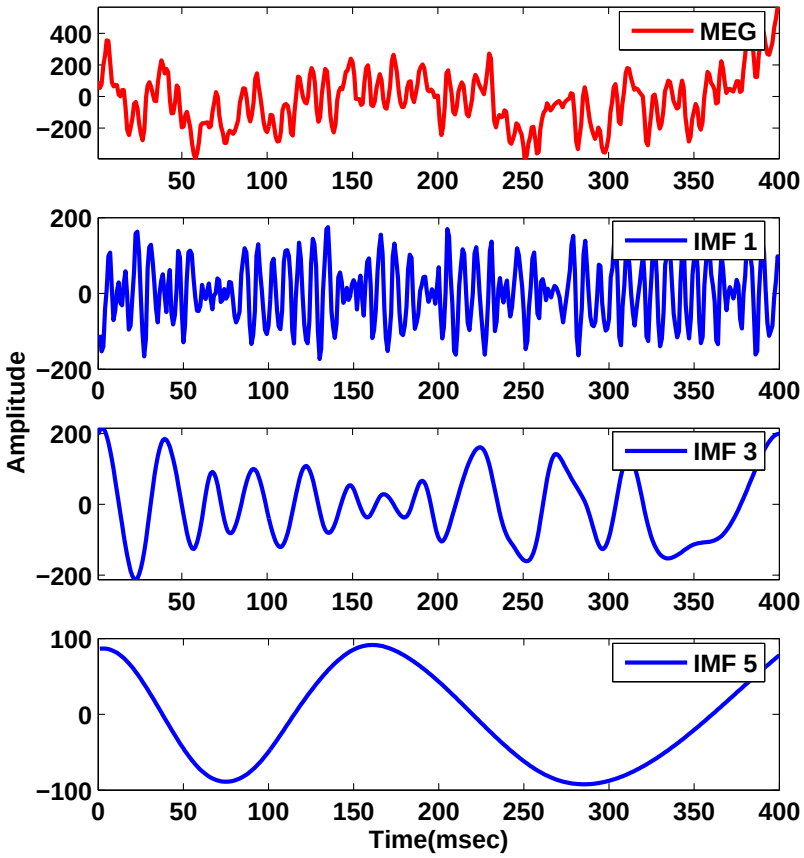

Figure 6.5: A single channel MEG recording and corresponding information-preserving IMFs.

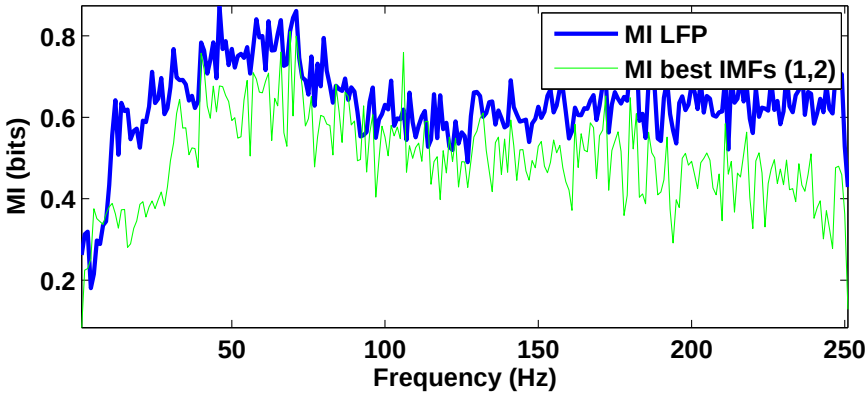

Figure 6.6: Neural population code analysis against a discrete visual stimulus.

population analysis as it will analyse activity of large neuronal networks in the regions covered by all the channels and gives insight into how the neurons in the observed area are encoding the stimuli.

MI analysis for the data (all channels) recorded against a visual grating is shown in Fig. 6.6. The data is recorded using 4×4 micro-electrode array and 4 channels were used as reference point and data was collected from 12 channels. The micro-electrodes which are used as reference points (without channel numbers), are connected often onto the brain surface. Data from the rest of the electrodes are then used for analytical purpose. The results show that only two IMFs carry most of the information. The extracted information carrying IMFs are shown in Fig. 6.7. The first IMF (about 90 Hz) indicates a high-gamma oscillation. The second IMF shows a low-gamma oscillation (about 50 Hz).

The population activity recorded from 10 MEG channels against wrist movement in 'right' and 'forward' direction is shown in Fig. 6.8. The activity for both stimuli is in the same frequency regions; the only difference is that the information level obtained in the first case is slightly higher than the second case. An MEG recording for the 'right' movement direction and the extracted IMFs (1,3,4) are shown in Fig. 6.9.

6.2.3 Information Connectivity Analysis

For multichannel recording experiments, it is possible to study the connectivities based on MI analysis. Connectivity between channels reveals synchronised firing patterns among these channels or population of neurons. An example of

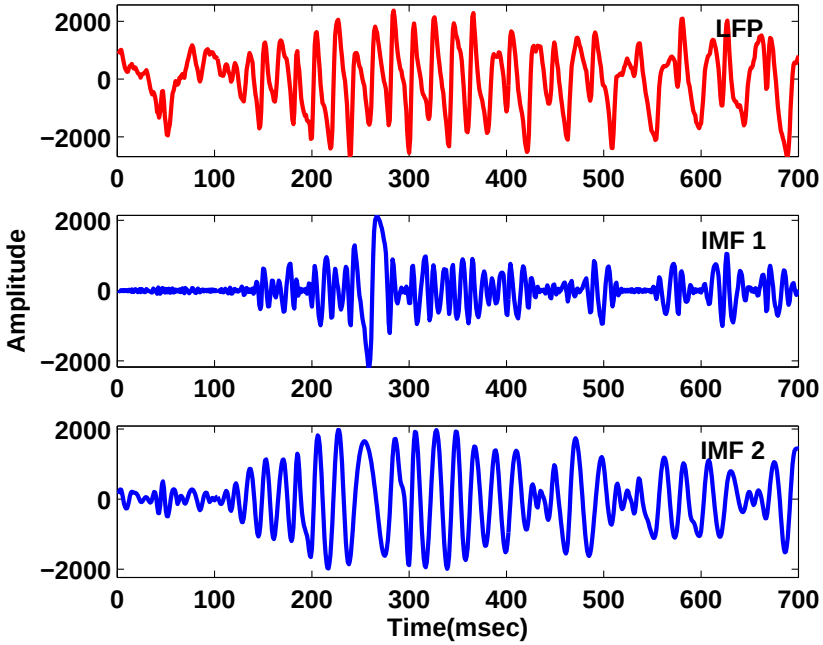

Figure 6.7: An LFP recording and the information carrying IMFs.

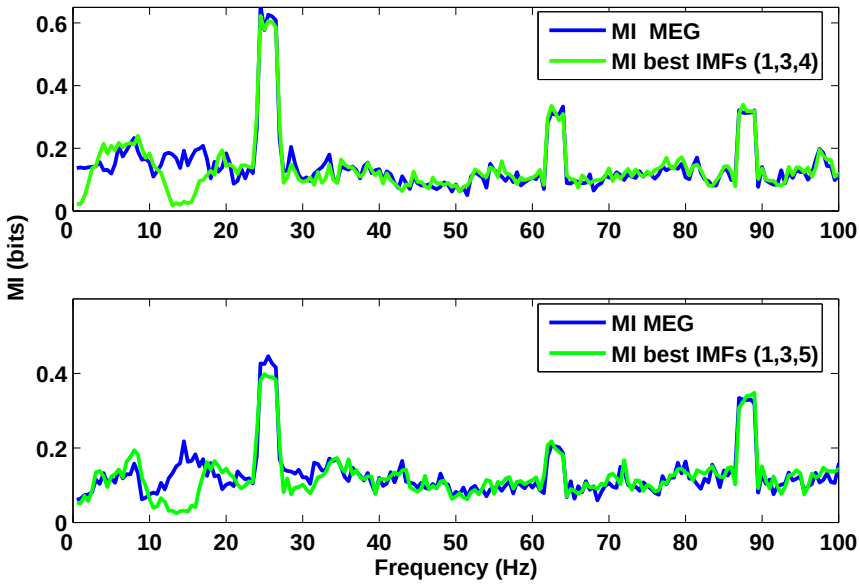

Figure 6.8: Population activity analysis (MI) against 'right' and 'forward' wrist directions. The responses were collected from a 8×8 microarray.

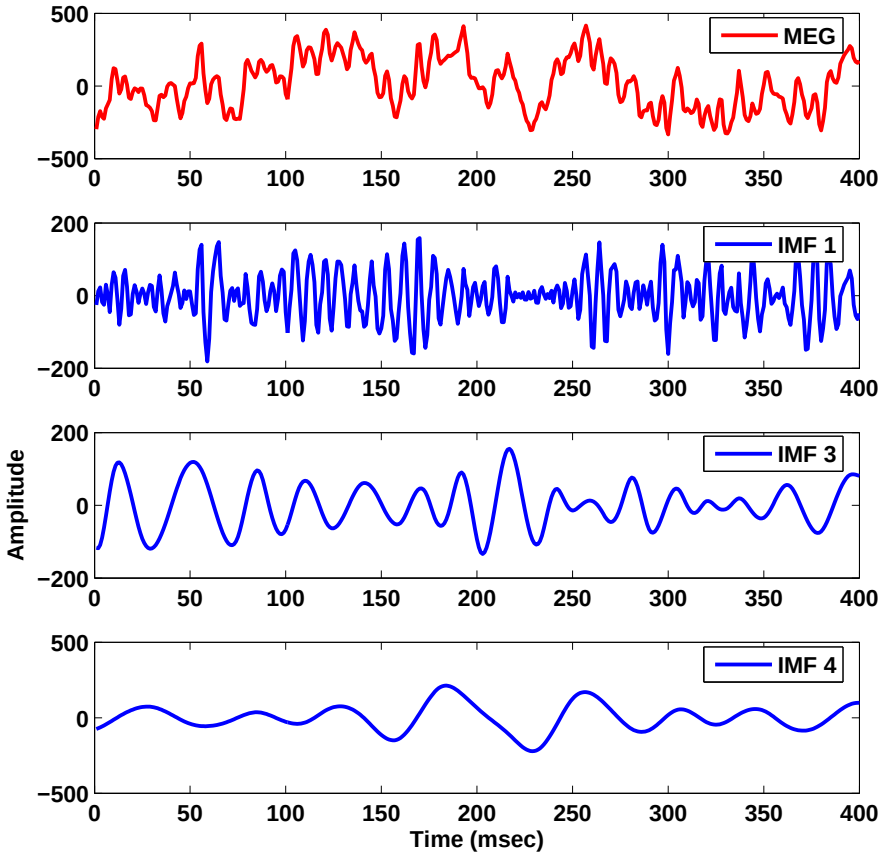

Figure 6.9: Population activity analysis (IMFs) against wrist movement in 'right' direction. The responses were collected from a 8×8 microarray.

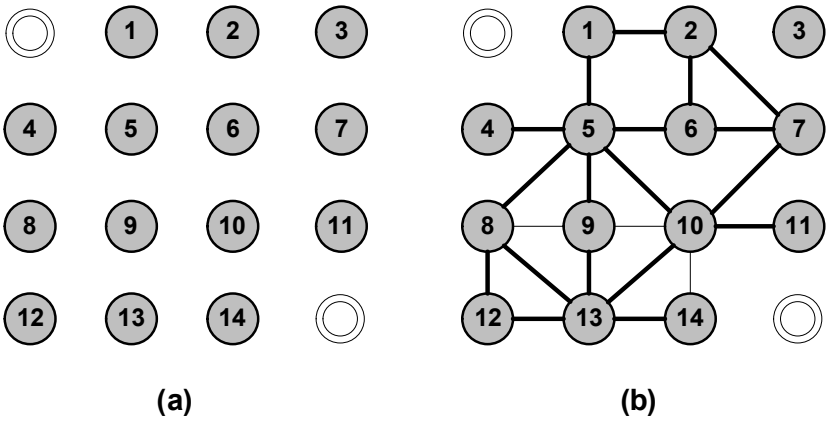

Figure 6.10: An example of a 4×4 microarray.

information connectivity diagram is shown in Fig. 6.10.

The spectral information connectivity among multiple channels can be calculated by calculating information contained in individual channels. The information connectivity analysis can be carried out by using Eq. 6.2.

$$MI(C; R_{Pwr}(f)) = \sum_{c} P(c) \sum_{R_{pwr}(f)} P(R_{pwr}(f)|c) \log_2 \frac{P(R_{pwr}(f)|c)}{P(R_{pwr}(f))} \tag{6.2}$$

where $R_{pwr}(f)$ can be power spectrum of the field potential responses or the informative IMFs in a given channel.

The comparison of MI of field potential recordings, or their informative IMFs, from different channels provide information connectivity between these channels and quantifies the information coherence between neighbouring channels. By introducing delays, one can further analyse causal relationships among different channels. Such analysis help understand information flow or information transfer between different brain areas. A typical method for analysing causal relationships between different regions of brain is by means of Granger causality (Granger 1969). We have tested information preserving IMFs to study causal relationships among different channels of LFP recordings. The data used is from an experiment on visual attention of a subject (Manyakov & Hulle 2008). The two stimuli presented are gratings of two different orientations. The subject was rewarded for one stimulus and not for the other. The stimuli are shown in Fig. 6.11.

The data was recorded from a 10×10 electrode array and four of the channels were un-wired for use as reference points. The proposed method can be applied

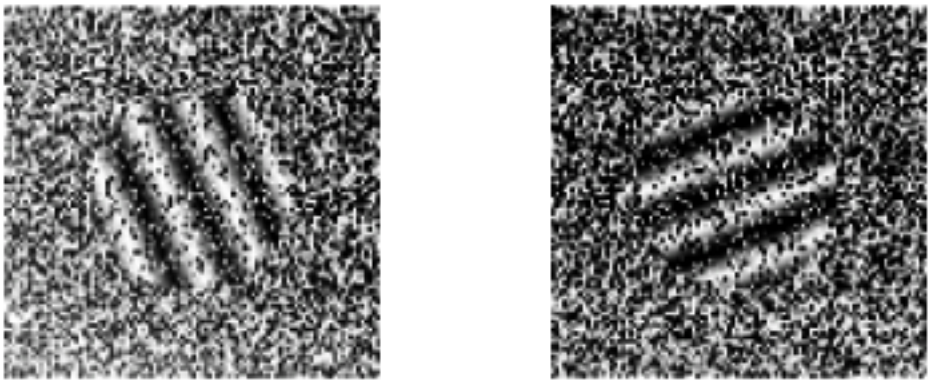

Figure 6.11: Discrete rewarded (right) and unrewarded (left) grating stimuli.

for information connectivity and synchronisation analysis.

The information connectivity diagram for a typical channel is shown in Fig. 6.12. For all its neighbouring channels, the first IMF was found to be the most informative one. The only exception was for channel 18, for which the information was so low that no IMF was found to be informative with the channel under study. The information profiles also show the levels of information transfer. The dotted lines show weak connectivity (with mean MI$<$0.025 bits) while the bold lines show strong connectivity (mean MI$\geq$0.25 bits) or synchronisation between the channels. Alternatively, one can use the thickness of the line to indicate the strength of connectivity.

The analysis has been tested on other channels and Fig. 6.13 shows the connectivity of 56 (out of 96) channels.

6.2.4 Hilbert Analysis

The information contained in a continuous signal is confined in its spectral attributes that includes both magnitude and phase. The information extracted from magnitude spectrum may not be sufficient to differentiate certain stimuli. For instance, the information analysis of power spectra (magnitude) of the LFPs with stimuli of Fig. 6.11 is depicted in Fig. 6.14. The two grating stimuli have different orientation. However, from Fig. 6.14, it can be seen that MI plots for both stimuli lie in the same frequency ranges and have similar profiles. Based on the MI profile, the stimuli are indistinguishable.

For both rewarded and unrewarded stimuli the first IMF was found to be

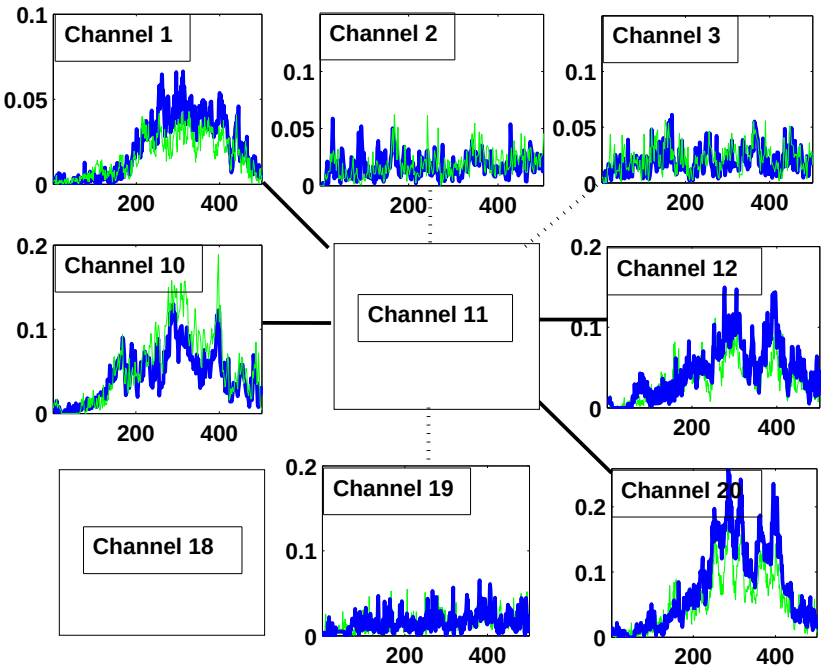

Figure 6.12: Information similarity between channel 11 and its neighbouring channels. The blue plots are for original recording and the green (dark) plots are the ones obtained using IP-EMD modes. Only the strong connectivity is shown.

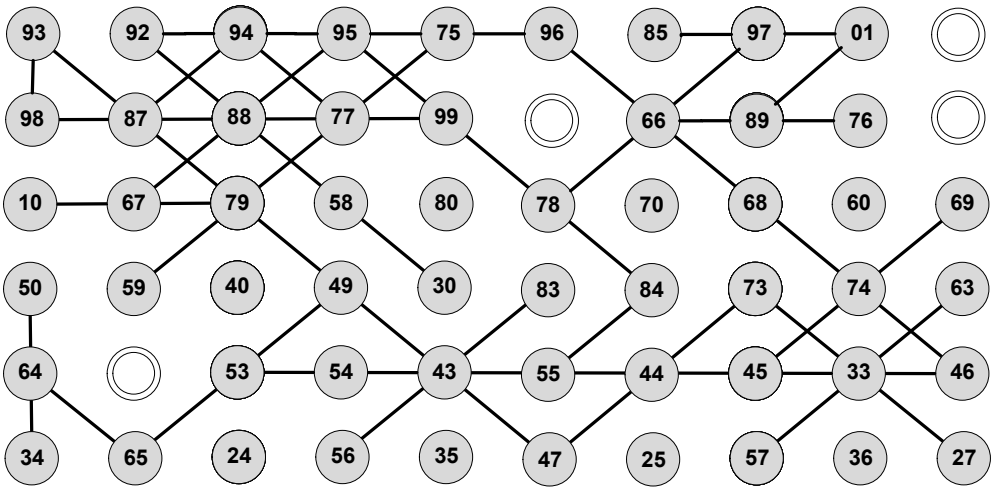

Figure 6.13: Information connectivity among channels. The figure only shows the information connections for 56 channels (out of 100 in total). Only the strong connections are shown here.

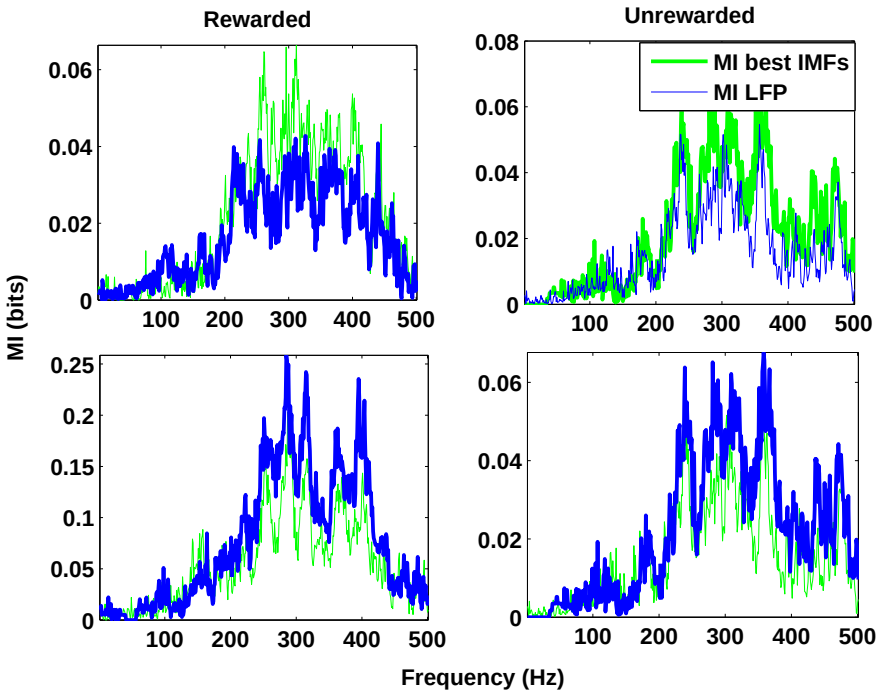

Figure 6.14: Indistinguishable information of the two channels for the rewarded and unrewarded stimuli.

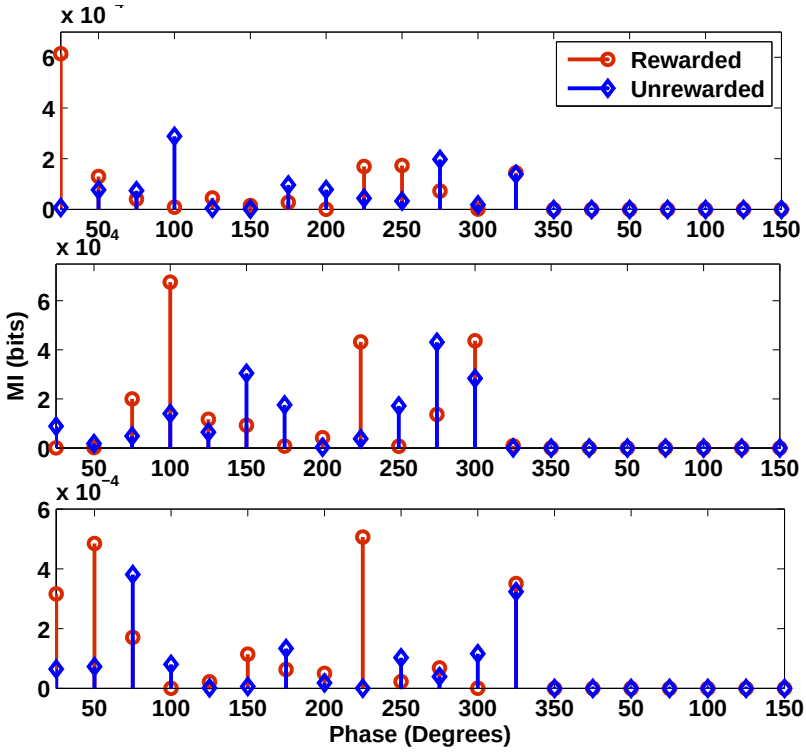

Figure 6.15: Information calculated from the phase of the first dominant IMF of both rewarded and unrewarded stimuli. Stems with circle and diamonds show the information for rewarded and unrewarded stimuli, respectively.

the dominant information carrier. We proposed to carry out additional analysis using phase information by employing the Hilbert analysis on extracted modes. The information obtained from the Hilbert phase (Eq. 6.3) of the first IMF of both rewarded and unrewarded stimuli was used for comparison. The results of three typical channels are shown in Fig. 6.15. As can be seen, the information of the phase spectra of the dominating IMFs differs markedly in these two stimuli. In this way IP-EMD might be used for stimuli discrimination and further for classification purpose.

$$I(S;\theta_{IMF}) = \sum_{s} P(s) \sum_{\theta_{imf}} P(\theta_{imf}|s) \log_2 \frac{P(\theta_{imf}|s)}{P(\theta_{imf})} \tag{6.3}$$

Although the Hilbert phase has been used in LFP and EEG analysis, most work has been on analysis of phase synchronisation and phase locking phenomena in different frequency bands, some of which are discussed earlier. Synchronisation analysis in EEG can help in distinguishing health issues (Kramer et al. 2007,

Table 6.3: Algorithm for neural data compression using IP-EMD.

1. Extract the IMFs for the given set of recordings.
2. Find the information preserving IMFs using algorithm given in Table 6.2.
3. Find the extrema for all the extracted modes.
4. Quantize and encode the extrema.

Ahmadlou & Adeli 2010). One of the recently proposed and tested approaches makes use of EMD and single trial phase locking (Sweeney-Reed & Nasuto 2007, 2009). The approach has been applied to EEG data. First, the EMD is carried out on EEG signal and then the Hilbert phase is calculated for all the IMFs obtained. For each IMF, the series of instantaneous phases are then obtained and phase locking is obtained between all the different IMF combinations by using single-trial phase locking values. Our approach is different in the sense that it employs the phase analysis using only the informative IMFs.

6.2.5 Neural Data Compression

We presented a proposal for neural data compression by using the IP-EMD generated IMFs (Mehboob & Yin 2010). Not much work has been done for neural data compression and due to advancements in micro-electronics technology, a huge number of data recordings are collected in experiments. Storing and processing of these neural recordings is not a trivial task and their storage and sharing requires an efficient compression algorithm. The idea for the compression algorithm is based on discarding the data points that do not contribute to stimulus coding so that the information loss in the compressed dataset is minimal or negligible.

We made initial investigations to develop a compression algorithm that can make use of the informative modes extracted by IP-EMD. The approach is similar to an EMD based audio compression (Khaldi et al. 2010) but in this schema all IMFs are used for compression. The compression algorithm is based on few simple steps, given in Table 6.3.

The compressed modes (and field potentials) can be reconstructed by interpolation and IMFs summation. We used the Huffman coding for encoding purpose. An example of spline interpolation of an IMF extrema and the reconstruction obtained from it is shown in Fig. 6.16.

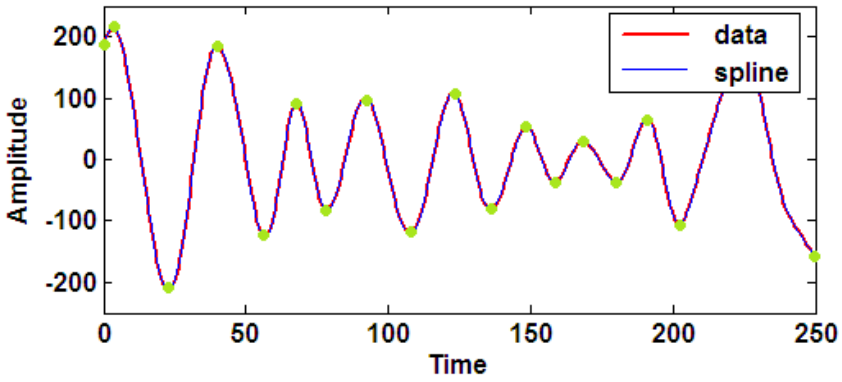

Figure 6.16: An original IMF and its reconstruction by spline interpolation. Green points are showing the extrema.

The algorithm can be improved by introducing thresholding for reducing the number of extrema in each IMF. But this should not effect the information level. In the initial study, we tested the approach by using all the extrema for compression. Using this approach, a compression ratio of 0.18 and lower has been achieved. The compression ration is defined as:

$$Compression\ Ratio = \frac{Magnitude\ of\ compressed\ data}{Magnitude\ of\ uncompressed\ data}$$

6.3 Conclusion

An improved version of information-coupled EMD framework has been developed for analysis of field potentials. It has been shown that EMD decomposes a non-stationary, nonlinear signal into a number of intrinsic oscillations. With the basic version of IP-EMD some biasing was observed in a few cases. This issue has been resolved by improving IMFs spectrum quantization. The enhanced version uses CorrE for informative modes extraction and extracts most informative IMFs only (usually 1–4). These information carrying IMFs reveal the dominating oscillations in the signal, thus can greatly simplify the analysis of potentially complex signals and facilitate their interpretation. The proposed method has been applied to LFPs and MEG from single and multiple channels and shows the information carrying frequency bands that otherwise are not directly visible in the signals.

The method can also be applied for information connection analysis among recording channels. The Hilbert analysis of informative IMFs can further help

identify discriminating features against different stimuli, when the magnitude information is not sufficient. Further research can incorporate time delay in mutual information analysis in order to reveal information flow (directions) among channels. A toolbox has been built to offer the analysis for wider applications and research purpose, the details of which are presented in Chapter 7.

The initial analysis of the approach adopted for compression has also shown some promising results. Further investigation can be conducted to achieve better compression rates with minimal information loss. It has been shown that the improved IP-EMD framework offers many advantages for field potentials analysis. Some examples are presented in this chapter. Some of the possible application of IP-EMD and modes obtained from IP-EMD analysis are summarised in Fig. 6.17. The upper main block is listing the basic steps involved in IP-EMD algorithm.

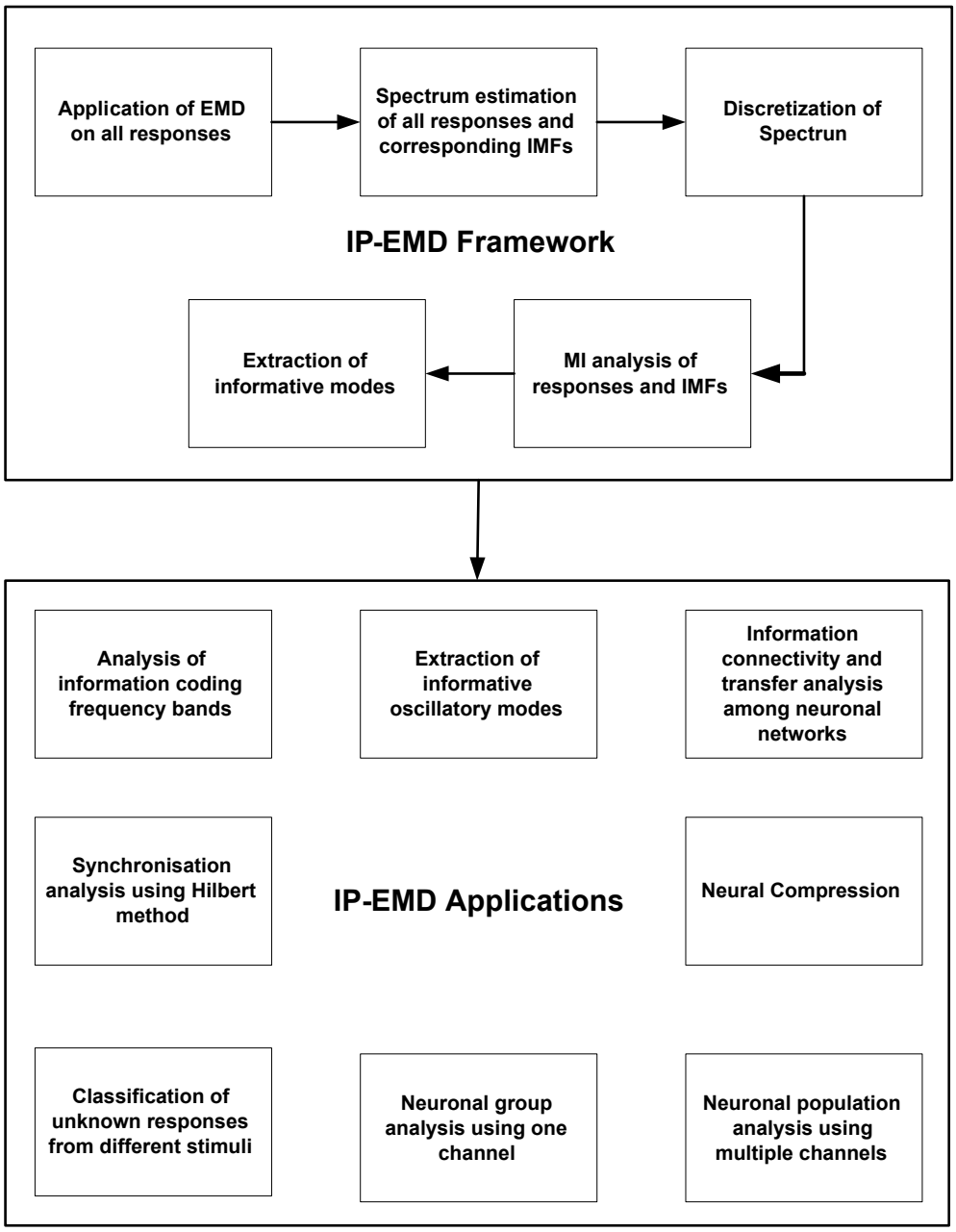

Figure 6.17: Summary of IP-EMD algorithm and its applications.

Chapter 7

Information-Preserving EMD Toolbox -ENIP v.1.0

The proposed framework has been developed into a MATLAB (Moler n.d.) toolbox for wider generic applications. This section describes the initial design and implementation of this toolbox. This is also available as a freeware (Mehboob & Yin 2011). The list of implemented features are:

7.1 Key Features

- Single channel recordings analysis.
- Population activity analysis.
- Information connectivity analysis between channels.

The information-preserving EMD based toolbox is available with the title 'ENIP' (EMD based neural information processing). The toolbox is built using MATLAB because it is one of the widely used languages for neural data analysis. The following sections discuss briefly the design and implementation of the toolbox.

7.2 Toolbox Design

The flowchart for the toolbox is presented in Fig. 7.1. The figure shows the working flow of the toolbox.

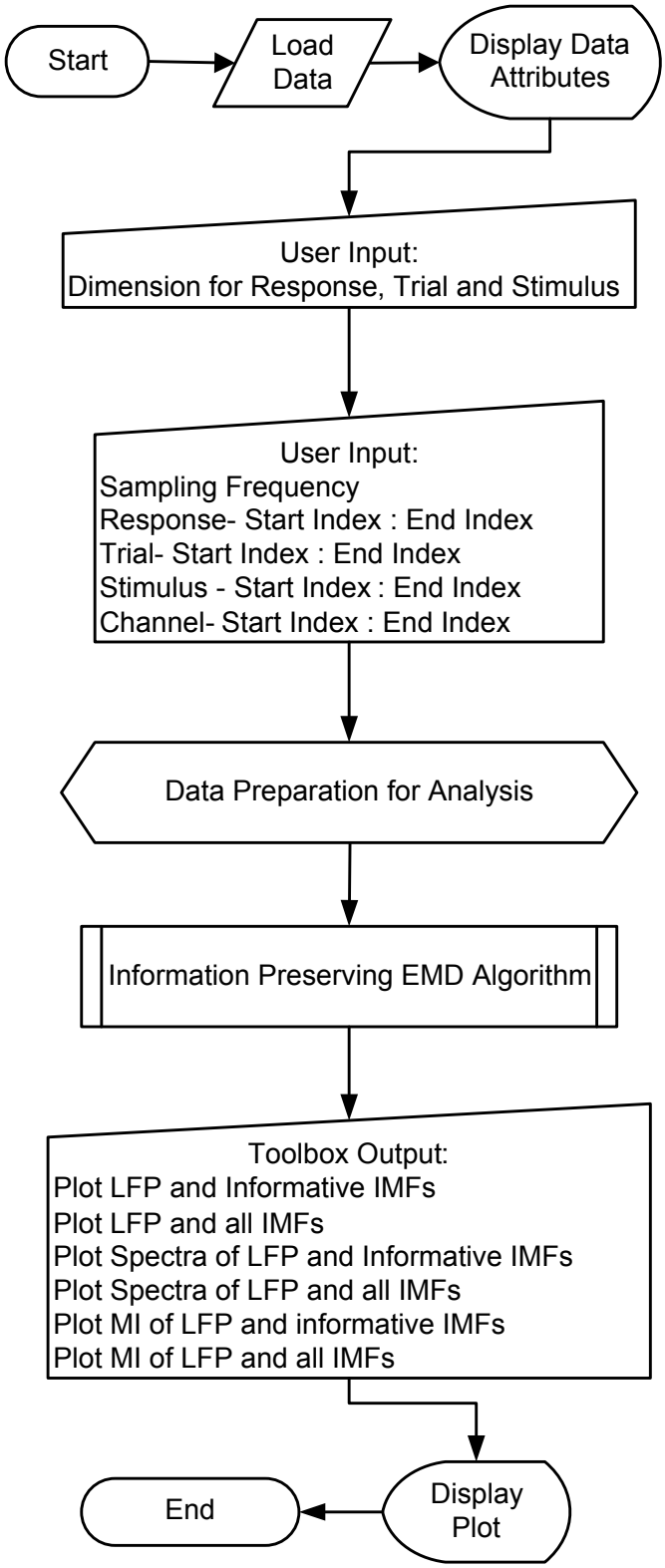

Figure 7.1: Flowchart showing the ENIP toolbox GUI implementation.

The interface is divided into three main blocks as can be seen in Fig. 7.2. The right most block is for the input and the left two are used for displaying plots for the IP-EMD analysis. Some textual information about the number and order of extracted modes is also displayed in the text box above the 'Reset' button of the input panel.

7.2.1 Data Input

The toolbox takes the data file in MATLAB format and assumes that data has already been arranged in a format as described in Chapter 5.

$$Response \times Trial \times Stimulus \times Channel\,(RTSC)$$

If this is not the case, user can enter the correct dimensions and then toolbox computes information based on the dimensions and parameters given for analysis. When a data file is loaded, its size and dimension information are displayed and then user can enter the other parameters for analysis. A snapshot for the input panel is given in Fig. 7.3.

7.2.2 Input Parameters

7.2.2.1 Data File

The data dimension parameter can take a value of 1–4 depending on the format of data file. Currently MATLAB data files with extension .mat are supported.

7.2.2.2 Data Dimension

The 'Dimension Index' default values display indexes as:

Response dimension - 1

Trial Dimension - 2 and

Stimulus Dimension - 3 for the data loaded in to the toolbox.

If data is four dimensional, the fourth dimension is assumed to be for the channels. Users can change the orders and channel dimension is selected accordingly.

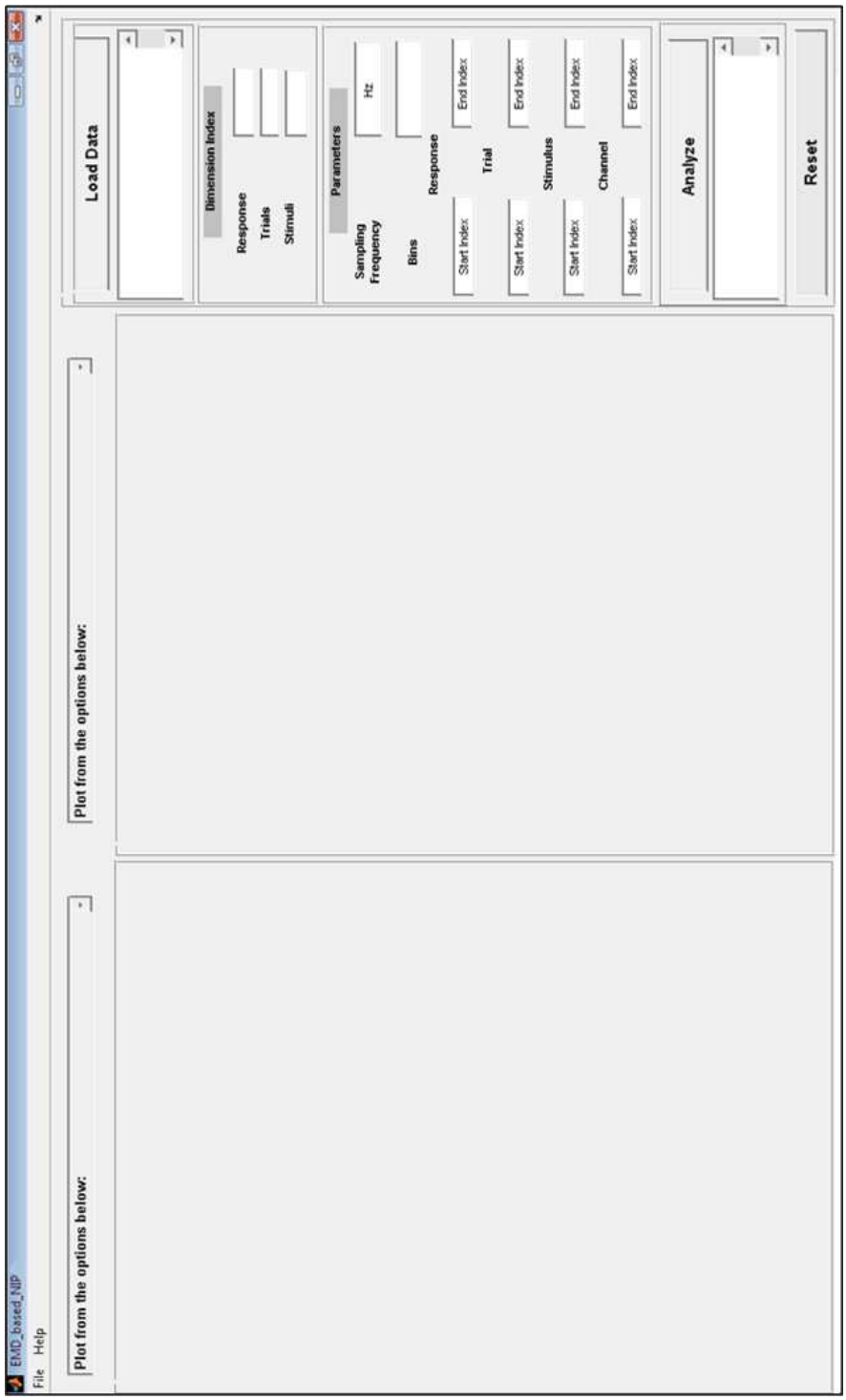

Figure 7.2: ENIP toolbox interface.

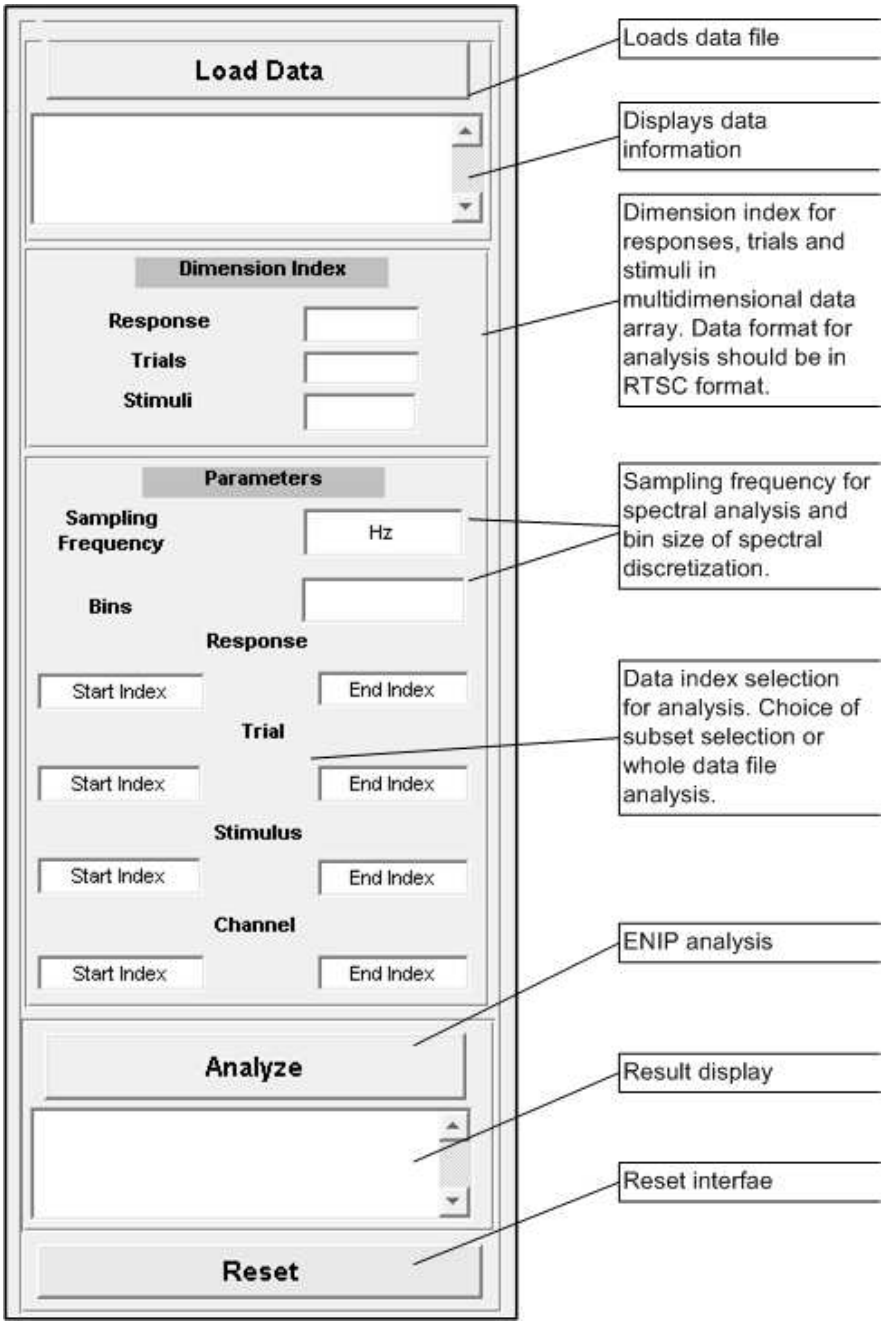

Figure 7.3: ENIP toolbox input panel.

7.2.2.3 Sampling Frequency

The default sampling frequency is set to 500 Hz and this is an important parameter since the spectra are calculated based on it and results can be misinterpreted because of it. For instance, 1 kHz sampling frequency will give spectra in a range of 500 Hz and 500 Hz sampling frequency gives spectra up to 250 Hz.

7.2.2.4 Binning

A binning size around 5 or higher can be used for analysis. The toolbox generates an error message regarding binning size if the bin size mentioned is less than 2 or greater than the total number of unique values present in the spectra.

7.2.2.5 Data Indexes for Analysis

The 'Data indexes' default values are set according to the input data file size in $RTSC$ format with R responses, T trials, S stimuli and C channels. For a three dimensional datafile C is assigned a value of 1. For instance, if a dataset with the dimension $200 \times 50 \times 6$ is loaded into the toolbox, the indexes take the values as:

Response : Start Index– 1 ———— End Index – 200

Trial : Start Index– 1 ———— End Index – 50

Stimulus : Start Index– 1 ———— End Index – 6

Channel : Start Index– 1 ———— End Index – 1

The user can change the index values to analyse a subset from the datafile. For example if it is important to analyse the data in the first 100 msec, the 'End Index' value should be changed from 200 to 100. Similarly if analysis is to be carried out on last 3 stimuli the 'Start index' value of Stimulus should be changed to 4.

Similarly, if a data file is loaded in $RTSC$ format with dimensions $1000 \times 200 \times 8 \times 10$, the indexes are assigned values as:

Response : Start Index– 1 ———— End Index – 1000

Trial : Start Index– 1 ———— End Index – 200

Stimulus : Start Index– 1 ———— End Index – 8

Channel : Start Index– 1 ———— End Index – 10

These default options will do the analysis on all channels recordings giving a population activity IP-EMD analysis. For single channel analysis the 'Channel Start Index' and 'Channel End Index' should be assigned the same values. The

toolbox gives information connectivity analysis between two neighbouring channels when the 'Channel Start Index' (e.g. 1) is assigned a value one less than the 'Channel End Index' (e.g. 2).

Toolbox will generate error message if an invalid index value is entered, for instance, a 'Start Index' smaller than 1 or an 'End Index' larger than R, T, S or C will give error. In the previous examples 'Responses End Index' value set to 1500 will give error. Also the 'Start Index' values should be less than (or equal to in case of channel) 'End Index'.

7.2.3 Toolbox Output

7.2.3.1 Output Options

- Field potential and (sum of) informative modes.
- Spectral distribution of field potentials and corresponding informative modes.
- Information quantification plots for field potentials and informative modes.
- Plot of all IMFs (informative and non-informative).
- Spectrum of all IMFs.

These list of options in the toolbox interface is shown in the snapshot of Fig. 7.4. The two panels for plots help in comparing informative and non informative IMFs and their subsequent frequency bands.

After the completion of analysis, the output window displays a FP trial, its corresponding IMFs and the information-preserving IMFs. User can also view the spectral distribution of the FP and IMFs. The MI of the original recording and the MI from the informative IMFs are also displayed. A snapshot from a FP result is shown in Fig. 7.5 and Fig. 7.6.

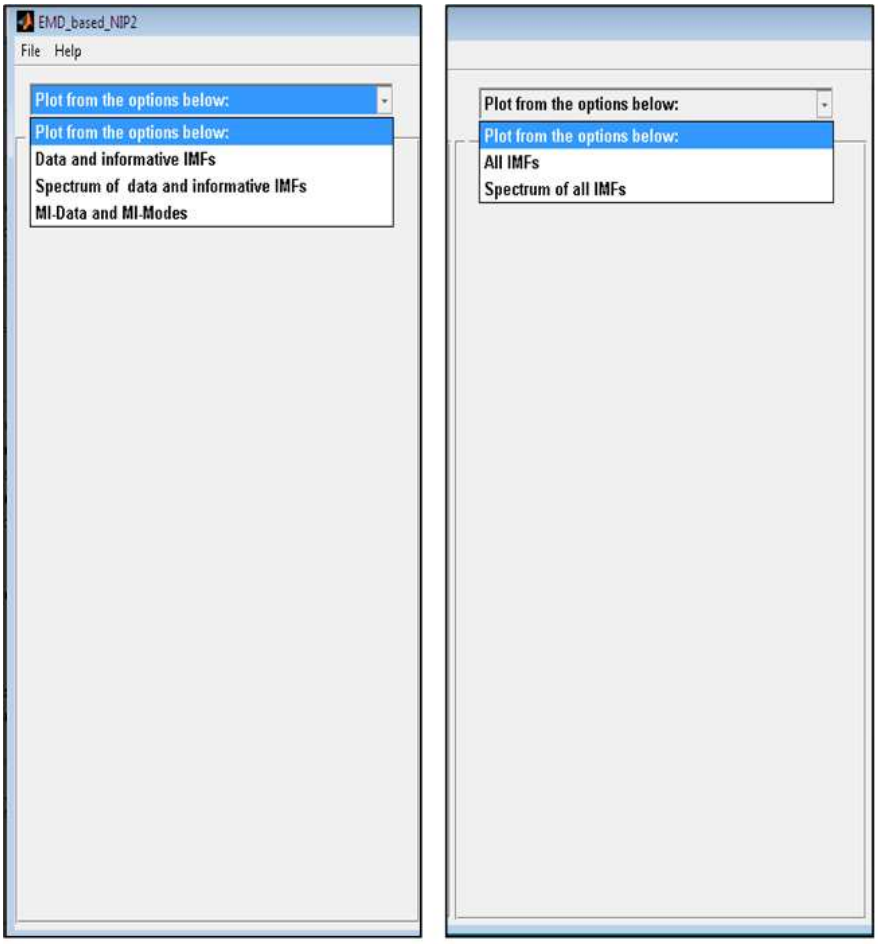

Figure 7.4: Toolbox output options.

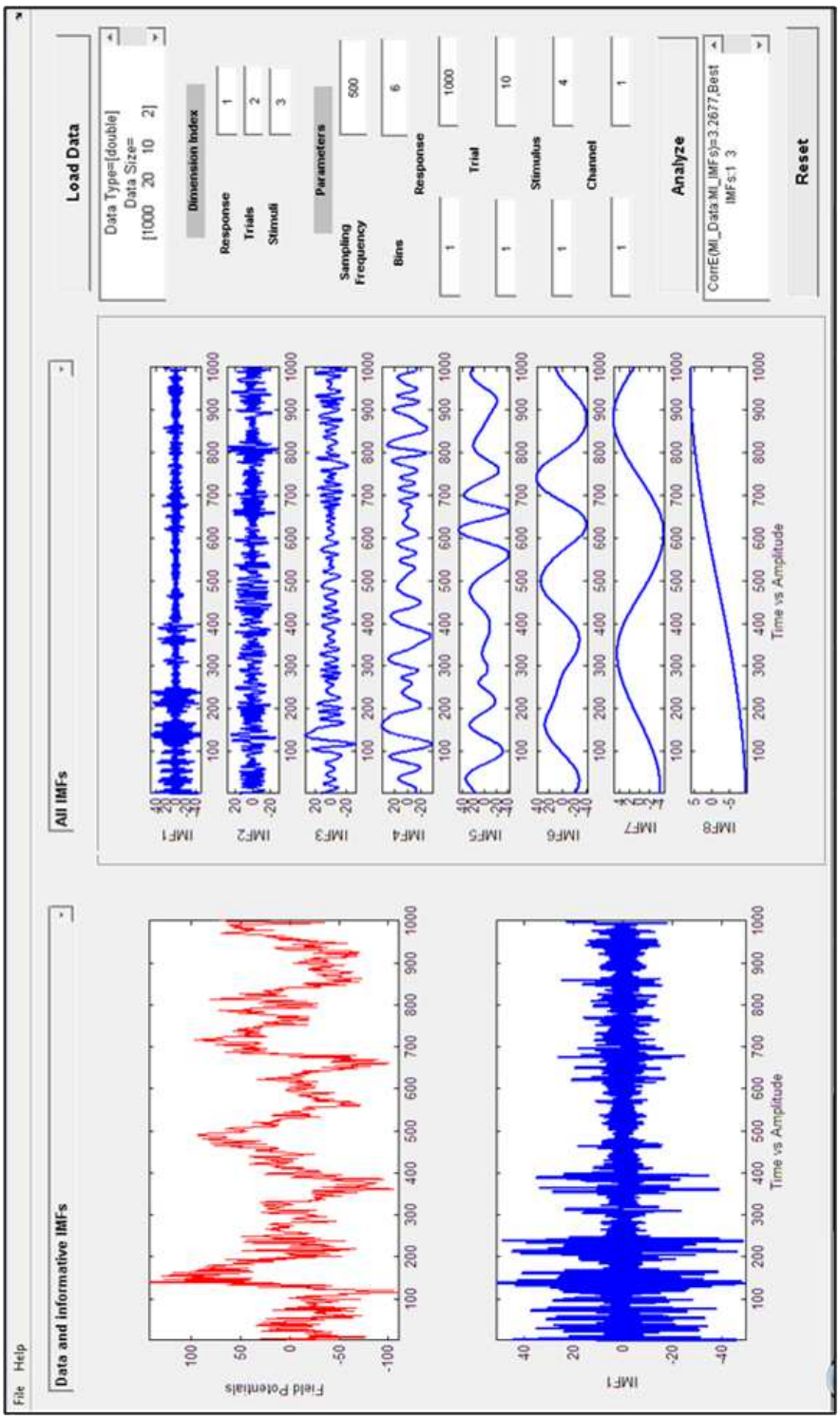

Figure 7.5: A snapshot of the ENIP output plots.

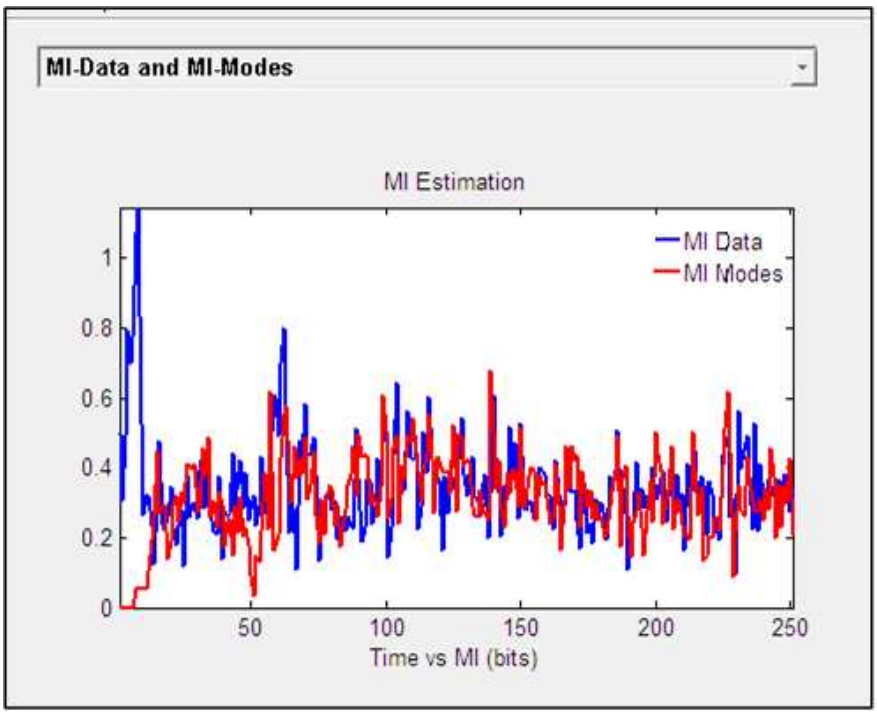

Figure 7.6: MI plots for the IP-EMD analysis.

Chapter 8

Conclusion and Future Work

The aim of this research and thesis was to explore and devise methods that can help in neural data analysis and give insight about neural coding mechanism. Algorithms have been developed for spike trains and various forms of field potentials. These methods and tool have been tested on real neural recordings and the findings confirm their significance and usefulness. The key results are listed in the following section.

8.1 Key Results and Conclusions

- Automated analysis of different forms of neural data recordings including spike train and field potentials. Algorithms have been developed that provide an adaptive solution for large spike train dataset and multi-channel electric and magnetic field potential recordings.
- The use of self-organizing maps for analysing, decoding and clustering multi-channel spike train data. The results show that discrete spike train when convolved with decaying exponential kernel gave better clustering results. For this reason, the decaying exponential kernel is preferred over Gaussian kernel.
- Insight of the neural coding mechanism can be obtained by SOM based clustering. This has been shown via information quantification of clusters. SOM generates clusters that are information-preserving.
- Design of algorithms for analysis of continuous neural recordings such as local field potentials (LFPs), magneto-encephalographs (MEGs) etc. The

algorithm called information preserving empirical mode decomposition (IP-EMD) combines information theory and EMD to decompose field potentials and extract information carrying oscillation in the field potentials which are not visible otherwise. This greatly simplifies the analysis of potentially complex signals and facilitate their interpretation and avoids the need for bandpass filtering followed by Fourier or wavelets analysis. The use of information-coupled empirical mode decomposition (EMD) thus extends the limitations of signal processing methods currently in use.

- IP-EMD gives information about stimulus coding oscillatory modes and corresponding frequency bands. This has several applications. It can be used for neuronal activity analysis of single and multiple channel recording against a stimulus or in a medical condition. It can also be used for synchronisation analysis and for analysing neuronal interaction via information connectivity analysis of different channels. The Hilbert analysis of informative modes can further help identify discriminating features against different stimuli, when the magnitude information is not sufficient. Further research will incorporate time delay in mutual information analysis in order to reveal information flow (directions) among channels. An attempt has also been made to use IP-EMD generated modes for field potentials data compression.

- IP-EMD framework has been tested on various electric and magnetic field potential datasets and its performance has been compared with other methods. An initial toolbox has been built to offer its advantages to the neuroscience community and for wider applications.

8.2 Future Work

The work carried out during this research can be further extended to many applications. Some of them are listed in the following.

- A SOM based clustering and classification toolbox can be developed that can be used for automated analysis for spike train recordings. Discrete spikes trains will be first convolved with decaying exponential kernel and will be used for SOM training. The information analysis of the clusters will

give insight into the information contained by cluster members and can give insight of the stimuli coding mechanism.

- Classification of unknown responses, belonging to different stimuli, can be carried out by using modes extracted by IP-EMD algorithm.
- The IP-EMD based information connectivity analysis among recording channels has been used to show strength of connectivity and information transfer among channels. Incorporation of transfer entropy or Granger causality can be used to find the direction of information flow among electrodes. This will help in analysing how different regions in brain are activated in response to stimuli.
- An initial investigation has been carried out to explore the use of informative modes for neural data compression. More experiments are required to develop this approach into a sophisticated compression algorithm.
- The results obtained from IP-EMD can be tested for use in brain-computer interface (BCI) applications.
- IP-EMD has been tested on field potential recordings. It can be extended to medical imaging data such as fMRI data. For imaging data bi-dimensional EMD (Damerval et al. 2005) can be employed.
- Performance of IP-EMD can also be tested on other non-stationary continuous data such as (electrocardiographs) ECG and financial series.

Bibliography

Abbot, L. & Dayan, P. (2001), *Theoretical Neuroscience: Computational and Mathematical Modeling of Neural Systems*, MIT Press.

Abeles, M., Vaadia, E., Bergman, H., Prut, Y., Haalman, I. & Slovin, H. (1993), 'Dynamics of neuronal interactions in the frontal cortex of behaving monkeys.', *Concepts in Neuroscience* **4**, 131–158.

Addison, P. S. (2005), 'Wavelet transforms and the ECG: a review', *Physiological Measurement* **26**, 155–199.

Adeli, H., Zhou, Z. & Dadmehr, N. (2003), 'Analysis of EEG records in an epileptic patient using wavelet transform.', *J. Neurosci. Meth.* **123**, 69?87.

Ahmadlou, M. & Adeli, H. (2010), 'Wavelet synchronization methodology: a new approach for EEG-based diagnosis of ADHD.', *Clinical EEG and Neurosci.* **41**, 1–10.

Andrade, A. O., Kyberdn, P. & Nasuto, S. J. (2008), 'The application of the Hilbert spectrum to the analysis of electromyographic signals', *Information Sciences* **178**, 2176–2193.

Arabzadeh, E., Panzeri, S. & Diamond, M. (2004), 'Whisker vibration information carried by rat barrel cortex neurons.', *Journal of Neuroscience* **24(26)**, 6011–6020.

Arabzadeh, E., Petersen, R. & Diamond, M. (2003), 'Encoding of whisker vibration by rat barrel cortex neurons: implications for texture discrimination.', *Journal of Neuroscience* **23(27)**, 9146–9154.

Awiszus, F. (1997), 'Spike train analysis', *J. Neurosci. Meth.* **74**, 155–166.

Bear, M. F., Connors, B. W. & Paradiso, M. A. (2007), *Neuroscience: exploring the brain*, Lippincot Williams & Wilkins.

Bedard, C., Krger, H. & Destexhe, A. (2004), 'Modeling extracellular field potentials and the frequency-filtering properties of extracellular space.', *Biophysical Journal* **86**, 1829–1842.

Bedard, C., Krger, H. & Destexhe, A. (2006), 'Model of low-pass filtering of local field potentials in brain tissue', *Physical Review E* **73**, 1–15.

Belitski, A., Gretton, A., Magri, C., Murayama, Y., Montemurro, M., Logothetis, N. & Panzeri, S. (2008), 'Low-frequency local field potentials and spikes in primary visual cortex convey independent visual information', *J. Neurosci.* **28**(22), 5696–5709.
URL: *http://www.jneurosci.org/cgi/content/abstract/28/22/5696*

Berens, P., Keliris, G. A., Ecker, A. S., Logothetis, N. K. & Tolias, A. S. (2008), 'Comparing the feature selectivity of the gamma-band of the local field potential and the underlying spiking activity in primate visual cortex', *Frontiers in systems neurosci.* **2**, 199–207.

Boudraa, A. O., Cexus, J. C. & Saidi, Z. (2005), 'EMD–Based signal noise reduction.', *Int. J. Information and Comm. Engineering* **1**, 33–37.

Brillinger, D. R. (1979), 'Confidence intervals for the crosscovariance function.', *Selecta Statistica Canadiana* **V**, 1–16.

Brown, E. N., Kass, R. E. & Mitra, P. P. (2004), 'Multiple neural spike train data analysis: state-of-the-art and future challenges', *Nature Neurosci.* **7**, 456–461.

Brown, G., Yamada, S., Luebben, H. & Sejnowski, T. (1998), 'Spike sorting and artifact rejection by independent component analysis of optical recordings from tritonia', *Soc. Neurosci. Abstr.* **24**, 1670.

Burns, B. D., Stean, J. & Webb, A. (1974), 'Recording for several days from single cortical neurons in completely unrestrained cats', *Electroencephalography and Clinical Neurophysiology* **36**, 314 – 318.

Buzsaki, G. (2004), 'Large-scale recording of neuronal ensembles', *Nat. Neurosci.* **7**, 446–451.

Carey, J. (1990), *Brainfacts, a primer on the brain and nervous system.* **URL:** *http://www.sfn.org/index.aspx?pagename=brainfacts*

Chang, C.-C. & Lin, C.-J. (2001), *LIBSVM.* Software available at http://www.csie.ntu.edu.tw/ cjlin/libsvm.

Christen, M., Ott, T. & Stoop, R. (2004), 'Spike train clustering using a lempel-ziv distance measure', *Inter. Symposium on Nonlinear Theory and its App. (NOLTA2004)* .

Chui, C. (1992), *An Introduction to Wavelets.*, San Diego: Academic Press.

Cohen, L. (1992), 'What is a multicomponent signal?', *IEEE International Conference on Acoustics, Speech, and Signal Processing (ICASSP-92)* **5**, 113–116.

Coles, M. G. & Rugg, M. D. (1996), *Electrophysiology of Mind*, Oxford Scholarship Online Monographs, chapter Event-related brain potentials: an introduction, pp. 1–7.

Cover, T. & Thomas, J. (1999), *Elements of Infomation Theory*, Wiley Interscience.

da Silva, F. L. (1991), 'Neural mechanisms underlying brain waves: from neural membranes to networks', *Electroencephalography and Clinical Neurophysiology* **79**, 81 – 93.

Damerval, C., Meignen, S. & Perrier, V. (2005), 'A fast algorithm for bidimensional emd, ieee signal process.', *IEEE Signal Process. Lett.* **12**, 701–704.

Date, A. (2001), An information theoretic analysis of 256-channel EEG recordings: Mutual information and measurement selection problem, *in* 'ICA conference', pp. 185–188.

Dermietzel, R. & von Bohlen und Halbach, O. (2006), *Neurotransmitters and neuromodulators:handbook of receptors and biological effects.*, 2 edn, Wiley-VCH, chapter Methods, pp. 21–42.

Dunn, J. (1974), 'Well separated clusters and optimal fuzzy partitions', *J.Cybern.* **4**, 95–104.

Ent, D. V., Manshanden, I., Ossenblok, P., Velis, D. N., de Munck, J. C., Verbunt, J. P. A. & da Silva, F. H. L. (2003), 'Spike cluster analysis in neocortical localization related epilepsy yields clinically significant equivalent source localization results in magnetoencephalogram (meg).', *Clinical Neurophysiology* **114**, 1948 – 1962.

Fellous, J., Tiesinga, P. H. E., Thomas, P. J. & Sejnowski, T. J. (2004), Discovering spike patterns in neuronal responses, *in* 'Hartigan JA', Vol. 24, Wiley, pp. 2989–3001.

Flandrin, P. & Gonçalvès, P. (2004), 'Empirical mode decompositions as data–driven wavelet–like expansions.', *International Journal of Wavelets, Multiresolution and Information Processing* **2**, 1–20.

Flury, B. (1988), *Common principal components and related multivariate methods.*, Wiley, New York.

Fotheringhame, D. & Baddeley, R. (1997), 'Nonlinear principal components analysis of neuronal spike train data', *Biol Cybern.* **77**, 283–288.

Fries, P. (2005), 'A mechanism for cognitive dynamics: neuronal communication through neuronal coherence', *Trends in Cognitive Sciences* **9**, 474 – 480.

Gerstein, G. L. & Clark, W. A. (1964), 'Simultaneous studies of firing patterns in several neurons', *Science* **143**, 1325 – 1327.

Gibbons, H. & Stahl, J. (2007), 'Response-time corrected averaging of event-related potentials.', *Clinical Neurophysiology* **118**, 197–208.

Grafakos, L. (2004), *Classical and Modern Fourier Analysis*, Prentice-Hall.

Gray, C., Maldonado, P., Wilson, M. & ., B. M. (1995), 'Tetrodes markedly improve the reliability and yield of multiple single-unit isolation from multi-unit recordings in cat striate cortex.', *Journal of Neuroscience Methods* **63**, 43–54.

Gunduz, A. & Principe, J. C. (2009), 'Correntropy as a novel measure for nonlinearity tests', *Signal Processing* **89**, 14–23.

Hämäläinen, M., Hari, R., Ilmoniemi, R. J., Knuutila, J. & Lounasmaa, O. V. (1993), 'Magnetoencephalography—theory, instrumentation, and applications

to noninvasive studies of the working human brain', *Rev. Mod. Phys.* **65**, 413–497.

Henrie, J. & Shapley, R. (2005), 'LFP power spectra in V1 cortex: the graded effect of stimulus contrast', *Journal of Neurophysiology* **94**, 479–490.

Hodgkin, A. & Huxley, A. (1952), 'A quantitative description of membrane current and its application to conduction and excitation in nerve.', *J. Physiol.* **117**.

Hsu, C.-W., Chang, C.-C. & Lin, C.-J. (n.d.), 'A pratical guide to support vector machine'.
URL: *http://www.csie.ntu.edu.tw/ cjlin/papers/guide/guide.pdf*

Huang, N. E., Shen, Z., Long, S. R., Wu, M. C., Shih, H. H., Zheng, Q., Yen, N. C., Tung, C. C. & Liu, H. H. (1998), 'The empirical mode decomposition and the hilbert spectrum for nonlinear and non-stationary time series analysis', *Proceedings of the Royal Society.* **454**, 903–995.
URL: *http://cat.inist.fr/?aModele=afficheN&cpsidt=10378737*

Huang, N., Wu, M.-L., Qu, W., Long, S., Shen, S. & Zhang, J. (2003), 'Applications of hilbert-huang transform to non-stationary financial time series analysis.', *Appl. Stoch. Models Bus. Ind.* **19**, 245–268.

Humphrey, D. R. & Schmidt, E. M. (1990), *Neurophysiological Techniques: Applications to Neural Systems*, Vol. 15, Springerlink, chapter Extracellular Single-Unit Recording Methods, pp. 1–64.

Humphrey, D. R. & Schmidt, E. M. (1991), Extracellular single-unit recording methods, *in* A. A. Boulton, G. B. Baker & C. H. Vanderwolf, eds, 'Neurophysiological Techniques', Vol. 15 of *Neuromethods*, Humana Press, pp. 1–64. 10.1385/0-89603-185-3:1.
URL: *http://dx.doi.org/10.1385/0-89603-185-3:1*

Ido Priness, O. M. & Ben-Gal, I. (2007), 'Evaluation of gene-expression clustering via mutual information distance measure', *BMC Bioinformatics* **8**(1), 1–11.
URL: *http://www.biomedcentral.com/1471-2105/8/111*

Jain, A., Murty, M. & Flynn, P. (1999), 'Data clustering: a review', *ACM Computing Surveys* **31**, 264–323.

Jeong, J., Gore, J. C. & Peterson, B. S. (2001), 'Mutual information analysis of the EEG in patients with alzheimer's disease.', *Clinical Neurophysiology* **112**(5), 827–835.

Kandel, E., Schwartz, J. & Jessell, T. (2000), *Principles of Neural Science*, 4th ed edn, McGraw-Hill, New York.

Katzner, S., Nauhaus, I., Benucci, A., Bonin, V., Ringach, D. & Carandini, M. (2007), 'The local field potential in primary visual cortex: how local is it?', *Journal of Vision* **7**(15), 72–72.
URL: *http://journalofvision.org/7/15/72/*

Khaldi, K., Alouane, M. T.-H. & Boudraa, A.-O. (2010), 'Voiced speech enhancement based on adaptive filtering of selected intrinsic mode functions', *Adv. in Adaptive Signal Analysis* **2**, 65–80.

Kim, D. & Oh, H. S. (2008), 'EMD: Empirical mode decomposition and Hilbert spectral analysis.'.
URL: *url: http://cran.r-project.org/web/packages/EMD/index.html*

Kitai, Stephen, T. & Melburn, P. R. (1991), Intracellular electrophysiological techniques, *in* A. A. Boulton, G. B. Baker & C. H. Vanderwolf, eds, 'Neurophysiological Techniques', Vol. 14 of *Neuromethods*, Humana Press, pp. 1–34. 10.1385/0-89603-160-8:1.
URL: *http://dx.doi.org/10.1385/0-89603-160-8:1*

Kohonen, T. (1997), *Self-Organizing Maps*, Springer.

Kramer, M. A., Chang, F. L., Cohen, M. E., Hudson, D. & Szeri, A. (2007), 'Synchronization measures of the scalp EEG can discriminate healthy from alzheimers subjects.', *Int. J. Neural Systems* **17**, 61–69.

Kraskov, A., Quiroga, R. Q., Reddy, L., Fried, I. & Koch, C. (2007), 'Local field potentials and spikes in the human medial temporal lobe are selective to image category.', *J. Cognitive Neurosci.* **19**, 479492.

Kreiman, G., Hung, C. P., Kraskov, A., Quiroga, R. Q., Poggio, T. & DiCarlo, J. (2006), 'Object selectivity of local field potentials and spikes in the macaque inferior temporal cortex', *Neuron* **49**, 433–445.

Lachaux, J.-P., Rodriguez, E., Martinerie, J. & Varela, F. J. (1999), 'Measuring phase synchrony in brain signals', *Human Brain Mapping* **8**(4), 194–208.

Lambert, M., Engroff, A., Dyer, M. & Byer, B. (2003), 'Emd'.
URL: *url: http://www.owlnet.rice.edu/elec301/Projects02/empirical Mode.*

Lau, C. (1992), *Neural Networks: Theoretical Foundations and Analysis*, IEEE Press.

Legatt, A. D., Arezzo, J. & Vaughan., H. (1980), 'Averaged multiple unit activity as an estimate of phasic changes in local neuronal activity: effects of volume-conducted potentials', *Journal of Neuroscience Methods* **2**, 203–217.

Lewicki, M. S. (1998), 'A review of methods for spike sorting: the detection and classification of neural action potentials', *Network: Computation in Neural Systems* **9**, 53–78.

Liang, H., Bressler, S. L., Buffalo, E. A., Desimone, R. & Fries, P. (2005), 'Empirical mode decomposition of local field potentials from macaque V4 in visual spatial attention.', *Biological Cybernetics* **92**(6), 380–392.

Logothetis, N. K., Pauls, J., Augath, M., Trinath, T. & Oeltermann, A. (2001), 'Neurophysiological investigation of the basis of the fmri signal', *Nature* **412**(6843), 150–157.
URL: *http://dx.doi.org/10.1038/35084005*

Lopez-Munoz, F., Boya, J. & Alamo, C. (2006), 'Neuron theory, the cornerstone of neuroscience,on the centenary of the nobel prize award to santiago ramn y cajal', *Brain Research Bulletin* **70**, 391–405.

MacLeod, K., Bcker, A. & Laurent, G. (1998), 'Who reads temporal information contained across synchronized and oscillatory spike trains?', *Nature* **395**, 693–698.

Mangiameli, P., Chen, S. & West, D. (1996), 'A comparison of som neural network and hierarchical clustering methods', *European J. of Operational Research* **93**, 402–417.

Manyakov, N. V. & Hulle, M. M. V. (2008), 'Discriminating visual stimuli from local field potentials recorded with a multi-electrode array in the monkey's visual cortex', pp. 157–162.

Mehboob, Z. & Yin, H. (2008), Analysis of non-stationary neurobiological signals using empirical mode decomposition., *in* 'Hybrid Artificial Intelligent Systems (HAIS)', pp. 714–721.

Mehboob, Z. & Yin, H. (2009), Information preserving empirical mode decomposition for filtering field potentials, *in* 'Intelligent Data Engineering and Automated Learning (IDEAL)', pp. 226–233.

Mehboob, Z. & Yin, H. (2010), Neural data analysis and reduction using improved framework of information-preserving EMD., *in* 'Intelligent Data Engineering and Automated Learning (IDEAL)', pp. 360–367.

Mehboob, Z. & Yin, H. (2011), 'Information quantification of empirical mode decomposition and applications to field potentials.', *Int. J. Neural Systems* **21**, 49–63.

Moler, C. (n.d.), 'The origins of MATLAB', Mathworks Newsletter.
URL: *http://www.mathworks.com/company/newsletters/news_notes/clevescorner/*

Nicolelis, M. A. (1999), *Methods for neural ensemble recordings*, CRC Press.

Oliva, A. (2005), 'Gist of the scene', *The Encyclopedia of Neurobiology of Attention* pp. 251–256.

Ortigueira, M. (2008), 'Empirical mode decomposition'.
URL: *http://www.mathworks.com/matlabcentral/fileexchange/21409-empirical-mode-decomposition*

Panzeri, S., Petersen, R., Schultz, S. & Diamond, M. L. M. (2001), 'The role of spike timing in the coding of stimulus location in rat somatosensory cortex', *Neuron* **29**, 769–777(9).

Panzeri, S. & Schultz, S. R. (2001), 'A unified approach to the study of temporal, correlational, and rate coding.', *Neural computation* **13**, 1311–1349.

Panzeri, S., Senatore, R., Montemurro, M. A. & Petersen, R. S. (2007), 'Correcting for the sampling bias problem in spike train information measures', *Journal of Neurophysiology* **98**, 1064–1072.

Percival, D. B. & Walden, A. T. (1993), *Spectral Analysis for Physical Applications:Multitaper and Conventional Univariate Techniques*, Cambridge University Press.

Pereda, E., Quiroga, R. Q. & Bhattacharya, J. (2005), 'Nonlinear multivariate analysis of neurophysiological signals', *Progress in Neurobiology* **77**, 1–37.

Petersen, R. S., Panzeri, S. & Diamond, M. E. (2001), 'Population coding of stimulus location in rat somatosensory cortex', *Neuron* **32**, 503–514.

Pfurtscheller, G. & Aranibar, A. (1977), 'Event-related cortical desynchronization detected by power measurements of scalp EEG.', *Electroenceph. clin. Neurophysiol* **42**, 817?826.

Picton, T., Lins, O. & Scherg, M. (1995), *Handbook of neuropsychology.*, Vol. 10, New York: Elsevier, chapter The recording and analysis of eventrelated potentials., pp. 3–73.

Quiroga, R. Q. (2007), 'Spike sorting', *Scholarpedia* **2**(12), 3583.

Quyen, M. L. V., Foucher, J., Lachaux, J.-P., Rodriguez, E., Lutz, A., Martinerie, J. & Varela, F. (2001), 'Comparison of Hilbert transform and wavelet methods for the analysis of neuronal synchrony.', *J. Neurosci. Meth.* **111**, 83–98.

Ray, S., Hsiao, S. S., Crone, N. E., Franaszczuk, P. J. & Niebur, E. (2008), 'Effect of stimulus intensity on spike-LFP relationship in secondary somatosensory cortex', *Journal of Neuroscience* **28**, 7334–7343.

Richmond, B. & Optican, L. (1987), 'Temporal encoding of two-dimensional patterns by single units in primate inferior temporal cortex. II. Quantification of response waveform', *Journal of Neurophysiology* **57**, 147–161.

Rieke, F., Warland, D., Deruytervansteveninck, R. & Bialek, W. (1999), *Spikes: Exploring the Neural Code (Computational Neuroscience)*, The MIT Press.

Rilling, G., Flandrin, P. & Gonçalvès, P. (2003), On empirical mode decomposition and its algorithms, *in* 'Proceedings of the 6th IEEE/EURASIP Workshop on Nonlinear Signal and Image Processing (NSIP '03), Grado, Italy'.

Roth, G. & Dicke, U. (2005), 'Evolution of the brain and intelligence', *Trends Cogn. Sci.* **9**, 250257.

Rousche, P. J., Petersen, R. S., Battiston, S., Giannotta, S. & Diamond, M. E. (1999), 'Examination of the spatial and temporal distribution of sensory cortical activity using a 100-electrode array.', *J. Neurosc. Meth.* **90**, 57–66.

Satoshi, Y., Michio, N., Kenji, M. & Satoru, S. (1993), 'Information theoretic analysis of action potential trains', *Biological Cybernetics* **68**, 215–220. 10.1007/BF00224854.
URL: *http://dx.doi.org/10.1007/BF00224854*

Schwartz, M., Bennett, W. R. & Stein, S. (1966), *Communication Systems and Techniques*, McGraw-Hill, New York.

Shannon, C. E. (1948), 'A mathematical theory of communication.', *Bell System Technical Journal* **27**, 623–656.

Shepherd, G. M. (1988), *Neurobiology*, Oxford University Press, chapter The Action Potential, pp. 101–121.

Stark, E. & Abeles, M. (2007), 'Predicting movement from multiunit activity', *The Journal of Neuroscience* **27**, 8387–8394.

Starr, C. & McMillan, B. (2007), *Human Biology*, 8 edn, Yolanda Cossio, chapter The Nervous System, pp. 239–265.

Strong, S. P., Koberle, R., de Ruyter van Steveninck, R. R. & Bialek, W. (1998), 'Entropy and information in neural spike trains.', *Physical Review Letters* **80**, 197200.

Sum, J. & Chan, L. (1994), 'Convergence of one-dimensional self-organizing map', *Proc. of Int. Symp. on Speech, Image Process. and Neural Networks* **1**, 81–84.

Swadlow, H. (1989), 'Efferent neurons and suspected interneurons in S-1 vibrissa cortex of the awake rabbit: receptive fields and axonal properties.', *J Neurophysiol* **62**, 288–308.

Sweeney-Reed, C. & Nasuto, S. (2007), 'A novel approach to the detection of synchronisation in EEG based on empirical mode decomposition', *Journal of Computational Neuroscience* **23**, 79–111.

Sweeney-Reed, C. & Nasuto, S. (2009), 'Detection of neural correlates of self-paced motor activity using empirical mode decomposition phase locking analysis.', *J. Neurosci. Meth.* **184**, 54–70.

Tamayo, P., Slonim, D., Mesirov, J., Zhu, Q., Kitareewana, S., Dmitrovsky, E., Lander, E. S. & Golub, T. R. (1999), Interpreting patterns of gene expression with self-organizing maps: Methods and application to hematopoietic differentiation., *in* 'Proc. of the National Academy of Sci. USA', Vol. 96, pp. 2907–2912.

Thorpe, S., Fize, D. & Marlot, C. (1996), 'Speed of processing in the human visual system', *Nature* **381**, 520–522.

Truccolo, W., Knuth, K. H., Shah, A., Bressler, S. L., Schroeder, C. E. & Ding, M. (2003), 'Estimation of single-trial multicomponent ERPs: Differentially variable component analysis (dVCA)', *Biological Cybernetics* **89**, 426–438. 10.1007/s00422-003-0433-7.
URL: *http://dx.doi.org/10.1007/s00422-003-0433-7*

Van Rossum M. C. W. (2001), 'A novel spike distance', *Neural Computation* **13**, 751–763.

Victor, J. D. (2006), 'Approaches to information-theoretic analysis of neural activity', *MIT Press* **1**, 302–316.

Walter, M., Stuart, L. & Borisyuk, R. (2003), 'The representation of neural data using visualization.', *The 9th IEEE int. symposium on information visualization (InfoVis03)* .

Wang, Z., Maier, A., Logothetis, N. K. & Liang, H. (2008), 'Single-trial classification of bistable perception by integrating empirical mode decomposition, clustering, and support vector machine', *EURASIP J. on Advances in Signal Processing* .

Weng, B., Xuan, G., Kolodzey, J. & Barner, K. E. (2006), 'Empirical mode decomposition as a tool for DNA sequence analysis from the terahertz spectroscopy measurements.', *IEEE Int. Workshop on Genomic Signal Processing and Statistics* pp. 63–64.

Williams, R. & Herrup, K. (1988), 'The control of neuron number', *Annual Review of Neuroscience* **11**, 423453.

Yeung, K. Y. & Ruzzo, W. L. (2001), 'Principal component analysis for clustering gene expression data', *Bioinformatics* **17**, 763–774.

Yin, H. (2002), 'Data visualization and manifold mapping using the ViSOM', *Neural Networks* **15**, 1005–1016.

Yin, H. (2008), 'On multidimensional scaling and embedding of self-organising maps', *Neural Networks* **21**, 160–169.

Yin, H., Mehboob, Z., Panzeri, S. & Diamond, M. E. (2008), Topological clustering of synchronous spike trains, *in* 'International Joint Conference on Neural Networks (IJCNN)'.

Yin, H., Panzeri, S., Mehboob, Z. & Diamond, M. E. (2008), Decoding population neuronal responses by topological clustering., *in* 'International Conference on Artificial Neural Networks (ICANN)'.